STUDIES ON THE PROPERTIES OF NUCLEAR REACTIONS INDUCED BY LOOSELY BOUND NUCLEI

A Thesis

SUBMITTED TO GAUHATI UNIVERSITY FOR THE
DEGREE OF DOCTOR OF PHILOSOPHY IN
(PHYSICS) IN THE FACULTY OF SCIENCE

Submitted by

Chinmoy Kumar Phookan

DEPARTMENT OF PHYSICS
GAUHATI UNIVERSITY
2014

Dr. Kushal Kalita
Assistant Professor
Department of Physics
Gauhati University
Guwahati-781014
Assam, INDIA

Ph : 91-361-2570531 (O)
9859936869 (M)
Fax : 91-361-2700311
e-mail : ku_kalita@yahoo.com
Address : Flat I, Unit 3
G. U. Campus
Guwahati-781014

CERTIFICATE

This is to certify that the work presented in this thesis entitled "STUDIES ON THE PROPERTIES OF NUCLEAR REACTIONS INDUCED BY LOOSELY BOUND NUCLEI" has been carried out in the Department of Physics, Gauhati University under my supervision. This work has been done by the candidate himself, and to the best of my (and candidate's) knowledge the work presented is original and has not been submitted for any other degree or diploma of this or any other University.

(Chinmoy Kumar Phookan)
Candidate

12.12.2014

(Dr. Kushal Kalita)
Thesis Supervisor
Assistant Professor
Department of Physics
Gauhati University

DECLARATION

I, Chinmoy Kumar Phookan, certify that the work embodied in this Ph.D. thesis is my own bonafide work carried out by me under the supervision of Dr. Kushal Kalita, Asst. Prof., Dept. of Physics, Gauhati University. To the best of my knowledge, no part of this work has been submitted elsewhere for the award of any other degree/diploma. I futher certify that I have not wilfully lifted somebody else's work and included them in my thesis and cited them as my own work.

Chinmoy Kumar Phookan
(Asst. Prof., Dept. of Physics)
(Haflong Govt. College)

Dedicated to
my Parents
my wife Mayuri and
my son Sankhaneel

Acknowledgements

I am highly grateful to my thesis supervisor, Dr. Kushal Kalita, for his constant help and encouragement in pursuing my research. I am especially thankful to him for allowing me to do theoretical work. I am also indebted to him for giving me permission to do part-time research work which allowed more flexibility and freedom in pursuing my research.

I am especially grateful to Dr. A. Gohain Barua, Head, Physics Dept., Gauhati University, for his constant cooperation and help. I also express my sincere thanks to Dr. Nimai Singh, Ex-Head, Physics Dept., Gauhati University, for his constant encouragement and keen interest in my work.

I also express my sincere thanks to Tapan Rajbonshi, Research Scholar, Physics Dept., Gauhati University, for his round the clock availability in helping me in innumerable ways. I also express my gratitude to Satyananda Singh, Research Scholar, Physics Dept., Gauhati University, for his constant help in the installation and use of Linux-softwares in my computers.

I am also grateful to Dr. Dipankar Misra, Asst. Professor, T. I. F. R., Mumbai for his valuable advice and sugggestions.

I am also thankul to Dr. Buddhadev Bhattacharjee and Dr. Kalyani Barua, faculty members at Physics Dept., Gauhati University, for their constant encouragement and valuable suggestions.

I am also grateful to Gautam Kumar Das, Ex-Principal, Haflong Govt. College, and Dr. Mizanur Rehman, Principal, Haflong Govt. College, for allowing me to pursue part-time research work.

I also express my sincere thanks to David Pegu, Basanta Pathak and Anjana Devi, Department colleagues at Haflong Govt. College, for their cooperation and help in pursuing my departmental work. .

Chinmoy Kumar Phookan
(Asst. Prof., Háflong Govt. College)

Research Publications

In Journals

1."A model for explaining fusion suppression using the classical trajectory method", C. K. Phookan and K. Kalita, *Journal of Phys. G : Nuclear and Particle Physics*, **40**, 125107 (2013).

2."Systematic study of Coulomb barrier of reactions induced by loosely bound projectiles using proximity potential",C. K. Phookan and K. Kalita, *Nuclear Physics A*, **899** 29, (2013).

3."Suppression of fusion in ^{6}Li+^{209}Bi using classical trajectory method", Chinmoy Kumar Phookan and Kushal Kalita, Vol. **53**, No. 2, page 63-68, *Journal of the Assam Science Society* (2012).

4."Analysis of reduced reaction cross section induced by radioactive projectiles", C. K. Phookan and Kushal Kalita, To be submitted to *Physical Review C*

Conference Presentations

1. "A model for explanation of fusion suppression using classical trajectory method", C. K. Phookan and K. Kalita, poster presentation at FUSION 14 International Conference, New Delhi, Feb. 24-28, 2014.

2. "Use of proximity potential in estimating the Coulomb barrier of reactions induced by loosely bound projectiles", Chinmoy Kr. Phookan, Kushal Kalita and Tapan Rajbonshi, oral presentation at National Conference of Theoretical Physics (NCTP), Tezpur University, Feb. 8-12, 2013."

3. "Classical trajectory model for extraction of fusion suppression on ^{6}Li+^{209}Bi reaction", Chinmoy Kr. Phookan, Baishali Saikia, Tapan Rajbonshi and Kushal Kalita, poster presentation at the One Day National Seminar on New Frontiers in Physics, Gauhati University, May 11, 2012.

4. "Classical trajectory model on fusion suppression of ^{6}Li+^{209}Bi", Chinmoy Kumar Phookan and Kushal Kalita, oral presentation at the 57^{th} Annual Technical Session of the Assam Science Society, March 16, 2012.

Contents

List of Tables

List of Figures

Preface

Studies on nuclear reactions with stable and unstable loosely bound projectiles has gained widespread popularity in recent years because of improved experimental facilities. This has been possible because of the availability of intense beams of stable loosely bound nuclei (^{6}Li, ^{7}Li and ^{9}Be) as well as unstable or radioactive loosely bound nuclei (^{6}He, ^{8}B, ^{7}Be, etc.). Hence, in the last two decades a large number of nuclear reactions have been performed around the world with loosely bound nuclei as projectiles. Having a low breakup threshold energy, these projectiles are easily susceptible to breakup and this gives rise to many new interesting features. The theoretical side is largely unexplored and the present thesis embodies theoretical work that has been carried out on some important properties of reactions induced by loosely bound projectiles.

From the analysis of experimental fusion cross section data, the empirical values of fusion barrier parameters of a large number of reactions induced by stable loosely bound projectiles on medium and heavy targets (^{209}Bi, ^{152}Sm, ^{144}Sm, ^{208}Pb, ^{124}Sn, etc.) have become available. We first determine the fusion barrier parameters of thirteen number of such reactions using eight different versions of the the proximity potential. The potentials chosen are Prox 77, Prox 88, Bass 73, Bass 77, Bass 80, CW 76, BW 91 and AW 95 as earlier work had shown that these potentials are highly effective in reproducing the barrier parameters of reactions induced by tightly bound projectiles. The results of all the potentials are found to be satisfactory. However, the potentials Bass 80 and BW 91 are found to be most effective in reproducing the

height (V_B) and position (R_B) of the barrier, respectively. The parametrized formula ($V_B = 1.44 Z_1 Z_2 (R_B - 0.75)/R_B^2$) connecting V_B and R_B has also been tested for the above reactions, and the formula is found to be extremely effective. For the reaction ^{6}Li+^{152}Sm, the deviations of the barrier parameters from the empirical values is found to be unusually large, and this is attributed to the large static deformation ($\beta_2 = 0.26$) of the target (^{152}Sm). On application of the correction of the Coulomb potential for the deformed target, the new values of the barrier parameters are found to be much closer to the empirical values. Study of the nature of the potentials for the case of deformed target reveals the emergence of distinct potential pocket for the potentials Bass 77, Bass 80, BW 91 and AW 95 in addition to the potentials Prox 77 and Prox 88 for which the pocket exists even for the spherical target case.

Then, fusion cross section for the reactions ^{6}Li+^{209}Bi, ^{9}Be+^{208}Pb, ^{7}Li+^{209}Bi and ^{6}Li+^{152}Sm is studied using the Wong's formalism and the barrier parameters are taken from the earlier results. The fusion cross section is also calculated from the single barrier penetration model (SBPM) using the code CCFULL. The fusion cross section calculated from Wong's formalism is found to be in agreement with the SBPM cross section, and is also found to be fractionally greater than the experimental cross section. The reason for the decrease of the experimental cross section is because of projectile breakup, and this phenomenon is called fusion suppression. Also, we find that fusion cross section calculated from Bass 80 barrier parameters gives a much better reproduction of the SBPM cross section. For the reaction ^{6}Li+^{152}Sm, fusion cross section is calculated considering the cases of spherical as well as deformed target. The fusion cross section for the case of deformed target is in much better agreement with the results of the SBPM cross section than the case of spherical target. This proves conclusively that deformation of nuclei has a great role to play in fusion cross section.

The most important part of our work is the semiclassical model for the explanation of fusion suppression. Technically speaking, fusion suppression is the ratio

between the experimental and the theoretical fusion cross section. The cause of fusion suppression, as noted earlier, is due to breakup of the projectile. We apply the model to the three ^{6}Li induced reactions : ^{6}Li+^{209}Bi, ^{6}Li+^{144}Sm and ^{6}Li+^{152}Sm. ^{6}Li has the lowest breakup threshold energy of 1.48 MeV, and easily breaks up into a deuteron and an α-particle. The experimental fusion suppression factors observed for the three reactions at energies $\approx$ 1.1 to 1.5 times the barrier energy are 0.36, 0.32 and 0.28, respectively. The basic idea of the model is to find out the cutoff impact parameter for fusion. Then the fraction of projectiles undergoing breakup within the cutoff impact parameter for fusion is determined which is then directly related to the fusion suppression factor. The cutoff impact parameter for fusion is determined by the single barrier penetration model (SBPM), as fusion cross section above the barrier can be approximated by the results of SBPM.

We apply the two-dimensional classical trajectory method for determining the fraction of projectiles undergoing breakup. From the three-body Lagrangian for the system of target and two-body projectile, the classical equations of motion are obtained. For obtaining numerical solutions, initial conditions have to be provided. For obtaining the initial conditions, we propose a semiclassical model of the ^{6}Li nucleus. The two postulates of the ^{6}Li ($\rightarrow$ ^{4}He+^{2}H) cluster model are : (a) The total energy of the deuteron and the α-particle system is equal to the breakup threshold energy (binding energy) of the ^{6}Li nucleus, and (b) The total angular momentum of rotation of the deuteron and the α-particle about an axis through its centre of mass is equal to $\sqrt{I(I+1)}\hbar$, where I is the spin quantum number of the ^{6}Li nucleus. From the calculations, the distance between the deuteron and the α-particle comes out to be 2.27 fm. Using the initial conditions, numerical solutions are obtained and the trajectories are studied. Three distinct types of trajectories are obtained and these are : scattering-like, incomplete fusion and no-capture breakup. We define a breakup condition for a trajectory or projectile. If the distance of separation between the deuteron and the α-particle is greater than 2.27 fm then its

a breakup trajectory, otherwise its a nobreakup trajectory.

Taking a sample of fifty trajectories at each impact parameter, the breakup fraction is determined. Then a formula is proposed for the explanation of fusion suppression according to which fusion suppression is given by the average of breakup fractions calculated at different impact parameters. The range of impact parameters lie between a head-on collision and the cutoff impact parameter for fusion. On application of the above formula to the three ^{6}Li induced systems, we find that there is excellent agreement between the experimental fusion cross section (σ_{exp}) and the calculated fusion cross section (σ_{cal}). However, for the reaction ^{6}Li+^{152}Sm there is slight disagreement at higher energies because of deformed nature of the target ^{152}Sm. Also, the relationship between the cutoff angular momentum for fusion (L_c) and energy (E_{cm}) is studied, and a linear relationship is establised. Using the proximity potential, the linear relationship is explained.

The last part of our study concerns the reduced reaction cross section of radioactive halo projectiles. For systematic analysis of reaction cross section data, Gomes' reduction procedure is widely followed in which the dependence of the cross section on the barrier radius (R_B) is eliminated, and the energy is scaled with respect to the barrier height (V_B). Study of reduced reaction cross section (σ_{red}) versus reduced energy (E_{red}) for a variety of systems has revealed that separate trajectories are followed for reactions induced by tightly bound, loosely bound, and radioactive halo projectiles. Also it has been pointed out that the reason for the separation of the trajectories of loosely bound and radioactive halo systems is that the Coulomb barrier is slightly lowered, and the barrier radius is marginally increased for radioactive systems in comparison with normal loosely bound systems. The reactions considered for radioactive halo systems are, ^{6}He+^{27}Al, ^{6}He+^{64}Zn, ^{6}He+^{209}Bi and ^{8}B+^{58}Ni. The corresponding reactions induced by normal nuclei are, ^{4}He+^{27}Al, ^{4}He+^{64}Zn, ^{4}He+^{209}Bi and ^{10}B+^{58}Ni. Using six different versions of global nuclear potentials on the above reactions we provide an explanation for the separation of

the barrier parameters. However, for the proton halo system ^{10,8}B+^{58}Ni, the change in the barrier parameters can only be accounted if proper radius of the halo nucleus ^{8}B and the normal nucleus ^{10}B is taken into account. This is because of the fact that experimentally the radius of the halo nucleus ^{8}B is found to be greater than ^{10}B, but all the six global nuclear potentials predict a decrease in the radius of ^{8}B. The study is extended to Be–projectile induced systems, and similar conclusions are drawn. Also, using the modified Wong's formula, the total reaction cross section is explained for the reactions ^{7}Be+^{27}Al and ^{6}He+^{27}Al. The modified Wong's formula is a phenemenonological formula containing three dimensionless parameters whose values are chosen by the χ^2 minimization technique.

There is potential future research prospect, particularly, in the semiclassical model of fusion suppression. The model of fusion suppression developed here is a two-dimensional classical trajectory model. The obvious generalization would be a three–dimensional model. It would be interesting to see whether the formula for fusion suppression proposed here for the two–dimensional model would still be applicable for the three–dimensional model. In the three–dimensional model, the orientation of the projectile is not necessarily confined to a single plane which is the case for the two–dimensional model. Finally, a fully quantum mechanical model of fusion suppression could be attempted in future even though it may be a highly challenging task. For this it would be necessary to develop a fully quantum mechanical version of the model of ^{6}Li nucleus that has been proposed here.

Chapter 1

Introduction

1.1 The nuclear interaction

Since the discovery of the neutron by Chadwick in 1932, there has been unprecedented attempts in understanding the nuclear force. In 1953, the noted physicist Hans Bethe stated that, "more man-hours have been given to this problem than to any other scientific question in the history of mankind". A variety of methods and procedures have been adopted in studying the problem. The nuclear force is powerfully attractive and operates at distances in the femtometer (10^{-15}m) regime. The magnitude of the force is maximum at distances around 1 fm, and quickly decreases to insignificance at distances greater than 2.5 fm. The first attempt at understanding the nuclear force problem was developed in 1935 by the Japanese physicist, Hideki Yukawa [1], who proposed that massive particles (called "mesons") were exchanged between the nucleons during their interaction. The theory was developed in analogy to the theory of electromagnetic interaction in which massless "photons" are exchanged between the particles. These models became known as one-boson-exchange models, and were very successful in explaining essentially all properties of the nucleon-nucleon interaction at low energies.

Apart from short-range and strong-attraction, some other remarkable properties

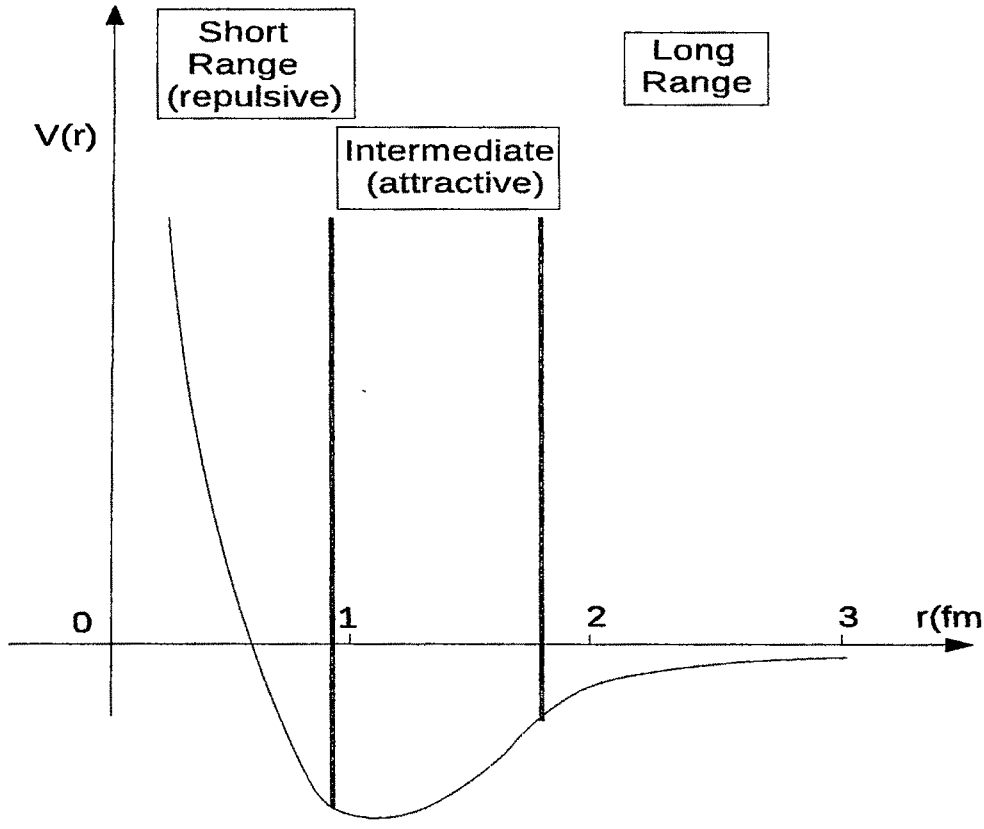

Figure 1.1: Diagram showing the nucleon-nucleon interaction.

of the nuclear force have been noted [2]. The nuclear force is dependent upon the direction of the spin of the nucleons due to which nuclear force has a tensor component. In heavier nuclei, a shell structure has been observed due to which it is essential to introduce a spin-orbit force. The nature of these forces can be studied through scattering experiments between nucleons. Moreover, the nucleon-nucleon force turns repulsive at distances shorter than 0.6 fm. Besides the force between two nucleons, there are also three-nucleon forces, four-nucleon forces, and so on. Their contribution is small, but crucial. The nuclear force or the nucleon-nucleon interaction is diagrammatically shown in Fig. 1.1. With all these properties the potential between two nucleons (the NN interaction) becomes quite complicated. Therefore, trying to solve the Schrodinger equation becomes a hopeless task even for the simplest nuclei. In the 60s and the early 70s, it became known that the

nucleons were no longer fundamental particles, but are instead composed of three quarks. Hence, it was realized that the fundamental theory of the nuclear force is quantum chromodynamics (QCD) and not meson theory [3]. Hence, the two-body nucleon problem becomes a six body quark problem. A lot of progress has been made, but still there are immense practical difficulties in trying to solve the six body problem by brute force. However, a true picture of the nuclear force has emerged. The modern view of the nuclear force is that it is a residual interaction of the even stronger force between quarks, which is mediated by the exchange of gluons and holds the quarks together inside a nucleon. This is somewhat similar to the van der waals interaction between neutral atoms, which is a residual interaction of the strong electromagnetic force between the electrons and the nuclei.

1.2 Heavy ion potentials

From the discussion in section 1.1, we can conclude that it would be a daunting task to study the nuclear force from a completely theoretical viewpoint. As such, the phenomenological approach has evolved in which simple nuclear models have been developed for explaining the results of experiments. A successful phenomenological approach is to ignore the individual nucleon-nucleon interaction and consider a single potential for the whole nucleus. Many heavy-ion systems may be understood in terms of empirical parametrizations of the nuclear potential. One such example is the optical model which is used for describing scattering data. The optical model potential has a real part and an imaginary part for describing the scattering and absorption, respectively. Phenomenological Woods-Saxon potential is used for describing both the real and imaginary parts of the optical potential. As many as two dozen other nuclear potentials are available in the literature. In chapter 2, we use a few nuclear potentials, and these are the two versions of the proximity potential (Prox 77 and Prox 88), three versions of the Bass potential (Bass 73, Bass 77 and

Bass 80), the Christensen and Winther potential (CW 76), the Broglia and Winther potential (BW 91), and the Aage Winther potential (AW 95). The proximity potential is obtained from the proximity theorem, whereas all the other potentials are obtained phenemenologically through analysis of scattering and fusion cross section data. Besides the above potentials, there are other potentials like the single folding potential, double folding potential [4], Skyrme energy density potential [5], etc. which are also successful in explaining a variety of phenomena.

1.3 Direct and compound-nucleus reactions

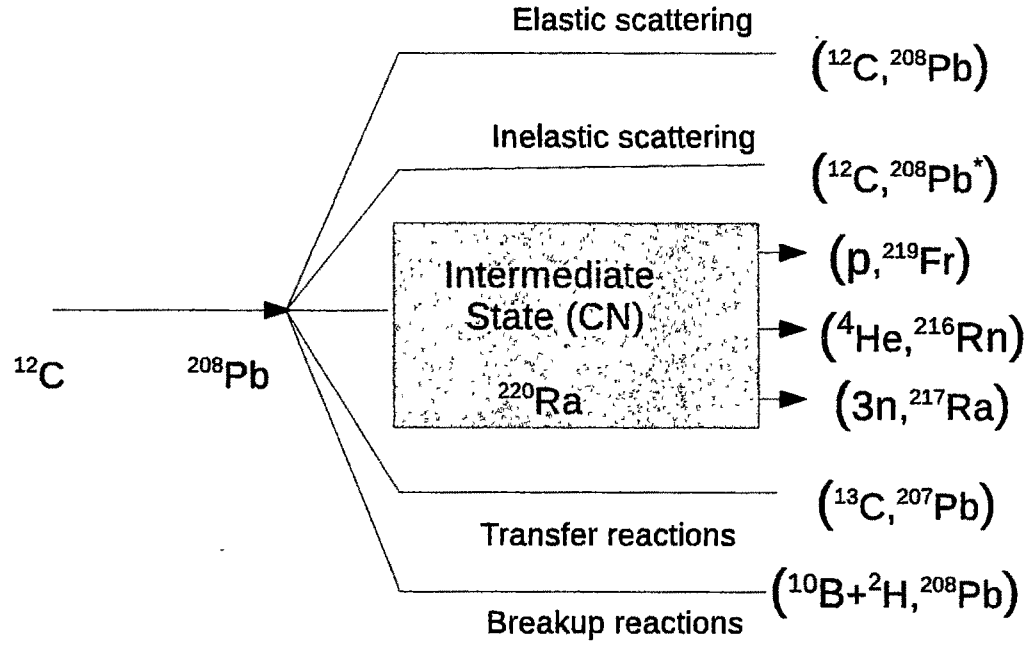

Figure 1.2: Diagram showing compound nucleus reactions and direct reactions for ^{12}C+^{208}Pb. Reactions proceeding from the rectangular box are the compound nucleus reactions, whereas the other reactions are the direct reactions.

A nuclei whose atomic number, A > 4, is called a heavy-ion by convention. Heavy-ion reactions have displayed properties which are quite different from reactions in which one of the participants is a light ion. Many different types of nuclear reactions [6] have been observed, and they are mainly categorized under two main

groups : direct reactions and compound-nucleus (CN) reactions. A third category, called deep inelastic collisions have also been categorized in recent years. In compound-nucleus reactions, the projectile and the target fuse to form a compound nucleus. In the formation of the compound nucleus, the total kinetic energy of the projectile is redistributed among all the nucleons of the compound nucleus. Hence, the compound-nucleus loses all memory of its formation process, and its decay is governed by the properties of the compound nucleus. The typical lifetime of a compound nucleus is 10^{-16} s, and they usually take place at smaller impact parameters or head-on collisions. All types of fusion reactions are examples of compound-nucleus reactions. At the opposite extreme we have direct reactions. Examples of direct reactions are elastic and inelastic reactions, transfer and breakup reactions, etc. These are diagrammatically shown in Fig. 1.2 with proper examples. Direct reactions are peripheral processes in which the incident particle interacts primarily at the surface of the target. Another criteria for direct reactions is that the incident particle must be highly energetic. As such the time of interaction between projectile and target in direct reaction is usually about 10^{-21} s, which is orders of magnitude smaller than that of compound nucleus reactions. Experimentally, these two incredibly short periods of time can be distinguished with present day facilities. Also, the angular distribution of the outgoing particles in direct reactions tend to be more sharply peaked in the forward direction. However, for compound-nucleus reactions the detected particles usually have forward and backward symmetry.

1.4 Types of heavy-ion nuclear reactions

Heavy-ion reactions are often treated in semi-classical approximation because of the complexities of the interaction between the two colliding nuclei. However, in view of the large masses it would be convenient to view the reaction first in the limit of classical scattering. Hence, the angular momentum of the projectile approaching a

target with energy, E, and impact parameter, b, is given by,

$$L = b\sqrt{2mE} \tag{1.1}$$

In the semi-classical approximation, we have, L=$\ell\hbar$, where, ℓ is the angular momentum of the projectile. Hence, in terms of the wave number, k=$\sqrt{2mE}/\hbar$, we may write,

$$\ell = b\frac{\sqrt{2mE}}{\hbar} = bk \tag{1.2}$$

In order to describe the different categories of heavy ion reactions with increasing energy, the grazing angular momentum (ℓ_g) may be defined,

$$\ell_g = kR_g \tag{1.3}$$

where, R_g is the grazing radius at which the colliding pairs start to feel the attractive nuclear force between them. It is usually taken to be slightly larger than the geometric "touching" distance between the two heavy-ions,

$$R = r_0(A_1^{1/3} + A_2^{1/3}) \quad ; \quad r_0 \approx 1.2 \text{ fm} \tag{1.4}$$

where, A_1 and A_2 are the mass numbers of the two heavy ions.

According to the relative values of ℓ and ℓ_g, heavy ion nuclear reactions may be classified as follows :

1.4.1 $\ell \gg \ell_g$

Reactions in this category doesn't involve transfer of mass or charge. Because of high impact parameter the Coulomb force is important in this category. Reactions under this category include the following :

Rutherford scattering

It takes place at the highest impact parameters and is also called the Coulomb scattering. Rutherford scattering can be entirely studied by applying classical laws. The Rutherford cross-section, originally derived by Rutherford using classical mechanics, matches the exact quantum mechanical cross section.

Coulomb excitation

In heavy ions, the Coulomb force is quite large, and this may cause excitations in both the target and projectile. Due to simplicity of the Coulomb force, the experimental results can be studied with great accuracy. The excited nucleus usually decays by the emission of γ-rays.

1.4.2 $\ell \geq \ell_g$

At these intermediate values of ℓ, the projectile reaches a distance close to the grazing radius (R_g). The nuclear effects start to dominate and as a result many new reaction channels open up. Transfer of a few number of nucleons are usually involved. For experimental reasons, these reactions are also called quasi-elastic. Reactions under this category include elastic nuclear scattering, inelastic scattering, nucleon-transfer reactions, knockout and breakup reactions and capture reactions.

Elastic Nuclear scattering

As the energy of the projectile is slowly increased, the Rutherford cross-section start showing deviations because of the nuclear force. The elastic nuclear scattering shows alternate maxima amd minima and bears a strong resemblance to the diffraction of light from an opaque object. All the participating partners remain in ground state before and after the scattering.

Inelastic scattering

This is similar to Coulomb excitation where either or both the target and projectile are excited to higher states. The excitation is primarily due to the nuclear interaction.

Nucleon transfer reactions

As the two nuclei come extremely close to each other, nucleon-transfer takes place due to quantum mechanical tunnelling. They can be either single nucleon transfer or multi-nucleon transfer reactions. Stripping and pick up reactions fall under single-nucleon transfer reactions. In stripping reactions, a nucleon is transferred from projectile to target. The reverse takes place in a pick up reaction. In multi-nucleon transfer reactions upto three-four nucleons may be exchanged between target and projectile.

Knockout and breakup reactions

In knockout reactions, a few nucleons are knocked out of the target or the projectile. In breakup reactions, the target breaks up into two or more fragments. Such reactions are only possible at very high energies.

Quasi-elastic scattering

The sum of the elastic scattering, inelastic scattering and transfer reactions is called quasi-elastic scattering. During measurement, when detector resolution is severe, the above reactions are not distinctly separated. Hence, they are grouped together under quasi-elastic scattering.

Capture reactions

In this type of reaction, an electron is captured by the target nucleus, and there is a decrease in the atomic number of the target by one unit. Eg : $^{7}\mathrm{Be}+e^{-} \rightarrow {}^{7}\mathrm{Li}$.

1.4.3 $\ell < \ell_g$

All compound-nucleus reactions fall under this category. Since, the life time of the compound nucleus is comparatively higher, hence, they are also called fusion reactions. The compound nucleus formed in fusion is usually unstable because they are generally proton-rich or neutron-deficient. For example, ^{40}Ca+^{90}Zr produces the compound nucleus ^{130}Nd which has 12 neutrons less than the most proton-rich stable neodymium isotope. Since, the collision process usually involves large masses at high velocities, hence, the compound-nucleus possesses high angular momentum, of the order of many tens to hundreds of $\hbar$. Depending upon the mode of disintegration of the compound nucleus, they are classified as :

Fusion-fission

For attaining stability, the compound nucleus decays by fission of two or more fragments of comparable mass. The angular momentum carried by the fission fragments is also large, and not much appears as spins of the fragments. Probability for fission is high only if the charge of the compound nucleus is greater than about 70.

Fusion-evaporation

On the other hand, if there are barriers against fission, the compound nucleus shall attain stability by evaporation of lighter particles (like neutrons, protons or α-particles) or through γ-ray emission. The angular momentum carried away by these lighter particles is usually small ($\leq$ 2-3 units of $\hbar$), and the residual nucleus is left with a very high spin. This process is called evaporation because it is similar to the evaporation of a liquid drop in which molecules escape from the surface. Fig. 1.3 shows the different types of fusion reactions.

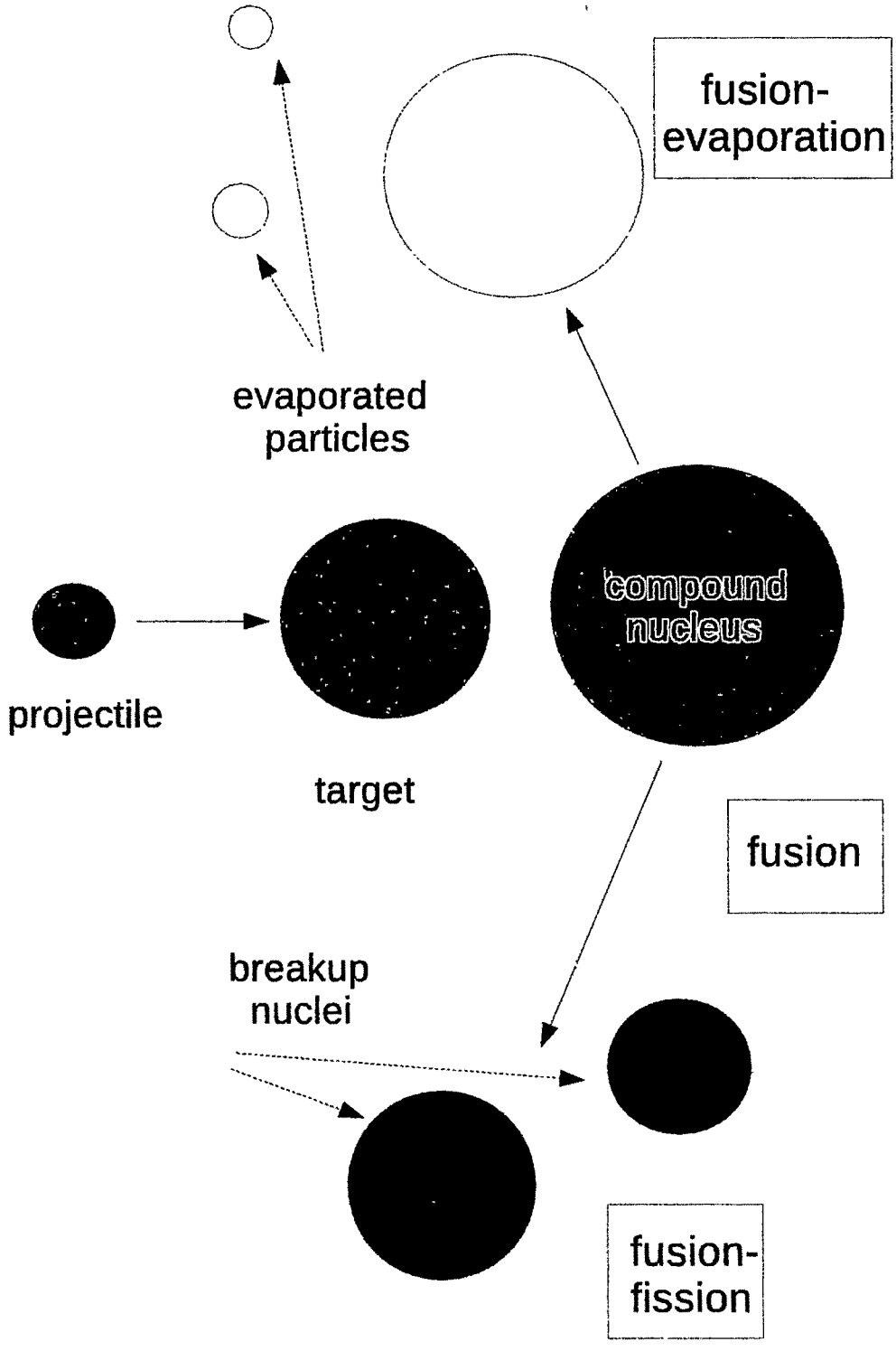

Figure 1.3: Three types of fusion reactions : (a) fusion (b) fusion-evaporation, and (c) fusion-fission

1.5 Heavy ion fusion reaction

As discussed above, fusion is defined as a reaction where two separate nuclei combine to form a composite system (compound nucleus) whose properties and mode of decay are independent of the formation process [7].

The two nuclei must collide at small impact parameters and must have sufficient energy to overcome the Coulomb barrier. The study of fusion of two nuclei is extremely important for a number of reasons. The process of nucleosynthesis (formation of new nuclei) in stars is due to the fusion of smaller nuclei to form heavier nuclei. In this process elements from carbon to iron are created. Experimentally, new radioactive nuclei are created which are far from the line of stability. The theoretical understanding of such processes has been a great challenge for the Physics community.

When the incident energy is not so large and the system is not so light, the reaction process is predominantly governed by quantum tunnelling over the Coulomb barrier created by the strong cancellation between the repulsive Coulomb force and the attractive nuclear interaction. The details of fusion cross section, including the single barrier penetration model (SBPM) and the Wong's formalism is given in section 3.4. Until about the early 1980s, fusion was understood in terms of a simple model of a single barrier whose parameters were varied to fit the measured cross-section. The results of a number of experiments during this period showed that the sub-barrier fusion cross-section is much larger than those expected from the simplified model. That this is not due to the ineffectiveness of the potential was elegantly showed by Balantekin [8]. He found that unphysical potentials are obtained if the experimental data is inverted to obtain the one-dimensional fusion barrier. The first successful explanation for this phenomenon came in terms of coupling-assisted tunnelling. Successive improvements in the couplings of the relative motion of the colliding nuclei provided better and better agreement between theory and experiment. The computer code CCFULL (coupled channels calculation for all

order couplings) [9], developed by K. Hagino, calculates the fusion cross section by solving the coupled second order differential equations and includes couplings upto all orders. Details of CCFULL code are given in section 3.5.

1.6 Loosely bound nuclei

Some of the lighter atomic nuclei (like ^6Li, ^7Li and ^9Be) are classified as loosely bound because they are easily susceptible to breakup into smaller nuclei [10, 11]. The breakup takes place because of low breakup threshold energy (binding energy) among its constituents. The breakup threshold energy is defined as the mass deficit (expressed in terms of energy) between the nucleus and its breakup fragments. Hence, if a nucleus, A, breaks up into fragments A_1 and A_2 (A $\rightarrow A_1 + A_2$) then the breakup threshold energy is given by,

$$S = (M_{A_1} + M_{A_2} - M_A)c^2 \tag{1.5}$$

where, M_A, M_{A_1} and M_{A_2} are the masses and c is the velocity of light. For the nuclei, ^6Li, ^7Li and ^9Be, the breakup channels along with their respective breakup threshold energies are given below,

$^6Li \rightarrow {}^4He + {}^2H \quad ; \quad S_\alpha = 1.475$ MeV

$^7Li \rightarrow {}^4He + {}^3H \quad ; \quad S_\alpha = 2.45$ MeV

$^9Be \rightarrow {}^4He + {}^4He + \mathrm{n} \quad ; \quad S_n = 1.67$ MeV

$^9Be \rightarrow {}^4He + {}^5He \quad ; \quad S_\alpha = 2.55$ MeV

We see that there are two prominent modes of decay for ^9Be. However, the first mode of decay is more probable because the breakup threshold energy is less. Besides the above stable loosely bound nuclei, radioactive (or unstable) loosely bound nuclei have become available in recent years. Examples of such nuclei are ^{6}He, ^{11}Li, ^{8}B,

^{7}Be and ^{11}Be [12, 13, 14, 15]. These nuclei are generally neutron-rich or proton rich, and most of them display halo properties, i.e., their r.m.s. matter radii are much greater than expected values. Out of the above nuclei, ^{11}Li, ^{11}Be and ^{6}He are neutron halo nuclei, whereas ^{8}B is a proton halo nucleus. In these nuclei, the separation energy of the last nucleon is extremely small (less than 1 MeV). The neutron (or proton) density distribution in radioactive loosely bound nuclei shows an extremely long tail, called the neutron (or proton) halo. Although the density of the halo is very low, it strongly affects the reaction cross section and leads to new properties in such nuclei.

1.7 Review work on reactions induced by loosely bound projectiles

With the availability of intense beams of loosely bound nuclei, a great deal of experimental work has become available. Most of this work concerns the study of fusion cross section (and fusion suppression) of these reactions. Fusion reactions induced by stable loosely bound projectiles have been studied on a wide range of medium and heavy targets like ^{209}Bi, ^{208}Pb, ^{159}Tb, ^{152}Sm, ^{144}Sm, ^{124}Sn, ^{89}Y, etc [10, 11, 16, 17, 18]. As discussed in the previous section, the loosely bound projectiles are easily susceptible to breakup into two fragments or in some cases even three fragments. The situation becomes more complicated than the case of fusion with a stable projectile. Experimentally, at least four different types of events have been identified [10, 19]. When the whole of the projectile fuses with the target without breakup, then it is called direct complete fusion (DCF). After breakup, if both the fragments fuse with the target, then it is called sequential complete fusion (SCF). If one of the breakup fragments fuse with the target, then it is called incomplete fusion (ICF). If none of the breakup fragments fuse with the target, then it is called no-capture breakup (NCBU). Because of projectile breakup, the experimental fu-

sion cross section falls below the theoretically expected fusion cross section. This phenomenon is called fusion suppression, and the ratio between σ_{exp} and σ_{theo} is called fusion suppression. The fusion suppression factor that has been observed for various loosely bound systems varies from $\approx$ 15–36 %. A detailed review of fusion suppression is given in chapter 4 in which we present a semiclassical model of fusion suppression.

Apart from the work undertaken by us, here we provide a brief review of the important work done with loosely bound projectiles. Some active groups are engaged in the analysis of elastic scattering data, and also in the simultaneous analysis of fusion and scattering data. The most popular and successful explanation is provided by the single-channel description of the process which is often called the optical model analysis. In the one channel description, the nuclear interaction can be written as the sum of two complex terms: the optical potential ($V_{opt}(r, E)+iW_{opt}(r, E)$) and the dynamic polarization potential ($V_{pol}(r, E)+iW_{pol}$(r,E)). The real part of the optical potential represents the static interaction between frozen nuclear matter distributions in the projectile and in the target, whereas its imaginary part accounts for the average flux lost to a large number of reaction channels. The dynamic polarization potential handles the strong coupling of these channels with the elastic channel. The real ($V_{opt}(r, E)$) and imaginary ($W_{opt}(r, E)$) parts of the optical potential are energy independent, or have a very weak dependence on E. On the other hand, the real ($V_{pol}(r, E)$) and imaginary (W_{pol}(r,E)) parts of the dynamic polarization potential are strongly dependent on the colliding energy. For the elastic scattering of tightly bound projectiles, a phenomenon called the threshold anomaly (TA) has been observed for a number of systems. This involves a characteristic peak in the energy dependence of V_{pol} around the Coulomb barrier, and the corresponding decrease in W_{pol} as the bombarding energy decreases below the Coulomb barrier. A different type of energy dependence from that of the TA is observed for the scattering of loosely bound projectiles ; this is often termed as the breakup threshold anomaly

(BTA). In the case of the BTA, a repulsive polarization potential is generated due to the coupling of breakup channels to the elastic channel, which causes an increase in the imaginary potential and corresponding decrease in the real part of the potential. Several works on the elastic scattering of ^{6}Li on various targets such as ^{27}Al [20], ^{64}Ni [21], ^{64}Zn [22], ^{80}Se [23], ^{90}Zr [24], ^{116,112}Sn [25],^{138}Ba [26], ^{144}Sm [27], ^{208}Pb [28], and ^{209}Bi [29] have indicated the presence of the breakup threshold anomaly (BTA). In these cases it has been observed that there is a small increase in the imaginary part of the optical potential rather than decreasing to zero at energies below the Coulomb barrier, indicating the absence of the normal TA. However, in the case of elastic scattering of ^{7}Li projectile on different targets such as ^{59}Co [30], ^{80}Se [23], ^{138}Ba [31], ^{208}Pb [32], and ^{232}Th [33] the conventional TA has been identified. This is attributed to the large breakup threshold energy of ^{7}Li in comparison to that of ^{6}Li. For ^{9}Be induced reactions, the usual TA is not present [34]. Since, ^{9}Be can breakup in two different ways (section 1.6) having comparable breakup threshold energies, hence the type of breakup is also crucial for an understanding of elastic scattering data. It was found that the cluster structure of ^{9}Be ($\rightarrow ^{4}He + ^{4}He$ + n) is able to explain the sub-barrier elastic scattering data for ^{9}Be+^{208}Pb, whereas the cluster structure of ^{9}Be ($\rightarrow ^{4}He + ^{5}He$) is needed to explain the elastic scattering data around and above the barrier [35].

1.8 Motivation for the thesis

In recent years a lot of experimental work has been done on nuclear reactions induced by loosely bound projectiles. This is due to the breakup properties of these projectiles (^{6}Li, ^{7}Li and ^{9}Be). Reactions induced by ^{6}Li is of particular interest because it has the lowest breakup threshold energy and hence, the highest breakup probability. The theoretical side of this huge amount of experimental work is largely unexplored, because within a short span of time a huge amount of experimental work

has been done. Hence, we would be pursuing theoretical work on some important properties of reactions induced by these projectiles. The properties investigated by us are the fusion barrier, fusion cross section and the fusion suppression for these reactions. Two factors which are very crucial in the study of fusion barrier and cross section is the nuclear potential, and the deformation properties of the target. Hence, a comparison among the predictions of different potentials is also a purpose of our study. Also a comparison of the results (with and without deformation) for the highly deformed target (^{152}Sm) is also done. The determination of fusion barrier parameters using global potentials has been extensively done for reactions induced by tightly bound projectiles. Since, such work has not been done for loosely bound systems, hence, as a first task we would be studying the fusion barrier parameters for loosely bound systems [10]. However, the most important motivation of our work is to provide an explanation of the phenemenon of fusion suppression. As far as we know no purely theoretical work on above barrier fusion suppression has been done. Although some authors (e.g., Diaz-Torrez [36]) have succeeded in explaining fusion suppression but they have done so only through the introduction of adhoc inputs like the breakup probability function. Reactions induced by ^{6}Li projectile is chosen because it has the highest breakup probability and also, the breakup of ^{6}Li is simpler compared to the breakup of ^{7}Li and ^{9}Be. The dominant channel for breakup of ^{7}Li involves a proton pickup from the target to form ^{8}Be, which then breaks up into two α-particles [37]. For ^{9}Be, the breakup process involves a neutron transfer to the target to form ^{8}Be, which finally breaks up into two α-particles [36]. However, the breakup of ^{6}Li takes place directly without any intermediate process like breakup of ^{7}Li or ^{9}Be. Finally we explain fusion suppression for the three reactions ; ^{6}Li+^{144}Sm, ^{6}Li+^{209}Bi and ^{6}Li+^{152}Sm [19]. The three reactions are chosen because precise experimental fusion cross section data is available for all the three systems, and also very high fusion suppression ($\approx 30\%$) is observed for all the systems. For obtaining the equations of motion of the three systems, we propose a

model for the ^{6}Li nucleus in which the deuteron and the α-particle revolve around their common centre of mass [19]. The model is semiclassical and is motivated by the Bohr's model of the hydrogen atom in which electrons revolve around the nucleus in classical orbits. In the last part of our work we are investigating the reaction cross section induced by radioactive projectiles. Recent analysis of the reduced reaction cross section of a variety of systems has revealed that the trajectories of radioactive halo systems and normal loosely bound systems are clearly separated. The above fact is explained in terms of the global parametrization of nuclear potentials.

1.9 Plan of the thesis

In chapter 1, we present the introductory information regarding our work which is mainly concerned with determination of barrier parameters, fusion cross section and explanation of fusion suppression for reactions induced by loosely bound projectiles. The introduction provides brief discussion about the nuclear force, heavy-ion potentials, different categories of nuclear reactions with special emphasis on fusion reactions, and loosely bound nuclei. Chapter 2 deals with the determination of barrier parameters of 13 numbers of reactions induced by ^6Li, ^7Li and ^9Be projectiles. For determination of the barrier parameters, we use 8 different versions of the nuclear proximity potential. The results are compared with experimental data, and a comparison of the potentials is also done in regard to their effectiveness in reproducing experimental data. In chapter 3 we investigate the fusion cross section for some reactions on the basis of the Wong's formula. A comparison with experimental fusion cross section is also done. We also present the complete theory of fusion cross section based upon the single barrier penetration model, and also the Wong's formula. Chapter 4 concerns the semiclassical model for the explanation of fusion suppression for the reactions ^{6}Li+^{144}Sm, ^{6}Li+^{209}Bi and ^{6}Li+^{152}Sm. We derive the classical equations of motion for the three systems. In the process, we

propose a model for the ^6Li nucleus through which we obtain the initial conditions of the differential equations [19]. Then, we define a breakup condition for a trajectory (projectile). Based upon this we propose a formula for explaination of fusion suppression, according to which fusion suppression is given by the average of the breakup fractions evaluated at impact parameters ranging from head-on collision up to the cutoff impact parameter. On application of the above formula, we discuss the results for the three systems. The relationship between the cutoff angular momentum (L_c), and the energy (E_{cm}) is also discussed. In chapter 5 we would be examining the reaction cross section induced by radioactive projectiles (^{6}He, ^{7}Be and ^{8}B). First, an explanation for the shift in the barrier parameters of radioactive halo systems with respect to normal loosely bound systems is provided, and this result is compared with the experimental shift obtained from reduced reaction cross section analysis. Next, the total reaction cross section of the reactions $^6He + {}^{27}Al$ and $^7Be + {}^{27}Al$ is explained in terms of the modified Wongs' formula (MWF). Finally, we give the conclusion in chapter 6. In each of the chapters 2, 3 and 4 we present an exhaustive review work concerning the determination of fusion barrier parameters, fusion cross section using Wong's formalism, and fusion suppression including projectile breakup, respectively.

Bibliography

[1] Bernard L. Cohen, *Concepts of Nuclear Physics*, Tata McGraw Hill (2004).

[2] R. R. Roy and B. P. Nigam, *Nuclear Physics*, New age International Limited (2011). ; Kenneth S. Krane, *Introductory Nuclear Physics*, Wiley-India Limited (2011).

[3] Ruprecht Machledt, article at www.scholarpedia.org/article /Nuclear_Forces.

[4] G. R. Satchler and W. G. Love, *Physics Reports*, **55**, 183, (1979)

[5] R.K. Puri and Raj K. Gupta, *Phys. Rev. C*, **45**, 1837, (1992) ; Raj Kumar, Manoj K. Sharma, and Raj K. Gupta, *Nucl. Phys. A*, **870-871**, 42-57, (2011)

[6] R. Bass, *Nuclear reactions with heavy ions*, Springer Verlag ; C. A. Bertulani and P. Danielewicz, *Introduction to nuclear reactions*, Institute of Physics Publishing (2004).

[7] M. Dasgupta, D. J. Hinde, N. Rowley and A. M. Stefanini, *Annu. Rev. Nucl. Part. Sci.*, **48**, 401, (1998) ; K. Hagino, Ph.D. thesis ; M. Beckerman, *Rep. Prog. Phys.*, **51**, 1047-1103 (1988).

[8] A. B. Balantekin, S. E. Koonin, and J. W. Negele, *Phys. Rev. C*, **28**, 1565, (1983).

[9] K. Hagino, N. Rowley and A.T. Kruppa, *Comp. Phys. Comm.*, **123**, 143, (1999).

[10] C. K. Phookan and K. Kalita, *Nucl. Phys. A*, **899**, 29, (2013).

[11] M. Dasgupta, P. R. S. Gomes, D. J. Hinde, S. B. Moraes, R. M. Anjos, A. C. Berriman, R. D. Butt, N. Carlin, J. Lubian, C. R. Morton, J. O. Newton, and A. Szanto de Toledo, *Phys. Rev. C*, **70**, 024606, (2004).

[12] J. S. Al-Khalili and J. A. Tostevin, *Phys. Rev. Lett* , **76**, 3903 (1996)

[13] J. J. Kolata and E. F. Aguilera, *Phys. Rev. C*, **79**, 027603 (2009)

[14] I. Tanihata, *Journal of Phys. G*, **22**, 157-198 (1996)

[15] F. Carstoiu, L. Trache, C. A. Gagliardi, R. E. Tribble and A. M. Mukhamedzhanov , *Phys. Rev. C*, **63**, 054310 (2001)

[16] P. K. Rath, S. Santra, N. L. Singh, K. Mahata, R. Palit, B. K. Nayak, K. Ramachandran, V. V. Parkar, R. Tripathi, S. K. Pandit, S. Appanababu, N. N. Deshmukh, R. K. Choudhury, and S. Kailas, *Nucl. Phys. A*, **874**, 14, (2012).

[17] P.K. Rath, S. Santra, N. L. Singh, R. Tripathi, V. V. Parkar, B. K. Nayak, K. Mahata, R. Palit, Suresh Kumar, S. Mukherjee, S. Appannababu, and R. K. Choudhury , *Phys. Rev. C*, **79**, 051601, (2009).

[18] M.K. Pradhan, A. Mukherjee, P.Basu, A. Goswami, R. Kshetri, Subinit Roy, P. Roy Chowdhury, and M. Saha Sarkar ,*Phys. Rev. C*, **83**, 064606, (2011).

[19] C. K. Phookan, K. Kalita, *Journal of Phys. G : Nucl. and Part. Phys.*, **40**, 125107, (2013).

[20] J. M. Figueira et al., *Phys. Rev. C*, **75**, 017602 (2007).

[21] M. Biswas et al., *Nucl. Phys. A*, **802**, 67 (2008).

[22] M. Zadro et al., *Phys. Rev. C*, **80**, 064610 (2009).

[23] L. Fimiani et al., *Phys. Rev. C*, **86**, 044607 (2012).

[24] H. Kumawat et al., *Phys. Rev. C*, **78**, 044617 (2008).

[25] N. N. Deshmukh et al., *Phys. Rev. C*, **83**, 024607 (2011).

[26] A. M. M. Maciel et al., *Phys. Rev. C*, **59**, 2103 (1999).

[27] J. M. Figueira et al., *Phys. Rev. C*, **81**, 024613 (2010).

[28] N. Keeley, S. J. Bennett, N. M. Clarke, B. R. Fulton, G. Tungate, P. V. Drumm, M. A. Nagarajan, and J. S. Lilley, *Nucl. Phys. A*, **571**, 326 (1994).

[29] S. Santra, S. Kailas, K. Ramachandran, V. V. Parkar, V. Jha, B. J. Roy, and P. Shukla, *Phys. Rev. C*, **83**, 034616 (2011).

[30] F. A. Souza et al., *Phys. Rev. C*, **75**, 044601 (2007).

[31] A. M. M. Maciel et al., *Phys. Rev. C*, **59**, 2103 (1999).

[32] N. Keeley, S. J. Bennett, N. M. Clarke, B. R. Fulton, G. Tungate, P. V. Drumm, M. A. Nagarajan, and J. S. Lilley, *Nucl. Phys. A*, **571**, 326 (1994).

[33] Shradha Dubey et al. , *Phys. Rev. C*, **89**, 014610 (2014).

[34] A. Gomez Camacho,P. R. S. Gomes, J. Lubian and I. Padron, *Phys. Rev. C*, **77**, 054606, (2008).

[35] N. Keeley, K. W. Kemper, and K. Rusek, *Phys. Rev. C*, **64**, 031602(R) (2001) ; S. K. Pandit, V. Jha, K. Mahata, S. Santra, C. S. Palshetkar, K. Ramachandran, V. V. Parkar, A. Shrivastava, H. Kumawat, B. J. Roy, et al., *Phys. Rev. C*, **84**, 031601(R) (2011).

[36] R. Rafiei, R. du Rietz, D. H. Luong, D. J. Hinde, M. Dasgupta, M. Evers, and A. Diaz-Torres, *Phys. Rev. C*, **81**, 024601, (2010).

[37] M. Dasgupta, L.R. Gasquez, D.H. Luong, R. du Rietz, R. Rafei, D. J. Hinde, C.J. Lin, M. Evers, A. Diaz-Torres, *Nucl. Phys. A*, **834**, 147c, (2010).

Chapter 2

Fusion barriers for reactions induced by loosely bound nuclei

2.1 Introduction

The total potential energy between two interacting nuclei is given by the sum of the nuclear and Coulomb potential energies. The Coulomb potential energy is inversely proportional to distance, and hence, shows a smooth variation with distance. On the other hand, the nuclear potential energy is effective at short distances (few fm) between the two nuclei. At distances just outside the overlapping region of the two nuclei (7-12 fm), the nuclear potential energy has an order of magnitude almost equal (but slightly less) as that of the Coulomb potential energy, but with the opposite sign. This unique coincidence gives rise to the Coulomb (or fusion) barrier, and a potential well immediately inside the barrier. Fusion between two nuclei takes place, when the projectile overcomes the Coulomb (or fusion) barrier and enters the potential well (Fig 2.1).

In this chapter, we shall focus on the determination of the fusion barrier parameters of reactions induced by loosely bound nuclei (^{6}Li, ^{7}Li and ^{9}Be). For determination of the fusion barriers, eight different versions of nuclear potentials are being

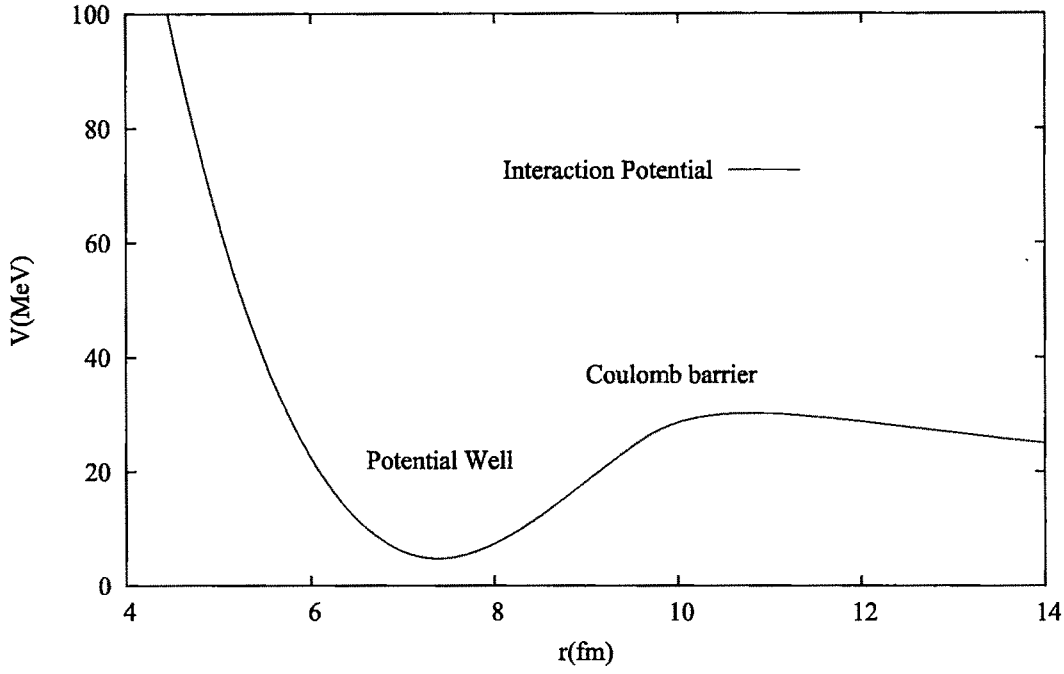

Figure 2.1: Total potential energy (MeV) between two nuclei vs distance (in fm).

used. The primary purpose of this exercise is to check the effectiveness of these nuclear potentials in reproducing the fusion barrier parameters. Secondly, these parameters are used for study of the fusion cross section of these reactions through the Wong's model (next chapter). Then, we check the validity of a parameterized formula connecting the barrier parameters. The above mentioned formula has also been tested for reactions induced by tightly bound projectiles. Lastly, we explain the large deviation of the barrier parameters of the reaction ^{6}Li+^{152}Sm in terms of the deformation of the target nucleus.

2.2 Review work on fusion barrier and nuclear potentials

The theoretical study of fusion barriers using global potentials has been done by a number of authors in the past. C. Ngo's group calculated the fusion barriers within the framework of the energy density formalism [1]. They proposed a graphical

method for the extraction of fusion barriers and found that experimental data is well reproduced up to $Z_1Z_2 \approx 2700$–2800. However, above this value, only an estimate was given, due to changes in the interaction energy curves. An improvement was made when the Fermi distribution of nuclear densities was used in the calculations [2]. Fl. Stancu and D.M. Brink used the Skyrme interaction density functional to study the interaction potential for several pairs of magic nuclei by taking into account exchange effects due to antisymmetrization [3]. An improvements over the previous results was noted when an approximation introduced by Kirzhnits and others for the kinetic energy density was included in the calculations [4]. In another study [5], L. C. Vaz and J. M. Alexander used the proximity potential for analysing the fusion cross section and the fusion barrier parameters of 48 pairs of colliding nuclei. They found that excellent fitting of the experimental data could be obtained by slight variation of the parameters (R, b and γ) of the proximity potential.

Next, the Panjab University group under R. K. Puri and Raj K. Gupta has made substantial contribution to the study of interaction potential and fusion barriers using a variety of nuclear potentials. In 1992 [6], they used the Skyrme interaction energy-density model to determine the fusion barrier parameters for light systems (each nucleus, $Z \leq 40$, and $A \leq 90$). They found that the calculated barrier heights lie within ± 1 MeV of the empirical estimates. Spin density effects were also studied, and it was found that such effects increased the barrier heights by ≈ 1 MeV, and shifted the barriers inside by 0.1–0.2 fm. More recently, they made a detailed study of light as well as heavy systems using as many as 12 different versions of the nuclear potential. They found that for symmetric colliding nuclei, the potentials could reproduce the experimental data, on average, within 8% [8] and for asymmetric colliding nuclei to within 10% [7]. In another study, they analysed the effects of various versions of the surface energy coefficients of the proximity potential on the fusion barriers. It was concluded that surface energy coefficients γ-MN 1976 and γ-MN 1995 may be better choices for studying fusion barriers [9]. Some Chinese

workers are also active in this field of study. C. L. Guo et al. [10], calculated the nuclear potential for symmetric systems by using the double folding model with density dependent NN interaction. They also obtained a Universal function of the proximity potential around the Coulomb barrier position by a parametric fitting of a simple Woods-Saxon type function. Using the Universal function they found that the fusion barrier parameters are reproduced satisfactorily for the systems studied.

We shall be using the same potentials that has been used by the Panjab University group in determining the fusion barrier parameters of reactions induced by loosely bound projectile. Also, we retain the same nomenclature in naming the potentials. The nuclear potentials are the two versions of the proximity potential (Prox 77 and Prox 88), three versions of the Bass potential (Bass 73, Bass 77 and Bass 80), the Christensen and Winther potential (CW 76), the Broglia and Winther potential (BW 91), and the Aage Winther potential (AW 95). Besides the study of fusion barriers, these potentials have been successfully used by the Panjab University group for the study of cluster radioactivity [11]. Cluster or heavy-ion radioactivity is an intermediate process between alpha decay and nuclear fission, where clusters heavier than alpha particles but lighter than fission fragments are produced. According to the preformed cluster model (PCM), the clusters are preborn in the parent nucleus with preformation probability P_0, hit the barrier with impinging frequency ν_0, and penetrate it with transmission coefficient P. The form of the nuclear potential comes into play in the determination of the barrier, and hence in the determination of the transmission coefficients by the WKB method. It was observed that the proximity potentials could reproduce the experimental half lives very well. Besides, the potentials Bass 80, CW 76 and BW 91 were found to be equally useful for the study of cluster dynamics.

In particular, the proximity potential has been used by a number of authors for studying a variety of phenomena. K. P. Santosh of Kannur University had used the potential for the study of fusion excitation functions and barrier distributions

for the fusion of ^{12}C, ^{16}O, ^{28}Si, and ^{35}Cl on ^{92}Zr target [12]. Then he used it for the study of α-decay of nuclei in the range $67 \leq Z \leq 91$ [13], as well as in the super-heavy region ($^{271-294}115$, $^{293,294}117$) [14, 15]. Also, he had used the above potential for working out a semi-empirical formula for spontaneous fission half life for nuclei in the mass range of ^{232}Th and $^{286}114$ [16]. Using the proximity potential in the Wong formula, Raj Kumar et al. had studied the capture cross-section data from $^{48}Ca+^{238}U$, $^{48}Ca+^{244}Pu$, and $^{48}Ca+^{248}Cm$ reactions in the super-heavy mass region, and also the fusion-evaporation cross section for the reactions $^{58}Ni+^{58}Ni$, $^{64}Ni+^{64}Ni$, and $^{64}Ni+^{100}Mo$, respectively [17].

2.3 Experimental determination of fusion barrier

The study of the fusion barrier (or Coulomb barrier) is very important, because it reveals a lot of information about the nucleus-nucleus interaction and also about the fusion mechanism. More recently, synthesis of super-heavy elements is a hot topic of research for which knowledge of the fusion barrier is crucial. Experimentally, the fusion barrier cannot be extracted by direct methods. It is indirectly obtained from analysis of precisely measured fusion cross section data. For energies greater than the fusion barrier, the extraction of the fusion barrier can be done from a fitting of the measured fusion cross section (σ) with Wong's formula (see chapter 3) [18],

$$\sigma = \frac{R_b^2 \hbar\omega_0}{2E} ln\Big\{1 + exp\Big[\frac{2\pi(E - E_0)}{\hbar\omega_0}\Big]\Big\} \tag{2.1}$$

where, $\hbar\omega_0$ is the curvature of the fusion barrier (ℓ=0). E_0 and R_B are the height and position of the fusion barrier, respectively, and E is the energy in the centre-of-mass frame. In a nutshell, V_B, R_B and $\hbar\omega_0$ are known as the barrier parameters. For energies (E) much above the barrier (E_0), the above formula reduces to the classical

equation for touching collision between spheres,

$$\sigma = \pi R_b^2 \left(1 - \frac{E_0}{E}\right) \tag{2.2}$$

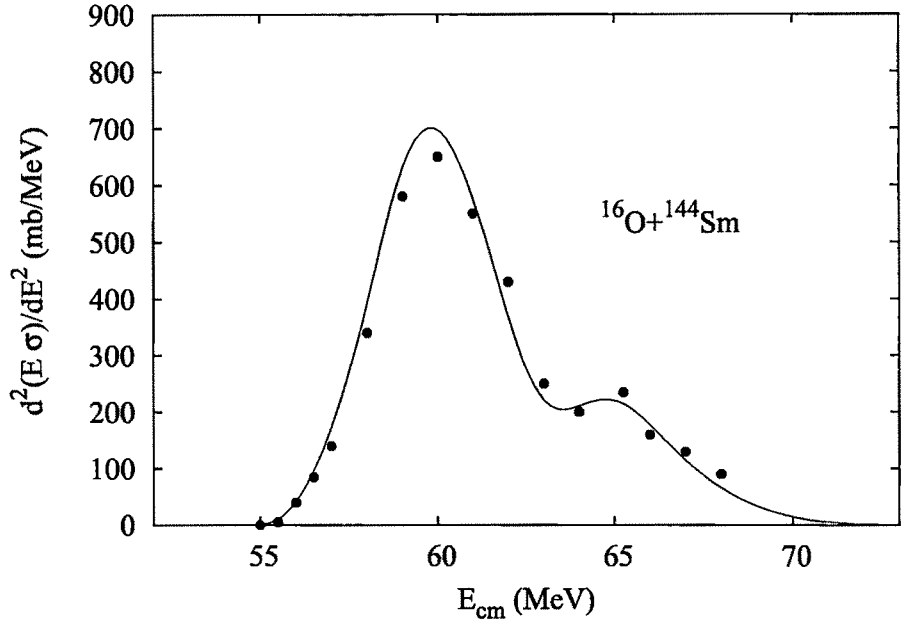

Figure 2.2: Diagram showing experimental and theoretical $d^2(E\sigma)/dE^2$ vs E_{cm}. Dots represent the experimental barrier distribution, whereas line represents the theoretical barrier distribution [19].

The most widely followed procedure is Rowley's method [19]. Rowley proposed in 1991 that the distribution of barriers could be extracted directly by taking the second derivative of the quantity (σE) with respect to E. Experimentally, it is obtained from a point-difference formula. At energy, E=$(E_1 + 2E_2 + E_3)/4$, it is given by,

$$\frac{d^2(E\sigma)}{dE^2} = 2\left(\frac{(E\sigma)_3 - (E\sigma)_2}{E_3 - E_2} - \frac{(E\sigma)_2 - (E\sigma)_1}{E_2 - E_1}\right)\left(\frac{1}{E_3 - E_1}\right) \tag{2.3}$$

for, equal energy steps, $\triangle E = E_2 - E_1 = E_3 - E_2$, we get,

$$D_{exp} = \frac{d^2(E\sigma)}{dE^2} = \frac{(E\sigma)_3 - 2(E\sigma)_2 - (E\sigma)_1}{\triangle E^2} \tag{2.4}$$

When, D_{exp} is plotted against energy (E), a distribution of barriers is obtained. The fusion (Coulomb) barrier corresponds to the prominent peak of the distribution. The above formula will only work if fusion cross section (σ) is evaluated at small intervals of energy (E). In Fig. 2.2 we have shown the experimental (dots) and the theoretical fusion barrier distribution (line) for the reaction $^{16}O+^{144}Sm$ as a function of the centre of mass energy (E_{cm}) [19]. The fusion barrier (occuring around 60 MeV) is clearly seen. A second resolved bump occurs because of the coupling to the target phonon states. Some other methods have also been proposed for extraction of fusion barrier parameters from fusion cross section.

2.4 Methodology for finding fusion barrier

The interaction potential between the target nucleus and the projectile can be written as the sum of nuclear, Coulomb and centrifugal potentials. Hence,

$$V = V_C(r) + V_N(r) + \frac{\hbar^2 l(l+1)}{2\mu r^2} \tag{2.5}$$

where, r is the distance between the centres of the target and projectile, l is the angular momentum quantum number, and μ is the reduced mass of the system. Assuming the size of the projectile to be much smaller than the radius of the target nucleus, r_c, the Coulomb potential V_C(r) can be approximated by the relation,

$$V_C = \begin{cases} \frac{Z_1 Z_2 e^2}{2r_c}\left(3 - \frac{r^2}{r_c^2}\right) & \text{if } r \leq r_c, \\ \frac{Z_1 Z_2 e^2}{r} & \text{if } r > r_c \end{cases} \tag{2.6}$$

where Z_1, Z_2 are the atomic numbers of the target and projectile. For ℓ=0 the maximum or peak value of the potential V is called the fusion barrier (or Coulomb barrier). The respective values of V and r are called the height (V_B) and position (R_B) of the fusion barrier. For V_N(r) we have used a total of eight different types

of nuclear potentials which are briefly discussed in the next section. In naming the potentials we have retained the same nomenclature as in Ref. [7].

Ideally, the fusion barrier heights and positions for the different potentials mentioned can be determined by applying the rules of calculus to the potential in Eq. (2.5),

$$\left.\frac{dV(r)}{dr}\right|_{r=R_b} = 0 \qquad and \qquad \left.\frac{d^2V(r)}{dr^2}\right|_{r=R_b} \leq 0 \tag{2.7}$$

However, the derivatives may become too complicated for a few of the nuclear potentials. An easier option is to obtain the potential (V) against distance (r) at small intervals of the distance (Δr=0.01 fm). Studying the output, V_B and R_B are easily obtained upto sufficient accuracy level. All calculations are done in the Fortran programming language.

2.5 Nuclear potentials

In recent years, a large number of nuclear models depending upon a variety of assumptions have been proposed. As many as two dozen potentials and their different versions are available in the literature. For the purpose of finding the fusion barrier we had chosen eight versions of commonly used nuclear proximity potentials. We have used these potentials in particular because earlier studies have shown that these potentials are reliable and effective for the study of fusion barriers [7, 8]. Moreover, the barrier parameters could be accurately determined with the minimum number of parameters. These potentials are described below :

2.5.1 Proximity 1977 (Prox 77)

The nuclear potential of Blocki [20] has its origin on the fact that the force between two bodies in close proximity is directly proportional to the interaction potential per unit area between two flat surfaces made of the same material and the mean

curvature of the two bodies provided the curvature is small. It leads to a formula for the interaction potential between two curved objects (eg., two atomic nuclei) which is the product of a universal function and a simple geometrical factor, characteristic of the material of which the objects are made. The potential is given by,

$$V_N(r) = 4\pi\gamma b\left[\frac{C_1C_2}{C_1+C_2}\right]\Phi\left(\frac{r-C_1-C_2}{b}\right) \text{ MeV} \tag{2.8}$$

where C_1, C_2 are the Sussmann central radius [21, 22] of the target and projectile, and is related to the sharp radius R_i as,

$$C_i = R_i - \frac{b^2}{R_i} \tag{2.9}$$

Here, b $\approx$ 1 fm, and R_i is given by the semi-empirical formula in terms of the mass number A_i,

$$R_i = 1.28A_i^{1/3} + 0.8A_i^{-1/3} - 0.76 \quad \text{fm} \quad (i = 1, 2) \tag{2.10}$$

The nuclear surface tension coefficient γ is given by

$$\gamma = \gamma_0\left[1 - k_s\frac{(N-Z)^2}{(N+Z)^2}\right] \tag{2.11}$$

where, N and Z are respectively the total number of neutrons and protons. γ_0 and k_s are respectively the surface energy constant and the surface asymmetry constant. Their values are given by the Myers-Swiatecki mass formula [23, 24] and are γ_0=0.9517 MeV/fm^2 and k_s=1.7826, respectively. The universal proximity function $\Phi(\xi)$ can be obtained using the nuclear Thomas-Fermi model with Seyler-Blanchard phenomenological nucleon-nucleon interaction [25, 26, 27]. For practical applications one uses a simple analytical representation of the function $\Phi(\xi)$. One such

approximation is given by the following "cubic exponential" pocket formula [20, 28],

$$\Phi(\xi) = \begin{cases} -\frac{1}{2}(\xi - 2.54)^2 - 0.0852(\xi - 2.54)^3 & \text{if } \xi \leq 1.2511, \\ -3.437exp(-\xi/0.75) & \text{if } \xi \geq 1.2511. \end{cases} \tag{2.12}$$

2.5.2 Proximity 1988 (Prox 88)

Based upon a refined mass formula, the value of the co-efficients γ_0 and k_s were later on modified by Moller and Nix [29] to the new set of values 1.2496 MeV/fm^2 and 2.3, respectively. In this model, the mass excess is given by the sum of a macroscopic and a microscopic term. The macroscopic part contains a term due to surface energy which is dependent upon the nuclear surface tension coefficient given by Eq. (2.11). All the constants appearing in the macroscopic term were determined by selective consideration of experimental data. The co-efficients γ_0 and k_s were determined from the experimental fission-barrier heights because fission-barrier heights are particularly sensitive to these constants.

2.5.3 Bass 1973 (Bass 73)

Based on the classical liquid drop model, Bass [30, 31] gave an expression of the nuclear potential. In this model, the surface energy of two spheres having half-density radii R_1 and R_2 is given by,

$$E_s = \gamma\Big[S_1 + S_2 - \frac{4\pi d R_1 R_2}{R_1 + R_2}\exp\Big(\frac{-s}{d}\Big)\Big] \tag{2.13}$$

where S_1 and S_2 are the surface areas of the two spheres, s is the distance between the nuclear surfaces, γ is the specific surface energy and d is the range parameter. The nuclear potential is now obtained as the difference in surface energies for infinite and finite separation s(= r$-R_{12}$).

It is given by ,

$$V_N(r) = -\frac{d}{R_{12}} a_s A_1^{1/3} A_2^{1/3} \exp\Big(-\frac{r - R_{12}}{d}\Big) \text{ MeV} \tag{2.14}$$

with $R_{12} = r_0(A_1^{1/3}+A_2^{1/3})$, $r_0 = 1.07$ fm, and $a_s = 4\pi\gamma r_0^2 = 17.0$ MeV. The value of d is obtained after fitting experimental fusion barrier and is given by 1.35 fm.

2.5.4 Bass 1977 (Bass 77)

It can be shown by use of the liquid-drop model and general geometrical arguments that the nuclear potential can be written as [30, 31, 32, 33],

$$V_N(r) = -\frac{R_1 R_2}{R_1 + R_2} \Phi(r - R_1 - R_2) \text{ MeV} \tag{2.15}$$

where, R_i is given as

$$R_i = 1.16A_i^{1/3} - 1.39A_i^{-1/3} \text{ fm} \tag{2.16}$$

Using the available data for fusion-cross section, Bass determined the experimental points for the function Φ(s) [33]. He found that the data can be fitted by an empirical function of the form,

$$\Phi(s) = \Big[A\exp\Big(\frac{s}{d_1}\Big) + B\exp\Big(\frac{s}{d_2}\Big)\Big]^{-1} \tag{2.17}$$

with A=0.03 MeV^{-1}fm, B=0.0061 MeV^{-1}fm, d_1=3.30 fm, and d_2=0.65 fm.

2.5.5 Bass 1980 (Bass 80)

Later Bass slightly modified the empirical function and also the radius parameter [23]. Here, Φ(s) is now given as,

$$\Phi(s) = \Big[0.033\exp\Big(\frac{s}{3.5}\Big) + 0.007\exp\Big(\frac{s}{0.65}\Big)\Big]^{-1} \tag{2.18}$$

where s= r - R_1 - R_2 (fm) measures the separation between the half-density surfaces of the interacting nuclei.

Central radius R_i is given as,

$$R_i = R_{si}\left(1 - \frac{0.98}{R_{si}^2}\right) \tag{2.19}$$

where R_{si} is given as,

$$R_{si} = 1.28A_i^{1/3} - 0.76 + 0.8A_i^{-1/3} \text{ fm} \tag{2.20}$$

2.5.6 Christensen and Winther 1976 (CW 76)

Christensen and Winther [34] derived the nucleus-nucleus interaction potential by analysing the heavy-ion elastic scattering data, based on the semiclassical arguments and the recognition that optical-model analysis of elastic scattering determines the real part of the interaction potential only in the vicinity of a characteristic distance. The potential has been tested for more than 60 reactions, and is given by,

$$V_N(r) = -50\frac{R_1 R_2}{R_1 + R_2}\Phi(r - R_1 - R_2) \text{ MeV} \tag{2.21}$$

The radius parameter is given as,

$$R_i = 1.233A_i^{1/3} - 0.978A_i^{-1/3} \text{ fm} \tag{2.22}$$

and the Universal function Φ(s) has the following form,

$$\Phi(s) = \exp\left(-\frac{r - R_1 - R_2}{0.63}\right) \tag{2.23}$$

2.5.7 Broglia and Winther 1991 (BW 91)

Broglia and Winther gave a Woods-Saxon parametrization of the nuclear potential from a knowledge of the densities of the colliding nuclei and an effective two-body force [23, 35, 36]. The potential is given by,

$$V_N(r) = -\frac{V_0}{1+\exp(\frac{r-R_0}{0.63})} \text{ MeV} \tag{2.24}$$

with,

$$V_0 = 16\pi\frac{R_1R_2}{R_1+R_2}\gamma a \tag{2.25}$$

Here, a=0.63 fm, and

$$R_0 = R_1 + R_2 + 0.29 \tag{2.26}$$

Radius, R_i is given by,

$$R_i = 1.233A_i^{1/3} - 0.98A_i^{-1/3} \text{ fm} \tag{2.27}$$

And, the surface energy co-efficient γ is given by,

$$\gamma = \gamma_0\Big[1 - k_s\Big(\frac{N_p - Z_p}{A_p}\Big)\Big(\frac{N_t - Z_t}{A_t}\Big)\Big] \tag{2.28}$$

where, γ_0=0.95 MeV/fm^2 and k_s=1.8. The subscripts 'p' and 't' refer to the projectile and target. The second term takes into account the mass asymmetry of the reaction. The parametrization has been constructed such that the force

$$-\frac{\delta V_N}{\delta r} = -\frac{V_0}{4(0.63)}cosh^{-2}(\frac{r-R_0}{1.26}) \tag{2.29}$$

has its maximum at r=R_0 and is equal to the maximum force predicted by the potential Prox 77.

2.5.8 Aage Winther 1995 (AW 95)

The parameters of the above potential were slightly refined by Winther [37] after an extensive comparison with experimental data for heavy-ion elastic scattering. The refined values of a and R_i are,

$$a = \left[\frac{1}{1.17(1+0.53(A_1^{-1/3}+A_2^{-1/3}))}\right] \text{ fm} \tag{2.30}$$

and,

$$R_i = 1.20A_i^{1/3} - 0.09 \text{ fm} \tag{2.31}$$

Here, R_0=R_1+R_2 only. The magnitude of the potential is given by,

$$V_N(r) = -\frac{V_0}{1+\exp(\frac{r-R_0}{0.63})} \text{ MeV} \tag{2.32}$$

with,

$$V_0 = 16\pi\frac{R_1R_2}{R_1+R_2}\gamma a \tag{2.33}$$

where, γ is given by Eq. (2.28).

2.6 Nature of the potentials

The interaction potential using the above nuclear potentials are shown in Figs. 2.3 and 2.4 for the reactions ^{6}Li+^{209}Bi, ^{7}Li+^{159}Tb and ^{9}Be+^{208}Pb [18]. As we had used a linear scale for the potential (y-axis) and since there is large variation of the potential at r $\leq R_B$, hence we have adjusted the distance (x-axis) so that the shape of the potential could be studied. The fusion barrier (Coulomb barrier) is shown by the peak of the potential. Apart from CW 76, the barrier is distinct for all the other nuclear models. At distances greater than the barrier radius (r > R_B), the force is repulsive because the Coulomb potential is dominant and the nuclear force is negligible. In the region immediately inside the barrier radius (r < R_B), the force

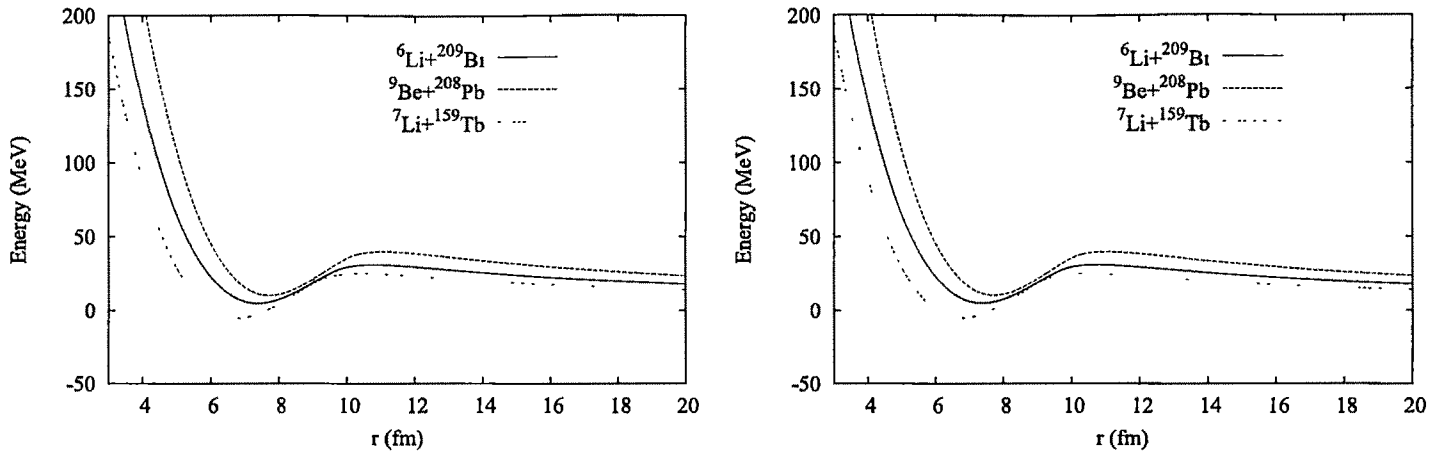

(a) Prox 77

(b) Prox 88

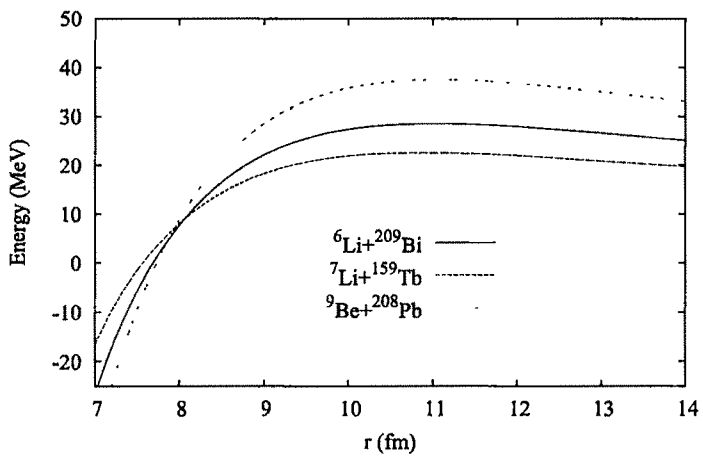

(c) Bass 73

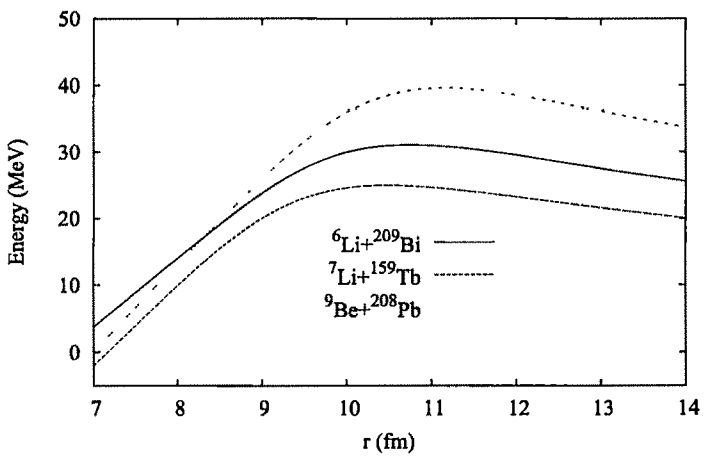

(d) Bass 77

Figure 2.3: Interaction potential for ^{6}Li+^{209}Bi, ^{7}Li+^{159}Tb and ^{9}Be+^{208}Pb for the potentials Prox 77, Prox 88, Bass 73 and Bass 77.

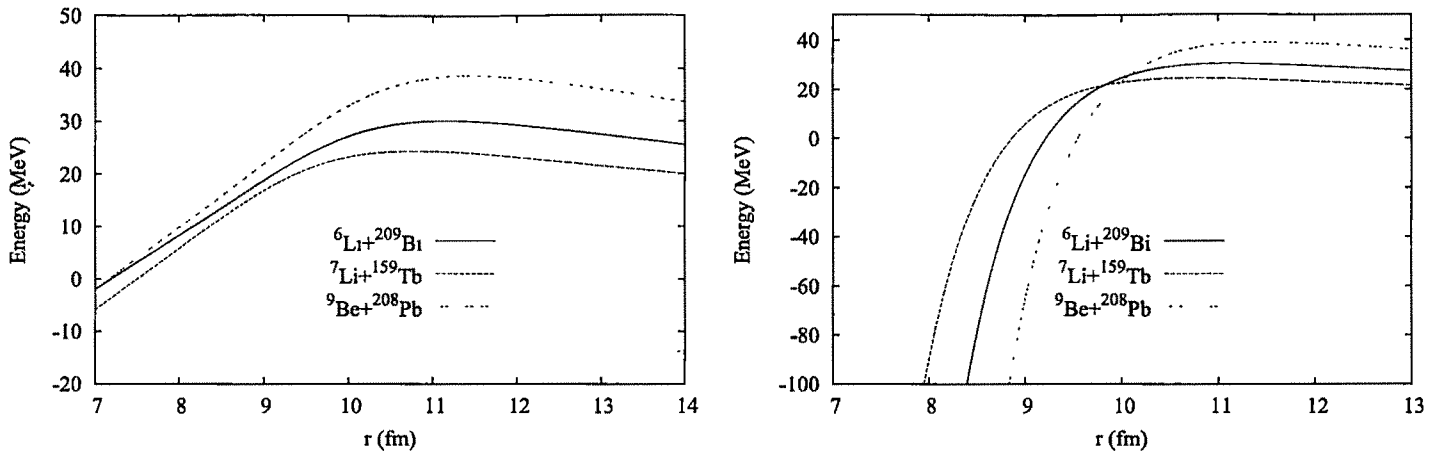

(a) Bass 80

(b) CW 76

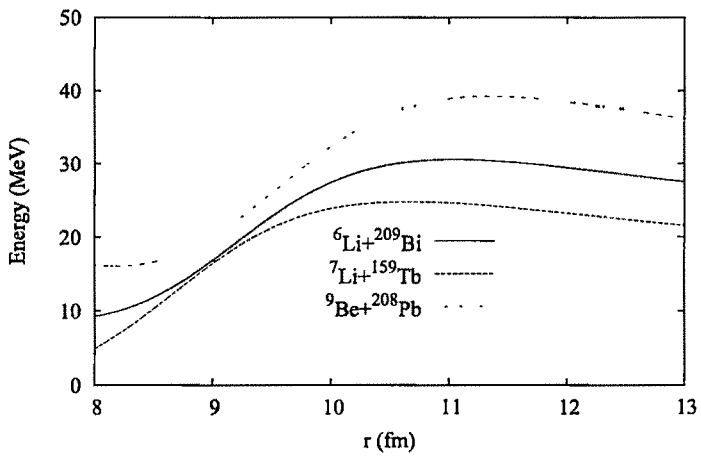

(c) BW 91

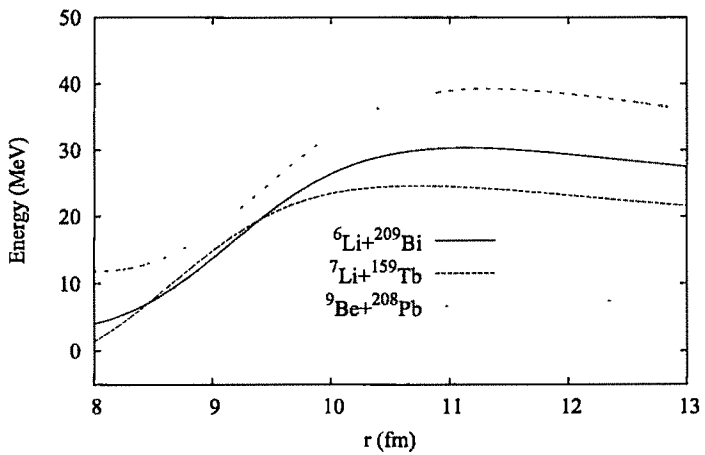

(d) AW 95

Figure 2.4: Interaction potential for ^{6}Li+^{209}Bi, ^{7}Li+^{159}Tb and ^{9}Be+^{208}Pb for the potentials Bass 80, CW 76, BW 91 and AW 95.

is attractive because the nuclear potential dominates the Coulomb potential. For the proximity potentials (Prox 77 and Prox 88), a distinct potential pocket exists because the force turns repulsive at smaller distances (r < 6 fm).

2.7 Results and Discussion

Our present study is conducted on a total of 13 reactions induced by loosely bound projectiles, namely, ^{6}Li, ^{7}Li and ^{9}Be. The reactions considered are : ^{6}Li+^{64}Zn, ^{6}Li+^{159}Tb, ^{6}Li+^{144}Sm, ^{6}Li+^{152}Sm, ^{6}Li+^{208}Pb, ^{6}Li+^{209}Bi, ^{7}Li+^{159}Tb, ^{7}Li+^{209}Bi, ^{9}Be+^{208}Pb, ^{9}Be+^{124}Sn, ^{9}Be+^{89}Y, ^{9}Be+^{144}Sm and ^{9}Be+^{209}Bi. All nuclei are considered to be spherical, except ^{152}Sm, for which both spherical and deformed cases (section 2.8) are considered. We find the height (V_B) and position (R_B) of the fusion barrier as explained in section 2.4. The results are shown in Tables 2.1 and 2.3 [18]. The results are compared with the empirical values of the heights and positions of the fusion barriers obtained from the literature.

The procedure for obtaining the empirical values of the fusion barriers needs to be briefly highlighted. Apart from the reaction ^{6}Li+^{64}Zn, V_B and R_B are obtained from analysis of fusion reaction data. For ^{6}Li+^{64}Zn, only V_B is obtained from analysis of elastic scattering data. Using the best fit parameters for the optical model, the maximum of the real nuclear plus Coulomb potential is extracted to give the value of V_B. For the other reactions, V_B is extracted from the peak of the barrier distribution (section 2.3). The standard procedure for obtaining R_B is through a fitting of the fusion cross section data by the fusion code CCFULL [38]. Then, R_B is obtained from the output of the CCFULL code. The parameters for the input nuclear Woods-Saxon potential are obtained by trial and error. For a few of the reactions R_B has not been reported, and we determine them by running the CCFULL code [38]. The parameters of the Woods-Saxon potential needed for the program are given as : ^{9}Be+^{144}Sm (V_0=140 MeV, r_0=1.06 fm, a=0.71 fm) [39],

Table 2.1: Fusion barrier heights (in MeV) and positions (in fm) using the potentials Prox 77, Prox 88 and Bass 73. The corresponding experimental values are also indicated.

Reaction	Prox 77		Prox 88		Bass 73		Empirical			Ref.
	V_B	R_B	V_B	R_B	V_B	R_B	V_B	R_B^{CC}	R_B^{par}	
$^{6}Li+^{64}Zn$	13.91	8.49	13.56	8.73	11.33	9.87	13.22	-	8.98	[42]
$^{6}Li+^{159}Tb$	25.97	10.01	25.44	10.23	22.98	10.67	24.48	10.53	10.66	[43]
$^{6}Li+^{144}Sm$	25.26	9.79	24.72	10.02	22.25	10.49	24.65	10.20	10.06	[44]
$^{6}Li+^{152}Sm$	24.96	9.92	24.46	10.14	21.99	10.63	25.10	9.98	9.86	[40]
$^{6}Li+^{208}Pb$	31.17	10.56	30.59	10.78	28.21	11.02	30.10	11.00	10.96	[45]
$^{6}Li+^{209}Bi$	31.53	10.57	30.94	10.78	28.58	11.00	30.10	11.24	11.11	[41]
$^{7}Li+^{159}Tb$	25.50	10.20	25.00	10.42	22.61	10.88	23.81	11.03	10.99	[46]
$^{7}Li+^{209}Bi$	30.99	10.76	30.42	10.98	28.12	11.21	29.70	11.40	11.27	[41]
$^{9}Be+^{208}Pb$	40.53	10.85	39.80	11.06	37.50	11.06	38.10	11.66	11.55	[41]
$^{9}Be+^{124}Sn$	27.02	9.85	26.47	10.07	23.86	10.52	25.87	10.25	10.32	[47]
$^{9}Be+^{89}Y$	22.26	9.27	21.76	9.51	19.17	10.16	21.60	9.63	9.59	[48]
$^{9}Be+^{144}Sm$	32.79	10.08	32.11	10.31	29.58	10.52	31.20	10.68	10.64	[39]
$^{9}Be+^{209}Bi$	41.00	10.85	40.25	11.07	37.98	11.05	39.40	11.30	11.33	[49]

Table 2.2: Percentage deviations of the theoretical values of V_B and R_B from the empirical values for the potentials Prox 77, Prox 88, Bass 73, Bass 77.

Reaction	Prox 77		Prox 88		Bass 73		Bass 77	
	ΔV_B	ΔR_B	ΔV_B	ΔR_B	ΔV_B	ΔR_B	ΔV_B	ΔR_B
$^{6}Li+^{64}Zn$	5.24	-	2.56	-	-14.29	-	2.53	-
$^{6}Li+^{159}Tb$	6.09	-4.94	3.93	-2.85	-6.12	1.33	4.22	-2.85
$^{6}Li+^{144}Sm$	4.34	-4.02	2.42	-1.76	-5.32	2.84	2.49	-1.76
$^{6}Li+^{152}Sm$	-0.54	-0.57	-2.57	1.63	-12.40	6.55	-2.37	1.73
$^{6}Li+^{208}Pb$	3.55	-4.00	1.63	-2.00	-6.28	0.18	2.06	-2.36
$^{6}Li+^{209}Bi$	4.73	-5.96	2.78	-4.09	-5.06	-2.06	3.29	-4.39
$^{7}Li+^{159}Tb$	2.47	-7.53	0.28	-5.53	-9.74	-1.36	0.69	-4.99
$^{7}Li+^{209}Bi$	7.10	-5.61	5.00	-3.68	-5.04	-1.67	4.83	-3.51
$^{9}Be+^{208}Pb$	5.96	1.63	4.05	-5.15	-1.96	-5.17	3.52	-4.43
$^{9}Be+^{124}Sn$	4.46	-3.95	2.33	-1.81	-7.78	2.66	1.19	-0.15
$^{9}Be+^{89}Y$	3.06	-3.70	0.73	-1.21	-11.23	5.48	-0.39	0.50
$^{9}Be+^{144}Sm$	5.10	-5.62	2.92	-3.46	-5.19	-1.50	2.28	-2.53
$^{9}Be+^{209}Bi$	4.06	-3.98	2.16	-2.03	-3.60	-2.21	1.70	-1.33

Table 2.3: Fusion barrier heights (in MeV) and positions (in fm) using the potentials Bass 77, Bass 80, CW 76, BW 91 and AW 95.

Reaction	Bass 77		Bass 80		CW 76		BW 91		AW 95	
	V_B	R_B	V_B	R_B	V_B	R_B	V_B	R_B	V_B	R_B
$^{6}Li+^{64}Zn$	13.55	8.80	13.22	9.05	13.41	8.99	13.49	8.91	13.19	9.13
$^{6}Li+^{159}Tb$	25.51	10.23	24.74	10.58	24.99	10.57	25.14	10.47	24.89	10.58
$^{6}Li+^{144}Sm$	24.82	10.02	24.08	10.35	24.33	10.34	24.48	10.23	24.20	10.37
$^{6}Li+^{152}Sm$	24.51	10.15	23.77	10.50	24.02	10.48	24.16	10.38	23.91	10.51
$^{6}Li+^{208}Pb$	30.72	10.74	29.72	11.35	30.00	11.13	30.17	11.03	29.97	11.12
$^{6}Li+^{209}Bi$	31.09	10.75	30.07	11.15	30.36	11.14	30.54	11.04	30.33	11.13
$^{7}Li+^{159}Tb$	24.96	10.48	24.33	10.78	24.54	10.78	24.74	10.65	24.60	10.72
$^{7}Li+^{209}Bi$	30.44	11.00	29.59	11.35	29.83	11.35	30.08	11.22	30.00	11.26
$^{9}Be+^{208}Pb$	39.60	11.14	38.70	11.43	38.85	11.49	39.18	11.35	39.27	11.33
$^{9}Be+^{124}Sn$	26.18	10.24	25.72	10.43	25.85	10.47	26.07	10.35	26.00	10.38
$^{9}Be+^{89}Y$	21.52	9.68	21.2	9.84	21.32	9.87	21.48	9.76	21.34	9.83
$^{9}Be+^{144}Sm$	31.91	10.41	31.31	10.64	31.43	10.69	31.67	10.57	31.64	10.59
$^{9}Be+^{209}Bi$	40.07	11.15	39.16	11.43	39.31	11.49	39.64	11.35	39.73	11.33

Table 2.4: Percentage deviations of the theoretical values of V_B and R_B from the empirical values for the potentials Bass 80, CW 76, BW 91 and AW 95.

Reaction	Bass 80		CW 76		BW 91		AW 95	
	ΔV_B	ΔR_B	ΔV_B	ΔR_B	ΔV_B	ΔR_B	ΔV_B	ΔR_B
$^{6}Li+^{64}Zn$	0.023	-	1.43	-	2.03	-	-0.22	-
$^{6}Li+^{159}Tb$	1.07	0.48	-6.07	0.38	2.70	-0.47	1.68	0.47
$^{6}Li+^{144}Sm$	-0.37	1.47	0.44	1.37	1.28	0.29	1.01	1.67
$^{6}Li+^{152}Sm$	-5.28	5.21	-4.30	5.00	-3.74	4.05	-4.74	5.28
$^{6}Li+^{208}Pb$	-1.26	1.36	-0.33	1.18	0.23	0.27	-0.43	1.09
$^{6}Li+^{209}Bi$	-0.10	-0.79	0.86	-0.87	1.45	-1.80	0.75	-1.02
$^{7}Li+^{159}Tb$	-2.31	-2.27	-1.30	-2.27	-0.69	-3.45	-1.83	-2.81
$^{7}Li+^{209}Bi$	2.18	-0.44	3.07	-0.44	3.91	-1.58	3.32	-1.23
$^{9}Be+^{208}Pb$	1.17	-1.98	1.56	-1.45	2.43	-2.67	2.66	-2.87
$^{9}Be+^{124}Sn$	-0.56	1.79	-0.07	2.15	0.76	0.96	0.49	1.29
$^{9}Be+^{89}Y$	-1.85	2.16	-1.31	2.44	-0.55	1.33	-1.20	2.08
$^{9}Be+^{144}Sm$	0.35	-0.38	0.74	0.09	1.51	-1.03	1.41	-0.85
$^{9}Be+^{209}Bi$	-0.61	1.15	-0.23	1.68	0.61	0.44	0.84	0.26

^{6}Li+^{152}Sm (V_0=131 MeV, r_0=1.01 fm, a=0.64 fm) [40], ^{6}Li+^{209}Bi (V_0=107 MeV, r_0=1.12 fm, a=0.63 fm), ^{7}Li+^{209}Bi (V_0=113 MeV, r_0=1.12 fm, a=0.63 fm), and ^{9}Be+^{208}Pb (V_0=198 MeV, r_0=1.10 fm, a=0.63 fm) [41]. We find that in general the agreement between the calculated barrier parameters and the empirical barrier parameters is quite satisfactory for all the potentials. However, there is marginal variation from potential to potential which has also been investigated.

There is a well known parametrized formula [50, 51, 52] which connects the height (V_B) and the position (R_B) of the Coulomb barrier. The formula has been tested for a large number of reactions induced by tightly bound projectiles. Here, we would like to test the validity of the formula for reactions induced by loosely bound projectiles. The parameterized formula is given as,

$$V_B^{par} = \frac{1.44 Z_1 Z_2}{R_B^{par}} \left(1 - \frac{0.75}{R_B^{par}}\right) \tag{2.34}$$

On the last column of Table 2.1, the parametrized value of the position of the Coulomb barrier (R_B^{par}) is evaluated. We use the following formula where V_B is the empirical value of the height of the barrier,

$$R_B^{par} = \frac{1.44 Z_1 Z_2 + \sqrt{2.0736 Z_1^2 Z_2^2 - 4.32 V_B Z_1 Z_2}}{2 V_B} \tag{2.35}$$

We note that the agreement between the empirical value of the position of the barrier (R_B^{CC}) and the parametrized value (R_B^{par}) is very good. The effectiveness of the parametrized formula in reproducing the value of R_B can be checked by finding the standard deviation ($\sigma_{R_B^{par}}$) of the parametrized value (R_B^{par}) with respect to the experimental value (R_B^{CC}). Hence, $\sigma_{R_B^{par}}$ is given by,

$$\sigma_{R_B^{par}} = \sqrt{\frac{\sum_{i=1}^{i=N} \left[\Delta R_B^{par}\right]^2}{N}} \tag{2.36}$$

where, ΔR_B^{par} is given by,

$$\Delta R_B^{par} = \frac{R_B^{par} - R_B^{CC}}{R_B^{CC}} \times 100 \tag{2.37}$$

The value of $\sigma_{R_B^{par}}$ comes out to be 0.89 %, which proves that the parametrized formula can reproduce the value of R_B within 1 % of the true value. This shows that the empirical formula connecting V_B and R_B is extremely effective for reactions induced by loosely bound projectiles.

In order to compare the predictions of the different potentials we compute the standard deviation (σ_{V_B} and σ_{R_B}) of the theoretical values over the experimental values for the barrier height and the position. These are given by,

$$\sigma_{V_B} = \sqrt{\frac{\sum_{i=1}^{i=N} \left[\Delta V_B\right]^2}{N}} \tag{2.38}$$

$$\sigma_{R_B} = \sqrt{\frac{\sum_{i=1}^{i=N} \left[\Delta R_B\right]^2}{N}} \tag{2.39}$$

Here, ΔV_B and ΔR_B are the percentage deviations and are given by,

$$\Delta V_B = \frac{V_B^{theor} - V_B^{expt}}{V_B^{expt}} \times 100 \tag{2.40}$$

$$\Delta R_B = \frac{R_B^{theor} - R_B^{expt}}{R_B^{expt}} \times 100 \tag{2.41}$$

where, V_B^{theor} is the theoretically calculated value of V_B, V_B^{expt} is the empirical value of V_B, R_B^{theor} is the theoretically calculated value of R_B, and R_B^{expt} is the empirical value of R_B. For R_B^{expt} we take the values of R_B^{CC} from Table 2.1. The percentage deviations ($\Delta V_B(\%)$, $\Delta R_B(\%)$) are shown in Tables 2.2 and 2.4 respectively. Using Eqs. (2.38) and (2.39), the values of σ_{V_B} and σ_{R_B} are determined and they are shown in Table 2.5 [18].

As seen from Table 2.5, the potentials Bass 80, AW 95 and BW 91 are most effective in reproducing the height of the fusion barrier as they have the minimum

Table 2.5: Standard deviations (σ_{V_B}, σ_{V_R}) of the theoretical values against the experimental values of V_B and R_B.

	Prox 77	Prox 88	Bass 73	Bass 77	Bass 80	CW 76	BW 91	AW 95
σ_{V_B}	4.66	2.85	8.03	2.73	1.89	2.39	2.04	2.02
σ_{R_B}	4.65	3.24	3.33	2.95	2.05	2.04	1.94	2.19

values of σ_{V_B} (around 1.9-2.05). This is in agreement with earlier work [7, 8] where it was concluded that the fusion barriers formed by the potentials of Bass 80, and the different versions by Winther and collaborators are close to experimental data. If we consider only the above three potentials the fusion barrier is best reproduced for the reaction $^{9}Be+^{124}Sn$, and is least accurate for the reaction $^{6}Li+^{152}Sm$. For, the position of the fusion barrier the top 3 potentials turn out to BW 91, CW 76 and Bass 80. Again if we consider only the 3 potentials, then the position of the fusion barrier is best reproduced for the reaction $^{6}Li+^{159}Tb$, and is least accurate for the reaction $^{6}Li+^{152}Sm$. The potential AW 95, having done a good job in reproducing the height of the fusion barrier, has dropped to the fourth place in reproducing the position of the fusion barrier. This is because of an unusually large deviation in reproducing the position of the fusion barrier for the reaction $^{6}Li+^{152}Sm$ as the target ^{152}Sm is a highly deformed one. The effect of target deformation is quite evident for the above reaction as the height of the fusion barrier for all the eight nuclear potentials used has been systematically lowered from the empirical value of 25.1 MeV. Also the position of the fusion barrier has been raised from the empirical value of 9.98 fm for all but one (Prox 77) of the nuclear potentials used.

2.8 Coulomb potential correction for the deformed target

For the reaction $^{6}Li+^{152}Sm$, we apply a correction to the Coulomb potential for the deformed target nucleus (^{152}Sm). Many methods are available in the literature

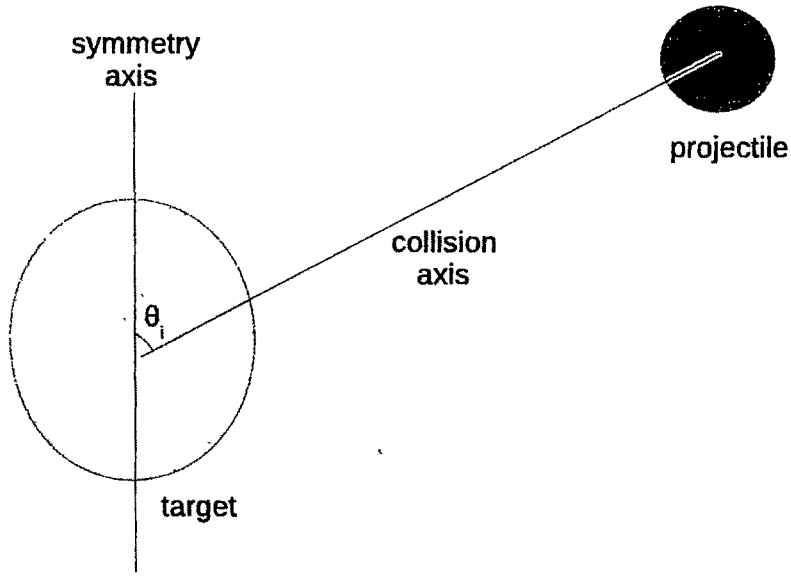

Figure 2.5: Diagram showing angle θ_i between collision axis and symmetry axis of the i^{th} nucleus.

for calculating the Coulomb interaction between two deformed and oriented nuclei. Here we apply Wong's correction [53] for two deformed charge distributions,

$$V_c(r,\theta) = \frac{Z_1 Z_2 e^2}{r} + \sqrt{\frac{9}{20\pi}}\frac{Z_1 Z_2 e^2}{r^3}\sum_{i=1}^{2} R_i^2 \beta_{2i} P_2(cos\theta_i) + \left(\frac{3}{7\pi}\right)\frac{Z_1 Z_2 e^2}{r^3}\sum_{i=1}^{2} R_i^2 [\beta_{2i} P_2(cos\theta_i)]^2 \quad (2.42)$$

here, θ_i is the orientation angle between the collision axis and the symmetry axis of the i^{th} nucleus (Fig. 2.5). The deformation parameter of the target nucleus (^{152}Sm) is taken as β_2=0.26 [40] and the projectile (^6Li) is assumed spherical. As the Coulomb potential is dependent upon the orientation of the target nucleus, hence, the effective Coulomb potential is found by averaging over all possible orientations. Because of symmetry, averaging over the angles from θ=0^0 to θ=90^0 is sufficient. Because of the target deformation, there is a slight raising of the total potential which is shown in Figs. 2.6 and 2.7 [18]. As a result we see that the effect of the

Table 2.6: Height and position of the fusion barrier for $^{6}Li+^{152}Sm$ after applying correction of the Coulomb potential for the deformed target. Values of V_B and R_B without correction are given in Tables 2.1 & 2.3.

	Prox 77	Prox 88	Bass 73	Bass 77	Bass 80	CW 76	BW 91	AW 95
V_B	25.36	24.82	22.32	24.87	24.11	24.36	24.51	24.25
R_B	9.88	10.11	10.58	10.12	10.47	10.45	10.36	10.48

target deformation is to make the potential more repulsive at shorter distances which is indeed expected. The effect is particularly pronounced for the potentials Bass 77, Bass 80, BW 91 and AW 95 where the repulsion is substantial at short distances for the deformed case as compared to the spherical case. For distances greater than R_B there is only a marginal difference between the spherical and deformed cases. However, for the potentials, Bass 73 and CW 76 there is no noticeable change even for short distances for the two cases. This is due to the exponential nature of the nuclear potentials due to which change of the Coulomb potential is overridden by large changes in the nuclear potential. A distinct feature of the potentials for the deformed case is the emergence of the potential pocket for the potentials Bass 77, Bass 80, BW 91 and AW 95. As we had observed earlier, for the spherical case potential pocket exists only for the proximity potentials. As can be seen from the Figs. 2.6 and 2.7, the height and position of the fusion barriers are shifted towards the empirical values. The new values of V_B and R_B for $^{6}Li+^{152}Sm$ are shown in Table 2.6 [18]. The correction for the barrier is about 0.35 MeV, and the correction for the position is about 0.03-0.04 fm with slight variation from potential to potential. Apart from Prox 77, all the corrections are in the right direction. This is probably due to the fact that Prox 77 had overestimated the measurements by about 4% [54].

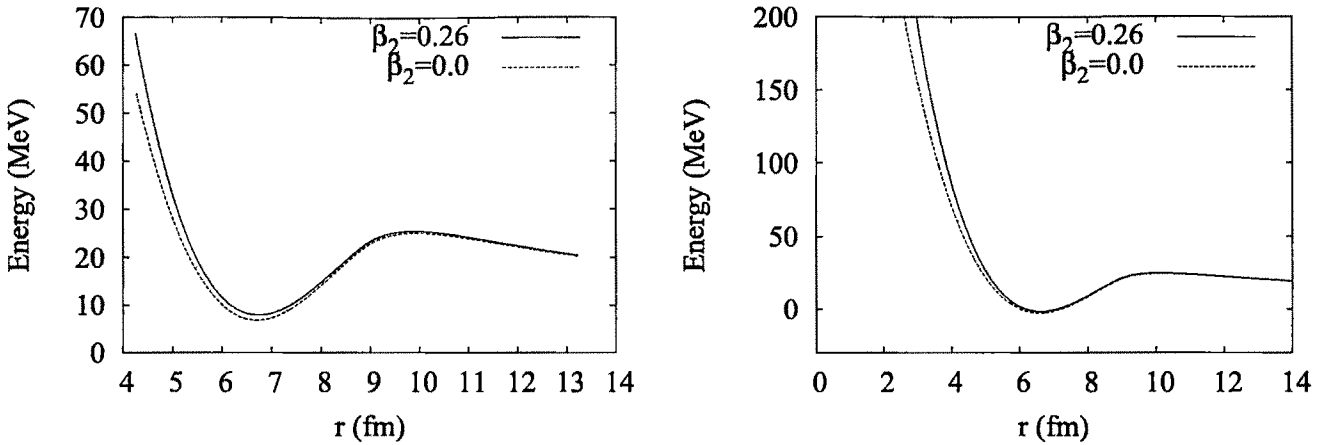

(a) Prox 77

(b) Prox 88

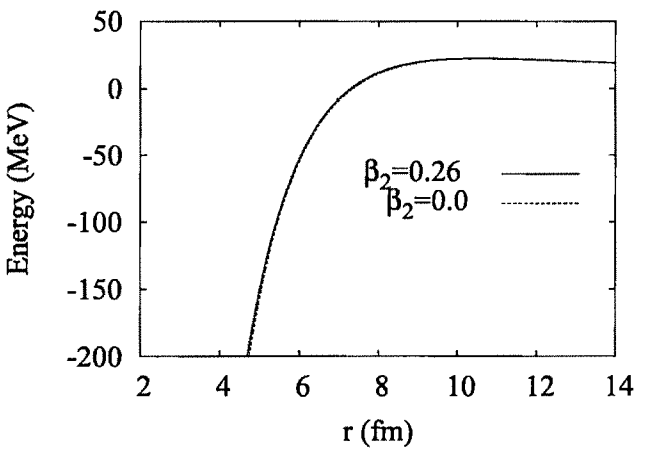

(c) Bass 73

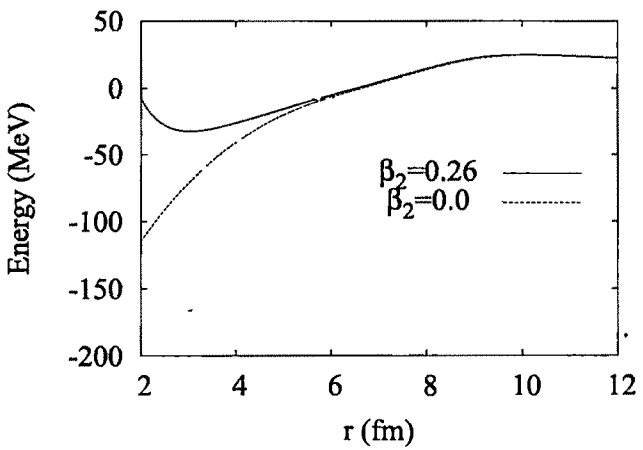

(d) Bass 77

Figure 2.6: Interaction potential for $^{6}Li+^{152}Sm$ assuming spherical (β_2=0) and deformed target (β_2=0.26) for the potentials Prox 77, Prox 88, Bass 73 and Bass 77 (as indicated).

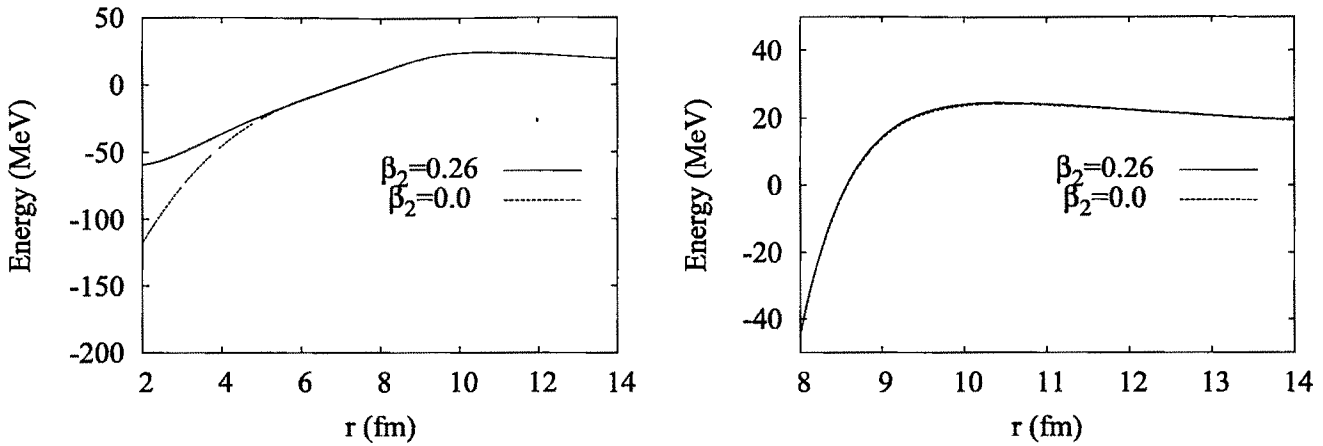

(a) Bass 80

(b) CW 76

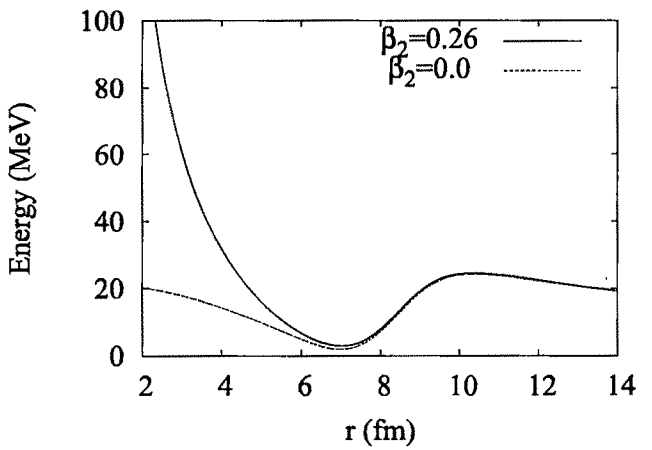

(c) BW 91

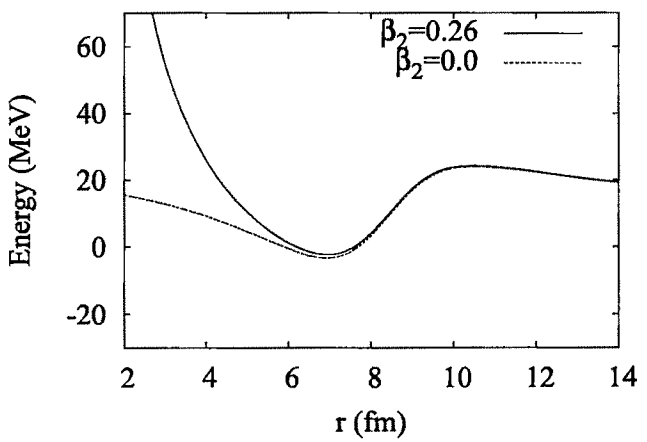

(d) AW 95

Figure 2.7: Interaction potential for $^{6}Li+^{152}Sm$ assuming spherical (β_2=0) and deformed target (β_2=0.26) for the potentials Bass 80, CW 76, BW 91 and AW 95 (as indicated).

2.9 Summary and Outlook

We determine the fusion barriers for thirteen number of reactions induced by loosely bound nuclei (^{6}Li, ^{7}Li, and ^{9}Be). For calculating the barriers, we use eight different versions of the nuclear potential. They are Prox 77, Prox 88, Bass 73, Bass 77, Bass 80, CW 76, BW 91 and AW 95. In general, all the potentials could reproduce the height and position of the barrier satisfactorily. In order to compare the predictions of the different potentials, we compute the standard deviation of the theoretical with respect to the experimental values (σ_{V_B}, σ_{R_B}). We find that the best potentials for reproducing the height (V_B) and position (R_B) of the barrier are Bass 80 and BW 91, respectively. The well known parametrized formula connecting V_B and R_B has also been checked. We find that the formula is well applicable to reactions induced by loosely bound projectiles as the prediction of the values of R_B is extremely accurate. For the reaction, ^{6}Li+^{152}Sm, the deviations of the barrier parameters from the empirical values is found to be unusually large. This is because of the deformed nature of the target (^{152}Sm). Applying correction to the Coulomb potential for the deformed target, we find that the new values of the barrier parameters are closer to the empirical values. The graphical plot of the potential for the deformed case of ^{6}Li+^{152}Sm shows the emergence of distinct potential pocket for the potentials Bass 77, Bass 80, BW 91 and AW 95, in addition to the potentials Prox 77 and Prox 88 for which potential pocket exists for both the spherical as well as the deformed cases.

Many other potentials are available in the literature, besides the ones that are considered here. Examples are the Denisov potential [55], the double-folding potential [56] with various versions of the NN interaction, the Skyrme nuclear interaction [6, 57], etc. In future, all these potentials could be used in order to find the barrier parameters of reactions induced by loosely bound projectiles. Some other parametrized formulae for V_B and R_B have been discussed by other authors, and these could also be studied in connection with the reactions discussed here. For

example, Puri and Gupta discusses a parameterized formula of the form [6],

$$V_B = k_1 \frac{Z_1 Z_2}{A_1^{1/3} + A_2^{1/3}} + k_2 \left(\frac{Z_1 Z_2}{A_1^{1/3} + A_2^{1/3}} \right)^2 \tag{2.43}$$

$$R_B = k_3 + k_4(A_1 A_2) + k_5(A_1 A_2)^2 + k_6(A_1 A_2)^3 \tag{2.44}$$

where, k_1, k_2, k_3, k_4, k_5 and k_6 are unknown constants which can be determined by fitting the data. For calculating the Coulomb potential between a spherical and a deformed target some other prescriptions (e.g., Takigawa et al. [58]) are also available which would give slightly improved results. Correction to the nuclear proximity potential for deformed nuclei can also be done. For the proximity potential (Prox 77 and Prox 88), the essential quantity is the shortest distance, s_0, between the two colliding nuclei. Various methods are discussed in the literature [59, 60, 61] for finding s_0 and hence, the nuclear proximity potential for deformed nuclei.

Bibliography

[1] C. Ngo, B. Tamain, J. Galin, M. Beiner, R.J. Lombard, *Nucl. Phys. A*, **240**, 353, (1975)

[2] H. Ngo and Ch. Ngo, *Nucl. Phys. A*, **348**, 140, (1980)

[3] Fl. Stancu and D.M. Brink, *Nucl. Phys. A*, **270**, 236, (1976)

[4] Fl. Stancu and D.M. Brink, *Nucl. Phys. A*, **299**, 321, (1978)

[5] Louis C. Vaz and John M. Alexander, *Phys. Rev. C*, **18**, 2152, (1978)

[6] R.K. Puri and Raj K. Gupta, *Phys. Rev. C*, **45**, 1837, (1992)

[7] I.Dutt and R.K. Puri, *Phys. Rev. C*, **81**, 064609, (2010)

[8] I.Dutt and R.K. Puri, *Phys. Rev. C*, **81**, 044615, (2010)

[9] I.Dutt and R.K. Puri, *Phys. Rev. C*, **81**, 047601, (2010)

[10] C. L. Guo, G.L. Zhang and X. Y. Le, *Nucl. Phys. A*, **897**, 54, (2013)

[11] Raj Kumar and Manoj K. Sharma, *Phys. Rev. C*, **85**, 054612, (2012)

[12] K. P. Santosh, V. Bobby Jose, Antony Joseph and K. M. Varier, *Nucl. Phys. A*, **817**, 35, (2009)

[13] K. P. Santosh, Jayesh George Joseph, and Sabina Sahadevan, *Phys. Rev. C*, **82**, 064605, (2010)

[14] K. P. Santosh, B. Priyanka, Jayesh George Joseph, and Sabina Sahadevan, *Phys. Rev. C*, **84**, 024609, (2011)

[15] K. P. Santosh, B. Priyanka, and M.S. Unnikrishnan, *Phys. Rev. C*, **85**, 034604, (2012)

[16] K. P. Santosh, R. K. Biju, and Sabina Sahadevan, *Nucl Phys. A*, **832**, 220, (2010)

[17] Raj Kumar, Manie Bansal, Sham K. Arun, and Raj K. Gupta, *Phys. Rev. C*, **80**, 034618, (2009)

[18] C. K. Phookan and K. Kalita, *Nucl. Phys. A*, **899**, 29, (2013)

[19] M. Dasgupta, D. J. Hinde, N. Rowley and A. M. Stefanini, *Annu. Rev. Nucl. Part. Sci.*, **48**, 401, (1998)

[20] J.Blocki, J.Randrup, W.J.Swiatecki, and C.F.Tsang, *Ann. Phy.*, **105**, 427, (1977)

[21] G. Sussmann, *Lawrence Berkeley Laboratory Report LBL-1615* (1973)

[22] W. D. Myers, *Nucl. Phys. A*, **204**, 465, (1973)

[23] W.Reisdorf, *Journal of Physics G*, **20**, 1297, (1994)

[24] W. D. Myers and W. J. Swiatecki, *Ark. Fys.*, **36**, 343, (1967)

[25] W. D. Myers and W. J. Swiatecki, *Ann. Physics*, **55**, 395, (1969)

[26] J. Randrup , *Nucl. Phys. A*, **259**, 253, (1976)

[27] R. G. Seyler and C. H. Blanchard, *Phys. Rev.*, **124**, 227, (1961);**131**, 355, (1963)

[28] W. J. Swiatecki, *Lawrence Berkeley Laboratory Report*, LBL-4296, (Sept. 1975)

[29] P. Moller and J. R. Nix, *Nucl. Phys. A*, **361**, 117, (1981)

[30] R. Bass, *Phys. Lett. B*, **47**, 139, (1973)

[31] R. Bass, *Nucl. Phys. A*, **231**, 45, (1974)

[32] J. Wilczynski, *Nucl. Phys. A*, **216**, 386, (1973)

[33] R. Bass, *Phys. Rev. Lett.*, **39**, 265, (1977)

[34] P.R. Christensen and A. Winther, *Phys. Lett. B*, **65**, 19, (1976)

[35] R.A. Broglia and A. Winther, *Heavy Ion Reactions, Parts I and II, Frontiers in Physics, vol. 84 (Addison-Wesley, 1991)*

[36] O Akyuz and A. Winther, *Proc. Enrico Fermi Intern. School of Physics 1979, eds. R.A. Broglia, C.H. Dasso and R. Ricci (North-Holland, Amsterdam, 1981)*

[37] A. Winther, *Nucl. Phys. A*, **594**, 203, (1995)

[38] K. Hagino, N. Rowley and A.T. Kruppa, *Comp. Phys. Comm.*, **123**, 143, (1999)

[39] P.R.S.Gomes, I. Padron, E. Crema, O. A. Capurro, J. O. Fernndez Niello, A. Arazi, G. V. Mart, J. Lubian, M. Trotta, A. J. Pacheco, J. E. Testoni, M. D. Rodrguez, M. E. Ortega, L. C. Chamon, R. M. Anjos, R. Veiga, M. Dasgupta, D. J. Hinde, and K. Hagino, *Phys. Rev. C*, **73**, 064606, (2006)

[40] P.K. Rath, S.Santra, N.L. Singh, K. Mahata, R. Palit, B.K. Nayak, K. Ramachandran, V.V. Parkar, R. Tripathi, S.K. Pandit, S. Appannababu, N.N. Deshmukh, R.K. Choudhury and S. Ḳailas, *Nucl. Phys. A*, **874**, 14-31, (2012)

[41] M. Dasgupta, P. R. S. Gomes, D. J. Hinde, S. B. Moraes, R. M. Anjos, A. C. Berriman, R. D. Butt, N. Carlin, J. Lubian, C. R. Morton, J. O. Newton, and A. Szanto de Toledo, *Phys. Rev. C*, **70**, 024606, (2004)

[42] M. Zadro, P.Figuera, A. Di Pietro, F. Amorini, M. Fisichella, O. Goryunov, M. Lattuada, C. Maiolino, A. Musumarra, V. Ostashko, M. Papa, M. G. Pellegriti, F. Rizzo, D. Santonocito, V. Scuderi, and D. Torresi, *Phys. Rev. C*, **80**, 064610, (2009)

[43] M.K. Pradhan, A. Mukherjee, P.Basu, A. Goswami, R. Kshetri, Subinit Roy, P. Roy Chowdhury, and M. Saha Sarkar, *Phys. Rev. C*, **83**, 064606, (2011)

[44] P.K. Rath, S. Santra, N. L. Singh, R. Tripathi, V. V. Parkar, B. K. Nayak, K. Mahata, R. Palit, Suresh Kumar, S. Mukherjee, S. Appannababu, and R. K. Choudhury , *Phys. Rev. C*, **79**, 051601, (2009)

[45] Y. W. Wu, Z. H. Liu, C. J. Lin, H. Q. Zhang, M. Ruan, F. Yang, and Z. C. Li, *Phys. Rev. C*, **68**, 044605, (2003)

[46] L. C. Vaz, J. M. Alexander and G. R. Satchler, *Physics Reports*, **69**, 373, (1981)

[47] V.V. Parkar, R. Palit, S.K. Sharma, B. S. Naidu, S. Santra, P. K. Joshi, P. K. Rath, K. Mahata, K. Ramachandran, T. Trivedi, and A. Raghav, *Phys. Rev. C*, **82**, 054601, (2010)

[48] C.S. Palshetkar, S. Santra, A. Chatterjee, K. Ramachandran, Shital Thakur, S..K. Pandit, K. Mahata, A. Shrivastava, V. V. Parkar, and V. Nanal, *Phys. Rev. C*, **82**, 044608, (2010)

[49] Z.H. Liu, C. Signorini, M. Mazzocco, M. Ruan, H.Q. Zhang, T. Glodariu, Y.W. Wu, F. Soramel,C.J. Lin, and F. Yang, *European Phys. J. A*, **26**, 73, (2005)

[50] N.G. Nicolis, *Eur. Phy. J. A*, **21**, 265, (2004)

[51] I.Dutt and R.K. Puri, *Phys. Rev. C*, **81**, 064608, (2010)

[52] R. A. Broglia and A. Winther, *Heavy-Ion Reactions Lecture Notes*, (Addison-Wesley, Redwood City, CA, 1981)

[53] C. Y. Wong, *Phys. Rev. Lett.*, **31**, 766, (1973)

[54] W.D. Myers and W.J. Swiatecki, *Phys. Rev. C*, **62**, 044610, (2000)

[55] V. Yu. Denisov, *Phys. Lett. B*, **526**, 315, (2002)

[56] G. R. Satchler and W. G. Love, *Physics Reports*, **55**, 183, (1979)

[57] Raj Kumar, Manoj K. Sharma, and Raj K. Gupta, *Nucl. Phys. A*, **870-871**, 42-57, (2011)

[58] Noboru Takigawa, Tamanna Rumin and Naoki Ihara, *Phys. Rev. C*, **61**, 044607, (2000)

[59] A. J. Baltz and B. F. Bayman, *Phys. Rev. C*, **26**, 1969, (1982)

[60] Raj Kumar, Narinder Singh and Monika Manhas, *Phys. Rev. C*, **70**, 034608, (2004)

[61] N. Malhotra and Raj. K. Gupta, *Phys. Rev. C*, **31**, 1179, (1985)

Chapter 3

Fusion cross section for reactions induced by loosely bound nuclei

3.1 Introduction

The study of fusion of heavy nuclei is extremely important for a number of reasons. In general, the fusion of two heavy nuclei produces a nucleus which is proton-rich and lies far away from the line of stability. The discovery and measurement of properties of previously unknown, proton-rich nuclei has formed a major part of the programme of heavy-ion fusion research. The study of heavy-ion fusion is also motivated by the search for superheavy or transuranic elements. Extrapolations of the nuclear shell model towards larger masses indicates that the next major shell closure should occur at Z=120, 124 or 126 and N=126 [1]. The recent progress in accelerator technologies has encouraged the experimentalists to reach this "island of stability". Heavy-ion fusion research is also important for astrophysical reasons as the heavier elements inside stars are formed by the successive fusion of lighter elements.

In this chapter we shall concentrate on the study of fusion cross-section of reactions induced by loosely bound projectiles. The study of fusion cross-section of

such nuclei is important because such nuclei are known to breakup in a nuclear reaction. Only a comparison of a carefully measured experimental fusion cross-section and the theoretical predictions can tell us whether breakup of such projectiles take place. In case of breakup, the experimental fusion cross-section must fall below the theoretically calculated cross-section. The contents of this chapter are as follows. In the next section, we shall give a brief review work of the study of fusion cross section. Then, we shall give a brief description of the experimental methods for the measurement of fusion cross-section. This will be followed by elaborate description of the theory of fusion cross-section, and the Wong's formula. Then we give a brief description of the CCFULL code for the calculation of fusion cross section. Finally our results are presented for the study of fusion cross-section of selected systems on the basis of the Wong's formula.

3.2 Review work on fusion cross section

The study of fusion cross section using the Wong's formalism has been done by a number of authors. K. P. Santosh of Kannur University had used the Wong's formula for the study of fusion cross section of reactions induced by ^{12}C, ^{16}O, ^{28}Si, and ^{35}Cl projectiles on ^{92}Zr target [2]. He found that near and above the barrier, Wong's formula satisfactorily explains the fusion cross section for these reactions. However, below the barrier, fusion cross section is well explained if Z_1Z_2 has a low value, and for higher values of Z_1Z_2 fusion cross section below the barrier is only explained with barrier parameters evaluated from Reisdorf's value of the nuclear surface tension coefficient. I. Dutt and R. K. Puri of Panjab University had studied the fusion excitation function of symmetric as well as asymmetric colliding nuclei using Wong's formalism. They found that for both the systems, the above barrier fusion cross section is well explained with barrier parameters evaluated from the potentials Bass 80, AW 95 and Denv 02 [3, 4]. Using Wong's formalism, Raj Kumar et al. had stud-

ied the capture cross-section data from $^{48}Ca+^{238}U$, $^{48}Ca+^{244}Pu$, and $^{48}Ca+^{248}Cm$ reactions in the super-heavy mass region, and also the fusion-evaporation cross section for the reactions $^{58}Ni+^{58}Ni$, $^{64}Ni+^{64}Ni$, and $^{64}Ni+^{100}Mo$ [5]. The fusion cross section for the ^{48}Ca based reaction is well explained by a slight modification of the Wong's formula where the ℓ-dependent barriers are introduced via the ℓ-summation. For the ^{58,64}Ni based reactions the experimental data is well explained only if a further modification of the barrier is introduced. Their calculations were done using the proximity potential, with effects of multipole deformations included upto hexadecapole term, and orientation degrees of freedom integrated for both the coplanar and noncoplanar configurations. In an improvement of the previous work [6], Raj Kumar studied the fusion cross section of the above reactions using various versions of the proximity potential with different isospin dependence. Among all the previous versions of proximity potential, they found that the results of Prox 88 are closest to experimental data. Then they introduced another variation of the Prox 88 potential (mod-Prox 88), which when used within the extended Wong's formalism could explain the fusion cross section for all the above reactions above and below the fusion barrier with a smooth variation of $\ell_{max}(E_{cm})$. More recently [7], Raj Kumar studied the fusion cross section of the above reactions using the Wong's model where the barrier parameters have been calculated using the semiclassical extended Thomas Fermi (ETF) approach within the Skyrme energy density formalism (SEDF). They found that the capture cross section data for Ca-induced reactions could be fitted to any Skyrme force, such as SIII, SV and GSkI, whereas the fusion-evaporation cross sections in Ni-induced reactions at sub-barrier energies required different Skyrme forces.

3.3 Experimental methods of determining fusion cross section

The measurement of the total fusion cross section is an intricate business, and requires extremely sophisticated experimental setup. As discussed earlier, fusion is defined as a reaction where two separate nuclei combine together to form a compound nucleus. As the compound nucleus formed in heavy-ion fusion is highly excited, hence, it decays either by emitting neutrons, protons, α-particles, γ and X-rays, or by fission. The probability for fission is high only if the charge of the compound nucleus is greater than 70, otherwise the compound nucleus decays by the former processes, i.e., evaporation. During evaporation, the decay product has a mass and charge close to the compound nucleus, and is called the evaporation residue. For a heavier compound nucleus, decay by fission competes successfully with evaporation. The total fusion cross section is defined by the sum of the fission and the evaporation residue cross section.

Detection of evaporation residues

Evaporation residue cross sections can be determined by direct detection of the evaporation residues or by detection of the radiation emitted in their deexcitation. In the direct detection methods, the evaporation residues which are forward peaked, must be physically separated from the direct beam and the intense flux of elastically scattered beam particles. One of the methods employed for separation is the compact velocity filter of the Canberra group [8]. Particles entering the velocity filter are subjected to orthogonal electric and magnetic fields. Assuming, the velocity of the particles to be in the z-direction, the electric and magnetic fields are imposed in the x- and y- directions, respectively. The force acting on the particles is then directed

towards the x-direction and its strength is given by,

$$F = q(\mathcal{E} - v\mathcal{B}) \tag{3.1}$$

where, q is the charge of the particle, v its velocity, and $\mathcal{E}$ and $\mathcal{B}$ are the strength of the electric and the magnetic fields, respectively. One can, therefore, select a particular ratio of the electric and the magnetic fields so that the force acting on a particle having a certain velocity is zero.

Detection of fission fragments

Kinematic coincidence in two detectors is a common method for identifying fission fragments [9]. Single detectors are also employed which uses energy-loss or time-of-flight information to detect these particles [10, 11]. Fission fragments are usually spread to all angles, giving good separation from beam particles. However, their angular distribution can change quite rapidly with beam energy, requiring careful placement of the detector or measurement of the angular distribution at many beam energies.

Once the number of events, Y, are determined, then the differential cross-section can be calculated from the following relation,

$$\frac{d\sigma(\theta, E)}{d\Omega} = \frac{Y(\theta, E)}{IN} \frac{1}{\Delta\Omega} \tag{3.2}$$

where, I is the number of beam particles per unit time, N is the number of target nuclei per unit area, and, $\Delta\Omega$ is the solid angle of the detector. The product IN can be determined by monitoring the the elastic scattering at a certain angle θ_M. If we assume that the cross section of scattering is well described by Rutherford scattering at θ_M, then

$$IN = \frac{Y_M(\theta_M, E)}{\Delta\Omega_M} \left(\frac{d\sigma_R(E, \theta_M)}{d\Omega} \right)^{-1} \tag{3.3}$$

where, Y_M is the number of elastically scattered events, and $\Delta\Omega_M$ is the solid angle of the detector. $d\sigma_R/d\Omega$ is the Rutherford differential cross section and is given by,

$$\frac{d\sigma_R(E,\theta_M)}{d\Omega} = \frac{1}{4}\Big(\frac{Z_P Z_T e^2}{2E}\Big)^2 \frac{1}{\sin^4(\theta_M/2)} \tag{3.4}$$

$$= 1.29\Big(\frac{Z_P Z_T}{2E}\Big)^2 \frac{1}{\sin^4(\theta_M/2)} \quad \text{mb/sr} \tag{3.5}$$

Usually the scattering cross section is measured in the laboratory system. We should multiply it with the Jacobian, J, in order to obtain the scattering cross section in the centre of mass system.

$$J = \frac{(1 - x^2 \sin^2\theta_L)^{1/2}}{\Big[x\cos\theta_L + (1 - x^2\sin^2\theta_L)^{1/2}\Big]^2} \tag{3.6}$$

where, x=M_P/M_T, M_P is the mass of the projectile, M_T is the mass of the target, and θ_L is the angle of scattering in the laboratory frame. Combining Eqs. (3.2) and (3.3) we get,

$$\frac{d\sigma(\theta,E)}{d\Omega} = \frac{Y(\theta,E)}{Y_M(\theta_M,E)} \frac{\Delta\Omega_M}{\Delta\Omega} \frac{d\sigma_R(E,\theta_M)}{d\Omega} \tag{3.7}$$

The total fusion cross section is then obtained by integrating Eq. (3.7) over all angles θ.

3.4 Theory of fusion cross section and Wong's formula

Let us first work out the classical cross-section for fusion. If a projectile is approaching a target nucleus with impact parameter b, then the collision cross-section is given by πb^2. Initially, the total energy of the system (E) is equal to the kinetic energy of the projectile. At the distance of closest approach (R), this energy appears partly as the kinetic energy (E') of the projectile, and partly as the potential energy (B)

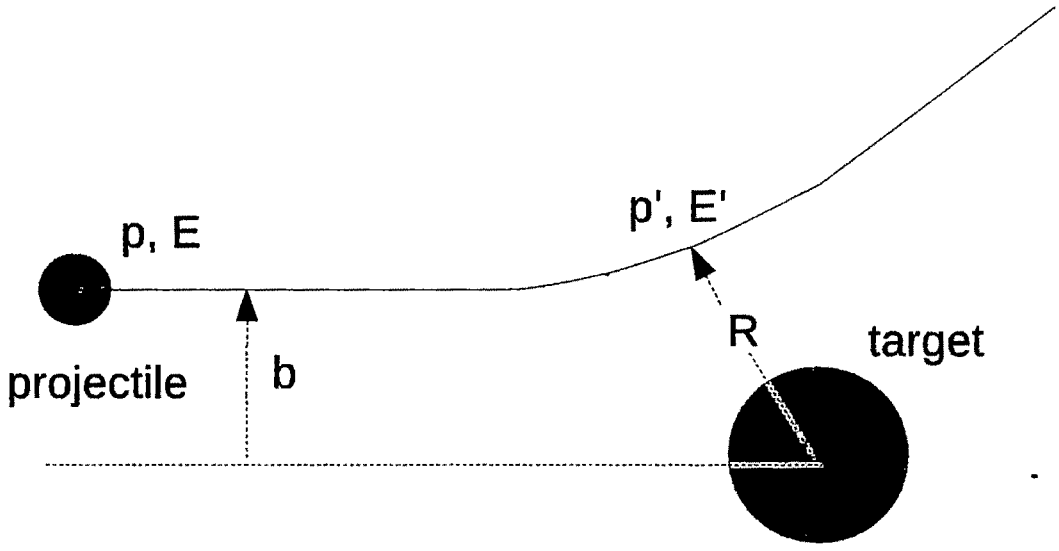

Figure 3.1: Diagram showing linear momentum and energy of the projectile at a distance far from the target (p, E) and at the distance of closest approach ($p^{'}$, $E^{'}$).

of the system of projectile and target. The potential energy is composed of the sum of the Coulomb potential energy and the nuclear potential energy. Hence,

$$E = E' + B$$

Applying law of conservation of momentum, we get,

$$L = pb = p'R$$

where, p and p', are the projectile momenta initially and at the distance of closest approach (Fig. 3.1). Since, E=$p^2/2m$, hence,

$$\frac{E'}{E} = \left(\frac{p'}{p}\right)^2 = \left(\frac{b}{R}\right)^2$$

from which it follows,

$$\sigma = \pi R^2 \frac{E'}{E} = \pi R^2 \left(1 - \frac{B}{E}\right) \qquad for \quad E \geq B \tag{3.8}$$

Fusion takes place when the projectile penetrates the fusion barrier, and enters the potential well or pocket. Hence, the classical cross-section for fusion is given by the above equation, where, B denotes the height of the fusion barrier, and R denotes the position of the fusion barrier. The above expression is only valid at high energies where the de-broglie wavelength of the projectile is small compared with the nuclear dimensions. At lower energies the de-broglie wavelength of the projectile is comparable to the nuclear dimensions and quantum effects become important. According to quantum mechanics, the angular momentum of the projectile can take integral values of $\hbar$, hence,

$$pb = \ell\hbar$$

$$b = \ell\frac{\hbar}{p} = \ell\frac{\lambda}{2\pi} = \ell\tilde{\lambda} \tag{3.9}$$

where, $\tilde{\lambda}$=$\lambda/2\pi$ is called the reduced de-Broglie wavelength, and also, $\tilde{\lambda}$=k^{-1}, the wave-number. Hence, for particles interacting between impact parameters $\ell\hbar$ and $(\ell+1)\hbar$, the area of interaction must be quantized, and is given by, $\pi[(\ell+1)^2\tilde{\lambda}^2 - \pi(\ell\tilde{\lambda})^2] = (2\ell+1)\pi\tilde{\lambda}^2$. Hence, the total cross-section is,

$$\sigma = \sum_{\ell=0}^{\ell_c}(2\ell+1)\pi\tilde{\lambda}^2 \tag{3.10}$$

where, ℓ_c is the cut-off angular momentum for the event under consideration. According to the quantum-mechanical description, fusion takes place when the projectile penetrates the fusion barrier with transmission coefficient (T_l). So, for each of these partial waves, the transmission coefficients must be evaluated, and the total fusion cross-section is given by,

$$\sigma = \frac{\pi}{k^2}\sum_{\ell=0}^{\infty}(2\ell+1)T_l \tag{3.11}$$

where, T_ℓ is the transmission coefficient for the ℓ^{th} partial wave, and k^2= $2\mu E_{cm}/\hbar^2$.

Using WKB approximation, the transmission co-efficients are given by [12],

$$T_l(E) = \frac{1}{1 + \exp\left[2\int_{x_a}^{x_b} dx \sqrt{\frac{2\mu}{\hbar^2}(E_l(x) - E)}\right]} \tag{3.12}$$

Here, x_a and x_b are the inner and outer turning points defined by $E_l(x)$=E, respectively. This formula is valid both below and above the Coulomb barrier. When the energy is well below the barrier, the second term dominates in the denominator in Eq. (3.12), and the formula in the primitive WKB approximation is obtained. For energies above the barrier, the turning points are found in the complex x plane. The integral in Eq. (3.12) is then carried out between the complex turning points. It was noted by Hill and Wheeler [13] that the fusion barriers can be approximately treated as inverted parabolas. Hence, the fusion barriers can be written as,

$$E_l(x) = E_{l(x=0)} - \frac{1}{2}\mu\omega_l x^2 \tag{3.13}$$

Evaluation of the integral in Eq. (3.12) leads to $\pi(E_{l(x=0)} - E)/\hbar\omega_l$, which gives the following expression for the transmission coefficients [13, 14],

$$T_\ell(E) = \frac{1}{1 + exp\left(\frac{2\pi}{\hbar\omega_l}(E_\ell - E)\right)} \tag{3.14}$$

where, E_ℓ=$E_{l(x=0)}$ is the fusion barrier for the ℓ^{th} partial wave, and $\hbar\omega_l$ is the curvature of the ℓ^{th} barrier. Eq. (3.14) gives the exact transmission coefficients for a parabolic potential because WKB approximation has the unique property that if the potential is quadratic, then Eq. (3.12) gives the exact solution. Replacing the sum by an integral, and assuming that the barrier position and curvature are independent of ℓ, we arrive at Wong's formula [15, 16] for the fusion cross-section,

$$\sum_\ell (2\ell + 1) = \sum_\ell (2\ell + 1)\Delta\ell = \sum_\epsilon \Delta\chi \longrightarrow \int d\chi$$

$$\sigma_F = \frac{2\pi}{k^2}\int_{1/4}^{\infty}\frac{d\chi}{1+exp[\frac{2\pi}{\hbar\omega_0}(V_B - E + \hbar^2\chi/2\mu R_B^2)]} \quad ; \quad \text{where,}\chi = \left(\ell+\frac{1}{2}\right)^2 \tag{3.15}$$

$$\sigma = \frac{R_b^2\hbar\omega_0}{2E}ln\Big\{1+exp\Big[\frac{2\pi(E-E_0)}{\hbar\omega_0}\Big]\Big\} \tag{3.16}$$

where, $\hbar\omega_0$ is the curvature of the fusion barrier (ℓ=0). E_0 and R_B are the height and position of the fusion barrier respectively. For E $\gg$ E_0, the above formula reduces to the classical formula (Eq. 3.8),

$$\sigma = \pi R_0^2\left(1-\frac{E_0}{E}\right) \tag{3.17}$$

The primary assumption of the Wong's formula is that the barrier parameters for the ℓ^{th} partial wave is approximated by the barrier parameters of the s-wave (ℓ=0). In this connection, Balantekin has improved Wong's formula by taking into account the angular momentum dependence of the barrier parameters. They make the assumption that the barrier position can be written as an infinite series,

$$R_l = R_0 + c_1\Lambda + c_2\Lambda^2 + ... \tag{3.18}$$

where, c_i are unknown constants, and Λ=$\ell(\ell+1)$. Retaining only the first order correction, the values of the barrier parameters are given by,

$$R_l = R_0 - \frac{\ell(\ell+1)\hbar^2}{\mu^2\omega^2R_0^3} \tag{3.19}$$

$$E_l = E_0 + \frac{\ell(\ell+1)\hbar^2}{2\mu R_0^2} + \frac{\ell^2(\ell+1)^2\hbar^4}{2\mu^3\omega^2R_0^6} \tag{3.20}$$

Making these corrections, Balantekin obtained a new expression for the fusion cross

section [17],

$$\sigma = \pi R_0^2\left(1 - \frac{E_0}{E}\right) - \frac{2\pi}{\mu\omega^2 E}(E - E_0)^2 \qquad (E \gg E_0) \tag{3.21}$$

The above equation suggests that Wong's formula slightly overestimates fusion cross section at energies well above the Coulomb barrier.

3.5 CCFULL code

The code CCFULL [18] is a FORTRAN 77 program that calculates the fusion cross section and the mean angular momenta of the compound nucleus in a heavy ion collision under the influence of coupling between the relative motion of projectile and target. The program essentially solves the coupled channel equations and includes all order couplings. For reducing the dimensions of the coupled-channel equations, the no-coriolis approximation is employed in which the angular momentum of the relative motion in each channel is replaced by the total angular momentum, J. The coupled channels equations then read,

$$\left[-\frac{\hbar^2}{2\mu}\frac{d^2}{dr^2} + \frac{J(J+1)}{2\mu r^2} + V_N^{(0)} + \frac{Z_P Z_T e^2}{r} + \epsilon_n - E\right]\psi_n(r) + \sum_m V_{nm}\psi_m(r) = 0 \tag{3.22}$$

where, E is the c.m. energy, μ is the reduced mass, and ϵ_n is the excitation energy of the n^{th} channel. V_{nm} are the matrix elements of the coupling Hamiltonian, which consists of the Coulomb and nuclear components in the collective model. The nuclear potential, $V_N^{(0)}$ is assumed to have a Woods-Saxon form and is given by,

$$V_N^{(0)}(r) = -\frac{V_0}{1 + exp((r - R_0)/a)}, \quad R_0 = r_0(A_P^{1/3} + A_T^{1/3}) \tag{3.23}$$

Table 3.1: Format of input file for CCFULL code

Line 1	AP, ZP, AT, ZT	
Line 2	RP, IVIBROTP, RT, IVIBROTT	
Line 3	OMEGAT, BETAT, LAMBDAT, NPHONONT	(if IVIBROTT=0)
	E2T, BETA2T, BETA4T, NROTT	(if IVIBROTT=1)
Line 4	OMEGAT2, BETAT2, LAMBDAT2, NPHONONT2	
Line 5	OMEGAP, BETAP, LAMBDAP, NPHONONP	(if IVIBROTP=0)
	E2P, BETA2P, BETA4P, NROTP	(if IVIBROTP=1)
Line 6	NTRANS, QTRANS, FTR	
Line 7	V0, R0, A0	
Line 8	EMIN, EMAX, DE	
Line 9	RMAX, DR	

The program calculates the transmission coefficients, $T_J(E)$, and the details of the theory can be found in Ref. [18]. The fusion cross-section is then given by,

$$\sigma_{fus}(E) = \frac{\pi}{k_0^2} \sum_J (2J+1) T_J(E) \tag{3.24}$$

The program considers either rotational or vibrational coupling for the target and projectile excited states. The program has the option of choosing the coupling and setting the parameters.

The input file of CCFULL has format shown in Table 3.1. The first line contains the parameters specifying the system. AP (AT) is the projectile (target) mass and ZP (ZT) is the projectile (target) charge. The second line is for the coupling Hamiltonian. RP (RT) is the radius parameter r_{coup} of the projectile (target) used in the coupling Hamiltonian. IVIBROTP (IVIBROTT) is an option which specifies the property of the intrinsic motion of the projectile (target). If it is set to be −1, the projectile (target) is assumed to be inert and the fifth (the third and the fourth) line will be ignored. The fusion cross sections in the absence of channel coupling can be therefore obtained by setting both the IVIBROTP and the IVIBROTT to −1. When IVIBROTP (IVIBROTT) is set to zero, the CCFULL assumes that the coupling in the projectile (target) is vibrational, while if it is set to one, the rotational coupling is assumed. The third line is for detailed information on the

target excitation. If IVIBROT is zero (i.e., the vibrational coupling), the CCFULL reads OMEGAT, BETAT, LAMBDAT, and NPHONONT. OMEGAT is the excitation energy of the single phonon state, BETAT is the deformation parameter, and LAMBDAT is the multipolarity of the vibrational excitation. NPHONONT is the maximum phonon number to be included. For example, if it is two, up to two phonon states are included in the calculation. If IVIBROTT is one (i.e., the rotational coupling), the CCFULL reads E2T, BETA2T, BETA4T, and NROTT. E2T is the excitation energy of the first 2^+ state in the ground rotational band of the target nucleus, BETA2T and BETA4T are the quadrupole and hexadecapole deformation parameters, respectively. NROTT is the number of levels in the rotational band to be included. For instance, if it is 3, the 2^+ , 4^+ and 6^+ states are included together with the ground state. The fourth line is for the second mode of excitation in the target nucleus. The meaning of OMEGAT2, BETAT2, LAMBDAT2 and NPHONONT2 is the same as OMEGAT, BETAT, LAMBDAT and NPHONONT, respectively. The second mode is not included when NPHONONT2 is set to zero. OMEGAT2, BETAT2, and LAMBDAT2 are then ignored. The fifth line is the same as the third line, but for the projectile excitations. The sixth line is for the pair transfer coupling. QTRANS is the Q-value for the pair transfer channel, while FTR is the coupling strength. NTRANS is the number of the pair transfer channel. In the present version of the CCFULL, NTRANS is restricted to be either one or zero. If it is zero, the pair transfer channel is not included and QTRANS and FTR are ignored. The seventh line is for the nuclear potential in the entrance channel (Eq. 3.23). V_0 is the depth parameter of the Woods–Saxon potential, R0 is the radius parameter R_0 in Eq. 3.23, and A0 is the surface diffuseness parameter a. EMIN, EMAX, and DE in the next line are the minimum and the maximum value of the colliding energy in the center of mass frame and the interval in the energy scale, respectively. The CCFULL constructs the distribution of partial cross sections σ_J as a function of J if a single value of the energy is entered, i.e. either when EMIN

= EMAX or DE = 0. The accuracy of the calculation is controlled by the matching radius RMAX and the mesh for the integration DR in the ninth line. For many applications, especially for asymmetric systems such as $^{16}O + {}^{144}Sm$, RMAX = 30 fm and DR = 0.05 fm provides sufficiently accurate results. For heavier systems, such as $^{64}Ni + {}^{92}Zr$, RMAX may have to be extended to a value as large as 50 fm.

3.6 Results and Discussion

We first apply Wong's formula to find the fusion cross-section for the reactions $^{6}Li+^{209}Bi$, $^{9}Be+^{208}Pb$ and $^{7}Li+^{209}Bi$, and the results are shown in Table 3.2. We need the values of the barrier parameters (V_B, R_B) for use in the Wongs' formula (Eq. 3.16), and these are taken from Tables 2.1 and 2.3 for all the potentials. The values of the curvature ($\hbar\omega_0$) are taken from Ref. [19] and are given by, 4.8 MeV, 4.4 MeV and 4.4 MeV, respectively, for the three reactions.

The results of the single BPM are obtained by running the code CCFULL [18]. Line 2 of the input file (Table 3.1) is taken as 1.2,–1,1.06,–1. Lines 3, 4, and 5 are automatically ignored as the target and projectile are assumed to be inert by setting the second and fourth parameter of line 2 as –1. NTRANS in line 6 is set to 0, and hence pair transfer coupling is ignored. Line 7 is for the parameters of the Woods-Saxon potential, and these values are the same as the ones mentioned in section 2.7. In line 8 we specify the energy interval, and in line 9 we put the values 0.05, 30 [18].

A graphical plot of the results are shown in Figs. 3.2 (a), 3.2(b) and 3.2(c) on a log scale [20]. For comparison both the experimental data points and the results of the single barrier penetration model (SBPM) are also shown. From the results, we observe that the experimental fusion cross section falls short of the theoretically expected results of single BPM. This is because fusion suppression is dominant in these reactions [21]. Hence, we make a comparison of the theoretical results with

Table 3.2: Fusion cross section for ^{6}Li+^{209}Bi, ^{9}Be+^{208}Pb and ^{7}Li+^{209}Bi.

	Prox77	Prox88	Bass73	Bass77	Bass80	CW 76	B W91	AW 95	SBPM
E_{cm} (MeV)	σ (mb) for ^{6}Li+^{209}Bi.								
25.27	.029	.066	1.505	.054	.221	.151	.117	.157	.517
27.22	.347	.781	16.58	.638	2.588	1.774	1.379	1.841	2.24
29.16	4.051	8.902	114.1	7.333	27.22	19.34	15.29	20.01	29.11
31.11	39.14	72.48	312.3	62.80	152.2	124.2	106.4	126.7	156.0
33.05	172.0	238.5	514.7	221.7	354.2	320.2	294.3	323.1	352.5
35.00	348.5	423.6	697.2	405.8	550.1	516.8	487.9	519.2	352.5
36.94	514.3	593.3	860.6	575.2	726.7	694.7	663.7	696.7	544.5
38.88	664.1	746.2	1008	728.0	885.7	855.0	822.0	856.5	715.7
40.83	799.7	884.6	1141	866.3	1030	1000	965.3	1001	868.0
42.77	923.0	1010	1262	992.0	1160	1132	1096	1133	1005
44.72	1036	1125	1372	1107	1280	1252	1215	1253	1126
46.66	1139	1231	1474	1212	1389	1363	1323	1363	1336
E_{cm} (MeV)	σ (mb) for ^{9}Be+^{208}Pb.								
32.59	.001	.003	.074	.004	.014	.012	.007	.006	.089
33.55	.004	.011	.283	.014	.055	.044	.027	.024	.051
35.47	.053	.155	4.038	.209	.794	.648	.395	.346	1.22
37.38	.768	2.24	44.11	3.01	10.90	9.01	5.60	4.93	18.35
39.30	10.48	27.27	181.1	34.83	88.53	78.71	56.41	51.34	117.6
41.22	81.64	140.2	347.0	159.3	252.6	240.6	203.7	194.7	287.6
41.13	224.8	297.7	502.2	319.9	422.2	412.2	371.4	361.7	456.7
45.05	371.4	448.1	644.4	471.9	578.8	571.1	527.6	517.7	612.6
46.01	440.7	518.9	711.0	543.4	652.3	645.7	601.0	591.0	685.2
47.93	571.0	651.9	836.4	677.6	790.50	785.8	738.9	728.7	821.3
48.88	632.4	714.5	895.4	740.8	855.5	851.8	803.8	793.5	883.2
49.84	691.4	774.7	952.1	801.6	918.0	915.2	866.2	855.9	943.7
E_{cm} (MeV)	σ (mb) for ^{7}Li+^{209}Bi.								
25.16	0.02	0.20	1.58	0.06	0.20	0.14	0.10	0.11	.08
28.06	1.37	10.76	64.17	3.11	10.76	7.75	5.36	6.03	9.89
31.93	125.7	299.9	471.7	186.9	299.9	270.7	235.3	246.3	287.2
34.83	401.8	609.5	761.2	479.8	609.5	581.6	540.0	553.0	588.4
36.77	571.9	790.5	929.0	654.6	790.5	764.1	719.8	733.6	763.7
38.70	725.2	953.4	1080	812.0	953.4	928.3	881.6	896.1	918.6
40.64	864.0	1101	1217	954.4	1101	1077	1028	1043	1058
42.57	990.1	1235	1341	1084	1235	1212	1161	1177	1182
44.51	1105	1357	1454	1202	1357	1335	1283	1299	1294
46.44	1211	1469	1558	1311	1469	1448	1394	1411	1395
48.38	1308	1572	1654	1410	1573	1552	1497	1514	1532
50.31	1398	1668	1742	1502	1668	1648	1591	1609	1571

Table 3.3: Fusion cross section for ^{6}Li+^{152}Sm considering both spherical (β_2=0) and deformed (β_2=0.26) target.

	Prox77	Prox88	Bass73	Bass77	Bass80	CW 76	BW 91	AW 95	SBPM
E_{cm} (MeV)	σ (mb) for ^{6}Li+^{152}Sm (β_2=0)								
20.20	0.14	0.30	9.96	0.28	0.84	0.59	0.48	0.69	.052
21.16	0.52	1.09	32.96	1.02	3.04	2.14	1.73	2.51	.299
22.13	1.89	3.94	91.13	3.69	10.76	7.66	6.22	8.94	1.49
23.09	6.78	13.76	190.5	12.92	35.07	25.77	21.21	29.68	6.33
24.05	22.78	43.05	310.1	40.76	93.68	73.44	62.46	82.28	22.48
25.01	64.67	106.5	430.7	102.4	188.2	159.0	141.2	172.3	62.94
25.97	139.3	198.6	545.2	193.4	298.4	265.8	243.7	281.2	132.7
26.94	232.0	299.8	652.2	294.6	408.5	375.3	350.9	391.4	220.9
27.90	327.1	399.0	752.2	394.0	513.1	480.3	454.3	496.7	311.9
28.86	418.4	492.9	845.5	488.3	611.3	579.1	551.7	595.6	399.9
29.82	504.4	581.2	932.8	576.9	703.3	671.7	643.1	688.4	482.8
30.78	585.2	663.9	1014	660.0	789.6	758.6	728.75	775.3	560.3
31.75	661.2	741.8	1091	738.1	870.7	840.2	809.3	857.0	633.4
32.71	732.7	815.0	1163	811.6	947.0	917.0	885.1	933.9	700.8
33.67	800.2	884.0	1232	881.0	1019	989.4	956.6	1006.4	763.8
34.63	863.8	949.2	1296	946.4	1087	1058	1024	1075	822.8
35.59	924.1	1010	1357	1008	1151	1122	1088	1140	878.1
36.56	981.2	1069	1416	1067	1212	1184	1148	1201	930.5
37.52	1035	1125	1470	1123	1270	1242	1206	1259	979.3
E_{cm} (MeV)	σ (mb) for ^{6}Li+^{152}Sm (β_2=0.26)								
20.20	0.08	0.18	6.31	0.17	0.52	0.37	0.29	0.43	
21.16	0.30	0.66	21.61	0.61	1.89	1.33	1.06	1.56	
22.13	1.08	2.39	64.56	2.23	6.77	4.80	3.84	5.61	
23.09	3.90	8.50	149.19	7.96	22.99	16.65	13.46	19.28	
24.05	13.60	28.08	262.1	26.48	66.92	55.10	42.46	57.91	
25.01	42.12	76.93	381.0	73.49	148.9	122.7	106.6	134.5	
25.97	102.5	158.9	495.6	154.1	254.1	222.8	201.5	237.4	
26.94	188.1	256.8	603.1	251.6	363.3	330.8	306.9	346.4	
27.90	281.4	355.6	703.5	350.6	468.3	436.0	410.5	452.0	
28.86	372.7	450.1	797.3	445.4	567.3	535.41	508.7	551.6	
29.82	459.2	539.0	885.1	534.6	660.0	628.7	601.0	645.1	
30.76	540.7	622.5	967.4	618.5	747.0	716.3	687.6	732.8	
31.75	617.2	701.0	1045	697.3	828.8	798.6	769.0	815.2	
32.71	689.3	774.8	1117	771.4	905.8	876.1	845.6	892.7	
33.67	757.3	844.5	1186	841.4	978.3	949.1	917.8	965.8	
34.63	821.5	910.2	1251	907.4	1047	1018	986.0	1035	
35.59	882.2	972.5	1312	969.9	1112	1083	1051	1100	
36.56	939.7	1031	1370	1029	1173	1145	1112	1162	
37.52	994.3	1087	1425	1085	1231	1204	1170	1221	

respect to the results of single BPM. We find that the potentials Bass 80 and BW 91 have an edge over the other potentials for the reaction $^{6}Li+^{209}Bi$. For the reactions $^{9}Be+^{208}Pb$ and $^{7}Li+^{209}Pb$ the potentials Bass 80 and CW 76 turn out to be better.

Similarly we calculate the fusion cross-section for the reaction $^{6}Li+^{152}Sm$ considering both spherical as well the deformed case [20] of the target nucleus. The results are shown in Table 3.3. The barrier parameters are taken from Tables 2.1 and 2.3 for the spherical target case, and from Table 2.6 for the deformed target case. The curvature of the barrier is taken to be 4.5 MeV [19]. Same as above, we make the comparison with respect to results of single BPM as there is a very high fusion suppression of 0.28 for this reaction [22]. The single BPM cross section is determined from CCFULL in exactly similar way as that mentioned above. The graphical plot of the results is shown in Figs. 3.3 (a), (b), (c) and (d). We see that for all the potentials the fusion cross-section for the deformed case (β_2=0.26) comes out closer to the results of single BPM than the spherical case (β_2=0). As such, the role of deformation of the target nuclei ^{152}Sm is clearly seen. Overall we see that the fusion cross-section for the potentials of CW 76 and BW 91 are better than the rest.

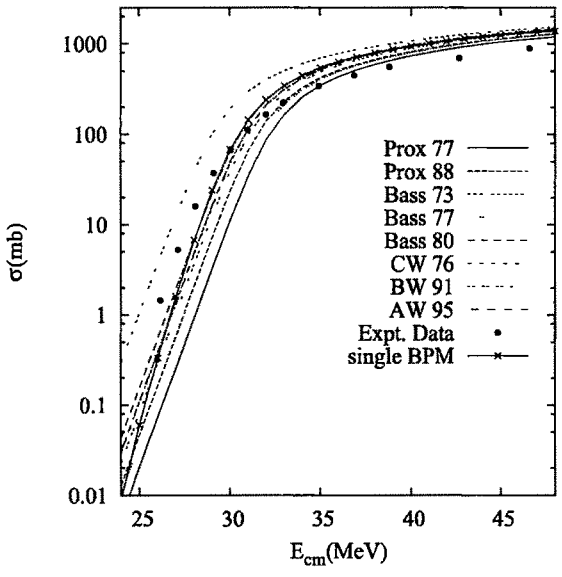

(a) $^{6}Li+^{209}Bi$

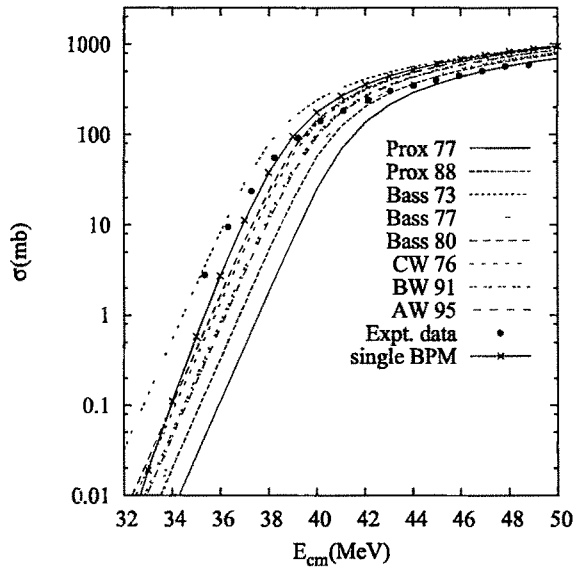

(b) $^{9}Be+^{208}Pb$

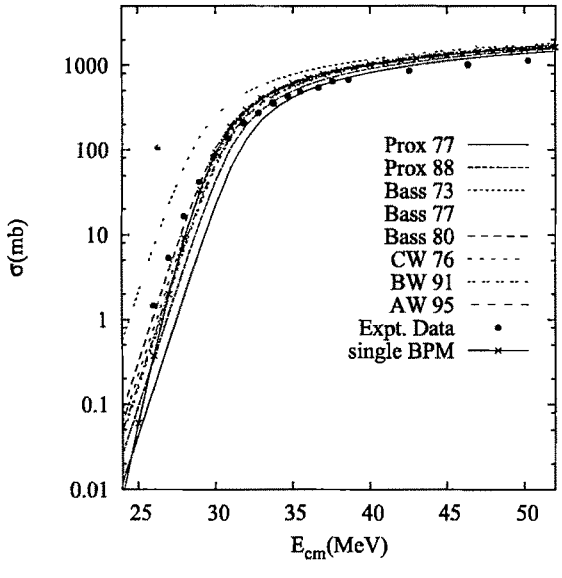

(c) $^{7}Li+^{209}Bi$

Figure 3.2: Fusion cross-section vs energy calculated from Wong's formula for eight versions of the nuclear Potential for the reactions (a) $^{6}Li+^{209}Bi$, (b) $^{9}Be+^{208}Pb$, and (c) $^{7}Li+^{209}Bi$. Expt. data are taken from Ref. [21].

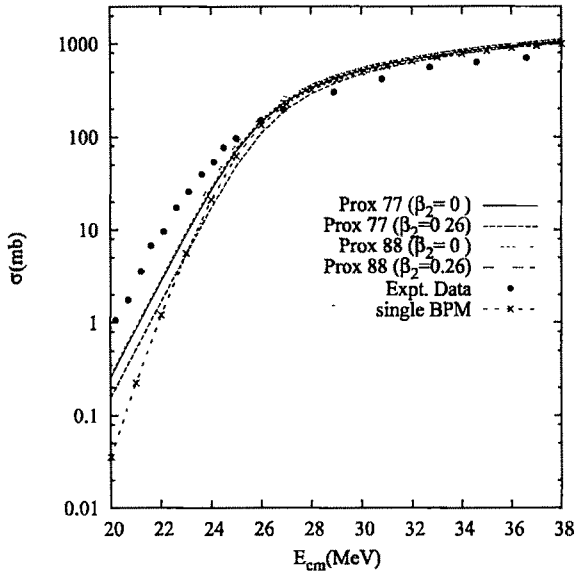

(a) Prox 77 and Prox 88

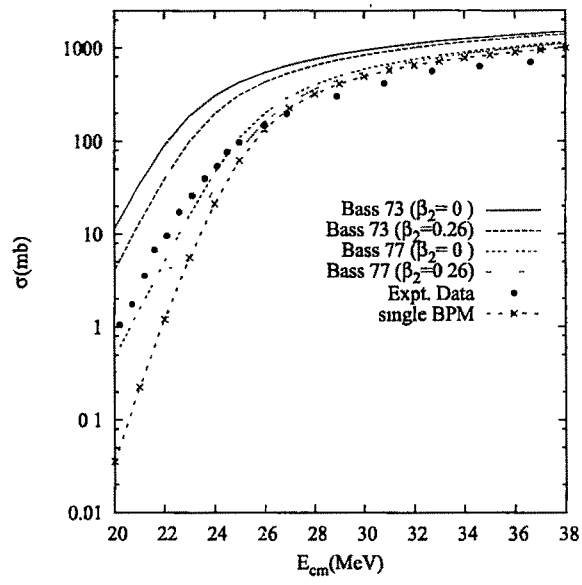

(b) Bass 73 and Bass 77

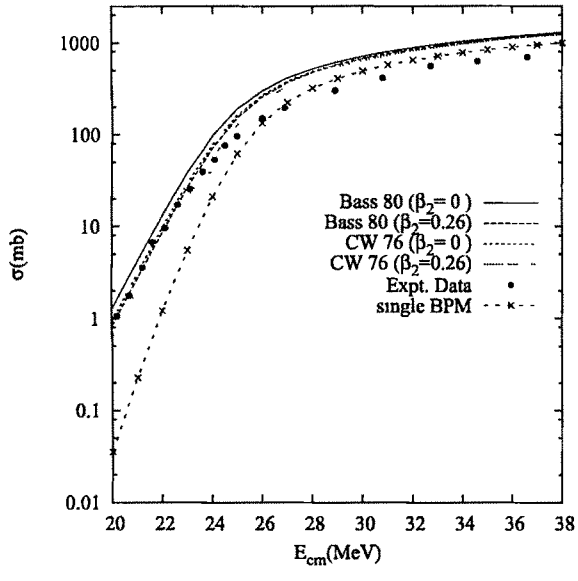

(c) Bass 80 and CW 76

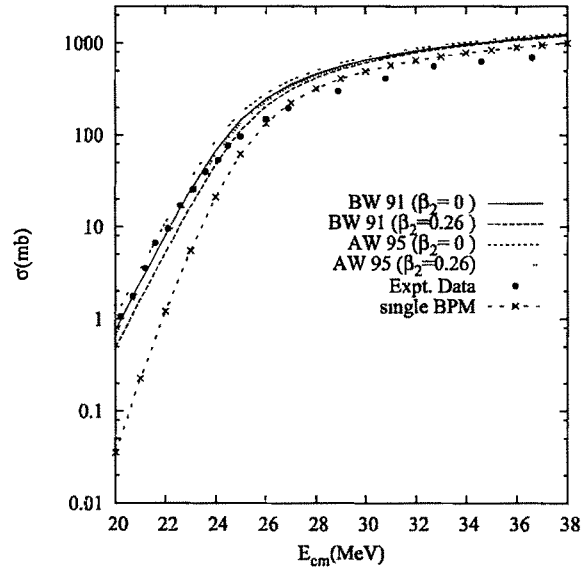

(d) BW 91 and AW 95

Figure 3.3: Fusion cross-section from Wong's formula for $^{6}Li+^{152}Sm$ assuming spherical (β_2=0) and deformed (β_2=0.26) target. Expt. data is taken from Ref. [22].

3.7 Summary and Outlook

Using Wong's formula, we find the fusion cross section for the reactions ^{6}Li+^{209}Bi, ^{9}Be+^{208}Pb and ^{7}Li+^{209}Bi. Values of the barrier parameters are taken from chapter 2. The fusion cross section is greater than the experimental fusion cross section, which is because of the fact that fusion suppression is dominant in these reactions. If comparison is made with respect to the results of single BPM (calculated from CCFULL), then we see that the prediction of the potential Bass 80 is better than the other potentials. For the reaction ^{6}Li+^{152}Sm, fusion cross section is determined on the assumption of spherical as well as deformed target. The results of fusion cross section for deformed target are closer to the results of single BPM. Hence, effects of deformation of the target nucleus ^{152}Sm is clearly seen.

The Wong's formalism gives accurate results for energies greater than about 1.2 times the barrier energy. For energies near or below the barrier one must resort to the exact coupled channels calculations which can be done with the code CCFULL with proper consideration of target (and projectile) excited (rotational or vibrational) states. For the reactions considered here the fusion cross section can also be studied through the Wong's formalism using the barrier parameters deduced from other nuclear potentials like the the Denisov potential, double-folding potential or the Skyrme nuclear interaction. Further improvement of fusion cross section can be done through the extended Wong's formalism in which the ℓ-dependent barriers are introduced via the ℓ-summation, or through Balantekin's improvement of Wong's formula (Eq. 3.21).

Bibliography

[1] K. P. Santosh, B. Priyanka, and M.S. Unnikrishnan, *Phys. Rev. C*, **85**, 034604, (2012)

[2] K. P. Santosh, V. Bobby Jose, Antony Joseph and K. M. Varier, *Nucl. Phys. A*, **817**, 35, (2009)

[3] I.Dutt and R.K. Puri, *Phys. Rev. C*, **81**, 064609, (2010)

[4] I.Dutt and R.K. Puri, *Phys. Rev. C*, **81**, 044615, (2010)

[5] Raj Kumar, Manie Bansal, Sham K. Arun, and Raj K. Gupta, *Phys. Rev. C*, **80**, 034618, (2009)

[6] Raj Kumar, *Phys. Rev. C*, **84**, 044613, (2011)

[7] J. R. Leigh, M. Dasgupta, D. J. Hinde, J. C. Mein, C. R. Morton, R. C. Lemmon, J. P. Lestone, J. O. Newton, H. Timmers, J. X. Wei, and N. Rowley , *Phys. Rev. C*, **52**, 3151, (1995)

[8] Raj Kumar, Manoj K. Sharma, and Raj K. Gupta, *Nucl. Phys. A*, **870-871**, 42-57, (2011)

[9] D.J. Hinde, C.R. Morton, M. Dasgupta, J.R. Leigh, J.C. Mein, H. Timmers, *Nucl. Phys. A*, **592**, 271, (1995)

[10] C. R. Morton, D. J. Hinde, J. R. Leigh, J. P. Lestone, M. Dasgupta, J. C. Mein, J. O. Newton, and H. Timmers, *Phys. Rev. C*, **52**, 243, (1995)

[11] J. D. Bierman, P. Chan, J. F. Liang, M. P. Kelly, A. A. Sonzogni, and R. Vandenbosch, *Phys. Rev. C*, **54**, 3068, (1996)

[12] D. M. Brink and U. Smilansky, *Nucl. Phys. A*, **405**, 301, (1983)

[13] D. L. Hill and J. A. Wheeler, *Phys. Rev.*, **89**, 1102, (1953)

[14] L. D. Landau and E. M. Lifschitz, *Quantum Mechanics*, 3rd ed.,(Permagon Press, Oxford, 1975) ; E. Kemble, *Phys. Rev.*, **48**, 549, (1935)

[15] C. Y. Wong , *Phys. Rev. Lett.*, **31**, 766, (1973)

[16] C. Y. Wong , *Phys. Lett. B*, **42**, 186, (1972)

[17] A. B. Balantekin and A. J. DeWeerd, *Phys. Rev. C*, **54**, 1853, (1996)

[18] K. Hagino, N. Rowley and A.T. Kruppa, *Comp. Phys. Comm.*, **123**, 143, (1999)

[19] L. F. Canto, P. R. S. Gomes, J. Lubian , L.C. Chamon and E. Crema, *Nucl. Phys. A*, **821**, 51, (2009)

[20] C. K. Phookan and K. Kalita, *Nucl. Phys. A*, **899**, 29, (2013)

[21] M. Dasgupta, P. R. S. Gomes, D. J. Hinde, S. B. Moraes, R. M. Anjos, A. C. Berriman, R. D. Butt, N. Carlin, J. Lubian, C. R. Morton, J. O. Newton, and A. Szanto de Toledo, *Phys. Rev. C*, **70**, 024606, (2004)

[22] P.K. Rath, S.Santra, N.L. Singh, K. Mahata, R. Palit, B.K. Nayak, K. Ramachandran, V.V. Parkar, R. Tripathi, S.K. Pandit, S. Appannababu, N.N. Deshmukh, R.K. Choudhury and S. Kailas, *Nucl. Phys. A*, **874**, 14-31, (2012)

Chapter 4

Semi-classical model of fusion suppression for reactions induced by ^{6}Li

4.1 Introduction

During the last decade and a half there has been marked improvement in experimental facilities, and also intense beams of loosely bound nuclei as well as the radioactive-ion beam have become available [1, 2, 3]. Hence, heavy ion collisions with loosely bound nuclei has become an active and exciting field of research [4, 5]. A huge amount of fusion cross-section data has been collected over the years. One common feature is that the experimentally measured fusion cross-section is fractionally less than the theoretically expected fusion cross-section. This fact has been noted in the previous chapter, where the theoretically calculated fusion cross-section from Wong's formula and the SBPM model is found to be somewhat greater than the experimentally measured fusion cross section. The theoretical fusion cross-section can be obtained from the one-dimensional barrier penetration model (for energies above the barrier), or from the code CCFULL (for low energies). The ratio between

the experimental (σ_{exp}) and theoretical fusion cross section (σ_{theo}) is called fusion suppression [6],

$$\text{Fusion Suppression} = \frac{\text{experimental fusion cross section}}{\text{theoretical fusion cross section}} = \frac{\sigma_{\text{exp}}}{\sigma_{\text{theo}}} \tag{4.1}$$

The reason for the decrease in the experimental fusion cross-section is attributed to the breakup of the loosely bound projectile. Because of the strong interaction with a heavy target nuclei (eg. ^{144}Sm, ^{209}Bi), the loosely bound projectile breaks up which results in a decrease of the fusion cross section. Here, at least four different types of events have been identified [6]. When the whole of the projectile fuses with the target without breakup, then it is called direct complete fusion (DCF). After breakup, if both the fragments fuse with the target, then it is called sequential complete fusion (SCF). If one of the breakup fragments fuse with the target, then it is called incomplete fusion (ICF). If none of the breakup fragments fuse with the target, then it is called no-capture breakup (NCBU). The four type of events are shown schematically in Fig 4.1.

In this chapter, we present a semiclassical model for the explanation of fusion suppression. In the next section (section 4.2), we provide the review work for fusion suppression, and also discuss the the theoretical work that has been done by various authors for explanation of projectile breakup and fusion suppression. This would be followed by a brief outline (section 4.3) of our approach in tackling the problem. Sections 4.4, 4.5 and 4.6 discuss the theory for obtaining the classical equations of motion. In the next section, we discuss the model of ^{6}Li that we have introduced for obtaining solutions. In sections 4.8 and 4.9 we discuss the method for obtaining numerical solutions and the nature of the solutions respectively. Section 4.10, 4.11 and 4.12 discusses the complete methodology for the explanation of fusion suppression including evaluation of cutoff impact parameter. In the next section, results and discussion are presented. Finally in section 4.15, we provide the summary and

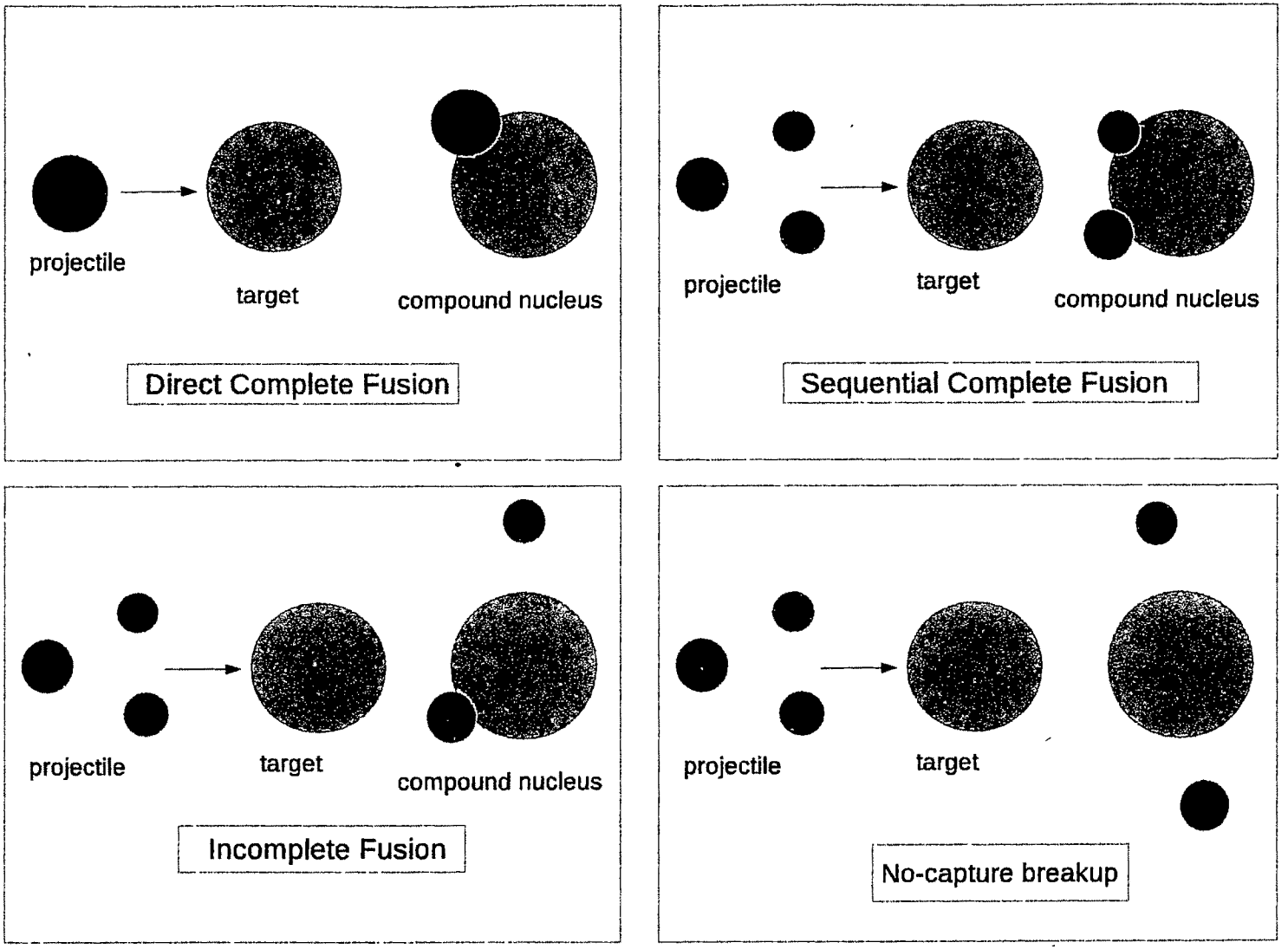

Figure 4.1: Four different types of events during collision of a loosely bound projectile with a heavy target.

also discuss possible future outlook.

4.2 Review work on projectile breakup and fusion suppression

As noted in section 4.1, reactions initiated by loosely bound projectiles (^{6}Li ,^{7}Li, ^{9}Be) have led to four distinct types of events. These are direct complete fusion (DCF), sequential complete fusion (SCF), incomplete fusion (ICF) and no-capture breakup (NCBU). These events are a direct consequence of the breakup of the projectile before they reach the target. As a result, the experimental cross section falls below the theoretically expected value, and the ratio between the two is often called fusion suppression. Fusion reactions induced by loosely bound projectiles have been studied on a wide range of medium and heavy targets like ^{209}Bi, ^{208}Pb, ^{159}Tb, ^{152}Sm, ^{144}Sm, ^{124}Sn, ^{89}Y, etc [7, 8, 9, 10, 11, 12, 13]. M. Dasgupta et. al. [7], studied the fusion cross section for the reactions ^{6}Li+^{209}Bi, ^{7}Li+^{209}Bi, and ^{9}Be+^{208}Pb at energies near and above the Coulomb barrier using the 14UD tandem accelerator at the Australian National University. By using three different and conclusive methods it was shown that fusion cross-section is suppressed by $\approx$ 30 % for the three reactions. Using the 14UD BARC-TIFR pelletron accelerator facility at Mumbai, P. K. Rath et al. performed fusion cross-section measurements of ^{6}Li on Samarium isotopes (^{144}Sm and ^{152}Sm) [8, 9]. For both the reactions evaporation of neutrons (1n, 2n, 3n, 4n and 5n) are the primary decay modes, and these were measured using the recoil catcher technique followed by off-line γ-ray spectrometry. Statistical model calculations using PACE code were done for estimating the contribution from the missing channels. After comparison with theoretical expectations, it was found that fusion cross section is suppressed by $\approx$ 32 % and 28 % for the reactions ^{6}Li+^{144}Sm and ^{6}Li+^{152}Sm, respectively. M. K. Pradhan found that the fusion suppression for the reaction ^{6}Li+^{159}Tb is $\approx$ 34 % [12]. Through a comparison of the fusion

suppression factors for the reactions ^{7}Li+^{159}Tb and ^{10}B+^{159}Tb, he could show that the suppression factor is inversely related with the α breakup threshold energy of the projectile. C. S. Palshetkar [14] found that the fusion excitation functions for ^{9}Be+^{89}Y is suppressed by (20±5)% as compared to the ones predicted by coupled-channels calculations that do not include couplings to the projectile continuum. Further confirmation of fusion suppression was obtained by comparison of fusion data for two more systems, namely, for ^{4}He+^{93}Nb and ^{12}C+^{89}Y, which involve tightly bound projectiles and form compound nuclei nearby to that formed in the reaction ^{9}Be+^{89}Y. Similar work involving ^{9}Be projectile has been done by other authors, namely, V. V. Parker on ^{124}Sn target [15], P. R. S Gomes on ^{144}Sm target [10], and Z. H. Liu on ^{209}Bi target [16]. The theoretically expected value of the fusion cross section in the absence of breakup can be calculated from the computer code CCFULL [17]. This code is remarkably successful in explaining the fusion cross section of tightly bound projectiles.

The calculation of breakup yields for reactions induced by loosely bound projectiles has been done by quantum as well as classical methods. The continuum-discretized coupled channels method (CDCC) [18] is the most widely applied quantum method for treating the breakup of a projectile. In the early seventies it became clear that the breakup of deuteron beams couldn't be well described by Born approximation, and required a careful treatment of the continuum. Since those early days, CDCC methods have evolved for the description of three-body as well as four-body breakup. A brief description of the three-body CDCC method is as follows. Here, the total wave function of the 3-body system (projectile + target) is expanded in terms of the complete eigen functions of the 2-body projectile. The eigen functions are composed of bound and continuum states and breakup of the projectile takes place when it reaches the continuum states. For practical applications, the continuum states are truncated at some maximum values of the angular momentum (ℓ_{max}) and the linear momentum (k_{max}). Accurate results may not always be pos-

sible [19, 20] with the CDCC method because of the above approximation and also due to discretization of the continuum. Also, CDCC methods cannot distinguish between complete fusion and incomplete fusion events because it requires a time dependent description of the process. These difficulties are overcome by the classical trajectory model in which the time evolution of the breakup fragments of the projectile can be studied through solutions of the Newtonian equations of motion.

The chief contributors towards the development of the classical model are K. Hagino, M. Dasgupta, Alexis Diaz-Torres, and others. Hagino's two-dimensional classical trajectory model [21] is developed by constructing the classical equations of motion of the three body (target+projectile) system. Events like scattering, incomplete fusion and no-capture breakup could be obtained from numerical solutions of the equations of motion. The loosely bound projectile is considered to be a two-body system held under the combined influence of Coulomb and nuclear potentials. However, the initial conditions for the equations of motion were obtained arbitrarily, without reference to any physical principles. He concluded by remarking that his work could be incorporated into the CDCC formalism. In Alexis Diaz-Torres's classical dynamical model [22, 23, 24], breakup of the projectile is determined through an empirically obtained breakup probability function. Sub-barrier no-capture breakup measurements are used for determining the parameters of this function. The method has been successfully used to determine the breakup yields of reactions induced by ^{9}Be on a number of targets, and also to predict the fusion suppression factors [24]. However, the method has a disadvantage as it can only work with inputs from precise experimental data in order to determine the breakup probability function. Classical trajectory method has been applied to study other problems like ionization of an atom. Ionization is in some respects similar to the breakup of a projectile as it involves the removal of an electron from an atom. In Ref. [25], ionization of the hydrogen atom in an intense laser field has been studied by classical trajectory method. It was found that the classical results match the

exact quantum mechanical results only if tunnelling is taken into account at the classical turning points.

4.3 Brief outline of our approach

In this work, we present a semi-classical model for determining the fusion suppression factor, and shall be applying it to the reactions ^{6}Li+^{209}Bi, ^{6}Li+^{152}Sm and ^{6}Li+^{144}Sm. The problem is separated into two parts. In the first part, the cutoff impact parameter (b_c) for fusion is determined, and in the second part we find out the fraction of projectiles undergoing breakup within this cutoff impact parameter. As fusion is a quantum mechanical barrier transmission problem, hence the cutoff impact parameter is evaluated by applying quantum mechanical methods. For determining the relative number of projectile breakup, we use Hagino's two-dimensional classical trajectory method [21]. Then the breakup fraction of the projectile is determined as a function of the impact parameter. A simple formula for explanation of fusion suppression is introduced, according to which fusion suppression is given by the average of the breakup fractions evaluated at impact parameters ranging from head-on collision up to the cutoff impact parameter.

The choice of the targets (^{209}Bi, ^{144}Sm and ^{152}Sm) have been motivated due to the availability of precise fusion excitation data for these reactions, and also due to the fact that very high fusion suppression is observed for these reactions. We have limited our work to ^{6}Li projectile because breakup of ^{7}Li and ^{9}Be involves complicated process. The dominant channel for breakup of ^{7}Li involves a proton pickup from the target to form ^{8}Be, which then breaks up into two α-particles [26]. For ^{9}Be, the breakup process involves a neutron transfer to the target to form ^{8}Be, which finally breaks up into two α-particles [24].

4.4 Lagrangian for the system

We first construct the Lagrangian in two dimensions for the system of projectile and target [21]. We consider the projectile to be composed of two point particles, and the target is assumed to be a sphere of radius r_c. The nuclear potential energy is assumed to have a Woods-Saxon form, whose parameters are obtained from optical model analysis of elastic scattering data. The Lagrangian assumes the form,

$$\mathcal{L} = \frac{1}{2}m_1(\dot{x}_1^2 + \dot{y}_1^2) + \frac{1}{2}m_2(\dot{x}_2^2 + \dot{y}_2^2) + \frac{1}{2}m_3(\dot{x}_3^2 + \dot{y}_3^2) - V_{12} - V_{13} - V_{23} \qquad (4.2)$$

where, subscripts 1 and 2 denote the two projectile fragments, and subscript 3 denote the target. V_{12} is the potential energy between the two components of the projectile, and is given by,

$$V_{12} = -\frac{v_1}{1 + exp^{(r-r_1)/a_1}} + \frac{e^2 Z_1 Z_2}{r} \quad , \quad r = \sqrt{(x_1 - x_2)^2 + (y_1 - y_2)^2} \qquad (4.3)$$

V_{13} is the potential energy between one component of the projectile and the target and is given by,

$$V_{13} = -\frac{v_2}{1 + exp^{(r-r_2)/a_2}} + U_{13} \quad , \quad r = \sqrt{(x_1 - x_3)^2 + (y_1 - y_3)^2} \qquad (4.4)$$

V_{23} is the potential energy between the remaining component of the projectile and the target and is given by,

$$V_{23} = -\frac{v_3}{1 + exp^{(r-r_3)/a_3}} + U_{23} \quad , \quad r = \sqrt{(x_2 - x_3)^2 + (y_2 - y_3)^2} \qquad (4.5)$$

here, (v_i, r_i, a_i) (i=1,2,3) are the parameters of the respective Woods-Saxon potential, and U_{ij} is the Coulomb potential energy between the projectile fragment and the target. As we had assumed the charge of the target nucleus to be uniformly

distributed over a sphere of radius r_c, hence,

$$U_{ij} = \begin{cases} \frac{Z_i Z_j e^2}{2r_c}\left(3 - \frac{r^2}{r_c^2}\right) & \text{if} \quad r \leq r_c, \\ \\ \frac{Z_i Z_j e^2}{r} & \text{if} \quad r > r_c, \end{cases} \tag{4.6}$$

where, r_c is the radius of the target nucleus and is given by, r_i=1.28$A_i^{1/3}$+0.8$A_i^{-1/3}$-0.76 fm [4, 5]. The boundary conditions of the problem are well defined in Cartesian coordinates. Hence, we rewrite the Lagrangian in Cartesian coordinates,

$$\mathcal{L} = \frac{1}{2}m_1(\dot{x}_1^2 + \dot{y}_1^2) + \frac{1}{2}m_2(\dot{x}_2^2 + \dot{y}_2^2) + \frac{1}{2}m_3(\dot{x}_3^2 + \dot{y}_3^2) - \frac{e^2 Z_1 Z_2}{\sqrt{(x_1 - x_2)^2 + (y_1 - y_2)^2}} + \frac{v_1}{1 + e^{\sqrt{(x_1-x_2)^2+(y_1-y_2)^2}-r_1)/a_1}} - U_{13} + \frac{v_2}{1 + e^{\sqrt{(x_1-x_3)^2+(y_1-y_3)^2}-r_2)/a_2}} - U_{23} + \frac{v_3}{1 + e^{\sqrt{(x_2-x_3)^2+(y_2-y_3)^2}-r_3)/a_3}} \tag{4.7}$$

The Coulomb potential energy between a component of the projectile and the target is given by,

$$U_{ij} = \begin{cases} \frac{Z_i Z_j e^2}{2r_c}\left[3 - \frac{(x_i-x_j)^2+(y_i-y_j)^2}{r_c^2}\right] & \text{if } \sqrt{(x_i - x_j)^2 + (y_i - y_j)^2} \leq r_c, \\ \frac{Z_i Z_j e^2}{\sqrt{(x_i-x_j)^2+(y_i-y_j)^2}} & \text{if } \sqrt{(x_i - x_j)^2 + (y_i - y_j)^2} > r_c. \end{cases} \tag{4.8}$$

4.5 Equations of motion for the system

From the Lagrangian given by Eqs. 4.7 and 4.8, we construct the equations of motion from Lagrange's equation,

$$\frac{d}{dt}\frac{\partial \mathcal{L}}{\partial \dot{q}_j} - \frac{\partial \mathcal{L}}{\partial q_j} = 0 \tag{4.9}$$

where, the generalized coordinate (q_j) stands for the the x and y coordinates of the three particles, i.e., x_1, x_2, x_3, y_1, y_2 and y_3. The equations of motion are given by,

$$m_1\ddot{x_1} = \frac{\partial \mathcal{L}}{\partial x_1} \tag{4.10}$$

$$m_1\ddot{y_1} = \frac{\partial \mathcal{L}}{\partial y_1} \tag{4.11}$$

$$m_2\ddot{x_2} = \frac{\partial \mathcal{L}}{\partial x_2} \tag{4.12}$$

$$m_2\ddot{y_2} = \frac{\partial \mathcal{L}}{\partial y_2} \tag{4.13}$$

$$m_3\ddot{x_3} = \frac{\partial \mathcal{L}}{\partial x_3} \tag{4.14}$$

$$m_3\ddot{y_3} = \frac{\partial \mathcal{L}}{\partial y_3} \tag{4.15}$$

The derivative of the Lagrangian with respect to the independent variables (x_1, y_1, x_2, y_2, x_3, y_3) are given below,

$$\frac{\partial \mathcal{L}}{\partial x_1} = -\frac{\partial U_{13}}{x_1} - \frac{\partial U_{23}}{x_1} + \frac{e^2 Z_1 Z_2 (x_1 - x_2)}{\left[(x_1 - x_2)^2 + (y_1 - y_2)^2\right]^{3/2}}$$

$$- \frac{(v_1/a_1) e^{\sqrt{(x_1-x_2)^2+(y_1-y_2)^2} - r_1)/a_1}}{\left[1 + e^{\sqrt{(x_1-x_2)^2+(y_1-y_2)^2} - r_1)/a_1}\right]^2} \frac{(x_1 - x_2)}{\sqrt{(x_1 - x_2)^2 + (y_1 - y_2)^2}}$$

$$- \frac{(v_2/a_2) e^{\sqrt{(x_1-x_3)^2+(y_1-y_3)^2} - r_2)/a_2}}{\left[1 + e^{\sqrt{(x_1-x_3)^2+(y_1-y_3)^2} - r_2)/a_2}\right]^2} \frac{(x_1 - x_3)}{\sqrt{(x_1 - x_3)^2 + (y_1 - y_3)^2}} \tag{4.16}$$

where,

$$\frac{\partial U_{13}}{x_1} = \begin{cases} -\frac{Z_1 Z_3 e^2}{R_c^3}(x_1 - x_3) & \text{if } \sqrt{(x_1-x_3)^2+(y_1-y_3)^2} \le r_c, \\ -\frac{Z_1 Z_3 e^2 (x_1-x_3)}{\left[(x_1-x_3)^2+(y_1-y_3)^2\right]^{3/2}} & \text{if } \sqrt{(x_1-x_3)^2+(y_1-y_3)^2} > r_c. \end{cases} \tag{4.17}$$

$$\frac{\partial U_{23}}{\partial x_1} = 0 \tag{4.18}$$

$$\frac{\partial \mathcal{L}}{\partial y_1} = -\frac{\partial U_{13}}{y_1} - \frac{\partial U_{23}}{y_1} + \frac{e^2 Z_1 Z_2 (y_1 - y_2)}{\left[(x_1-x_2)^2+(y_1-y_2)^2\right]^{3/2}}$$

$$- \frac{(v_1/a_1) e^{\sqrt{(x_1-x_2)^2+(y_1-y_2)^2}-r_1)/a_1}}{\left[1+e^{\sqrt{(x_1-x_2)^2+(y_1-y_2)^2}-r_1)/a_1}\right]^2} \frac{(y_1-y_2)}{\sqrt{(x_1-x_2)^2+(y_1-y_2)^2}}$$

$$- \frac{(v_2/a_2) e^{\sqrt{(x_1-x_3)^2+(y_1-y_3)^2}-r_2)/a_2}}{\left[1+e^{\sqrt{(x_1-x_3)^2+(y_1-y_3)^2}-r_2)/a_2}\right]^2} \frac{(y_1-y_3)}{\sqrt{(x_1-x_3)^2+(y_1-y_3)^2}} \tag{4.19}$$

where,

$$\frac{\partial U_{13}}{y_1} = \begin{cases} -\frac{Z_1 Z_3 e^2}{r_c^3}(y_1 - y_3) & \text{if } \sqrt{(x_1-x_3)^2+(y_1-y_3)^2} \le r_c, \\ -\frac{Z_1 Z_3 e^2 (y_1-y_3)}{\left[(x_1-x_3)^2+(y_1-y_3)^2\right]^{3/2}} & \text{if } \sqrt{(x_1-x_3)^2+(y_1-y_3)^2} \ge r_c. \end{cases} \tag{4.20}$$

$$\frac{\partial U_{23}}{\partial y_1} = 0 \tag{4.21}$$

$$\frac{\partial \mathcal{L}}{\partial x_2} = -\frac{\partial U_{13}}{\partial x_2} - \frac{\partial U_{23}}{\partial x_2} + \frac{e^2 Z_1 Z_2 (x_1 - x_2)}{\left[(x_1 - x_2)^2 + (y_1 - y_2)^2\right]^{3/2}}$$

$$\frac{(v_1/a_1) e^{\sqrt{(x_1-x_2)^2+(y_1-y_2)^2}-r_1)/a_1}}{\left[1 + e^{\sqrt{(x_1-x_2)^2+(y_1-y_2)^2}-r_1)/a_1}\right]^2} \frac{(x_1 - x_2)}{\sqrt{(x_1 - x_2)^2 + (y_1 - y_2)^2}}$$

$$- \frac{(v_3/a_3) e^{\sqrt{(x_2-x_3)^2+(y_2-y_3)^2}-r_3)/a_3}}{\left[1 + e^{\sqrt{(x_2-x_3)^2+(y_2-y_3)^2}-r_2)/a_2}\right]^2} \frac{(x_2 - x_3)}{\sqrt{(x_2 - x_3)^2 + (y_2 - y_3)^2}} \quad (4.22)$$

where,

$$\frac{\partial U_{23}}{\partial x_2} = \begin{cases} -\frac{Z_2 Z_3 e^2}{r_c^3}(x_2 - x_3) & \text{if } \sqrt{(x_2 - x_3)^2 + (y_2 - y_3)^2} \leq r_c, \\ -\frac{Z_2 Z_3 e^2 (y_2 - y_3)}{\left[(x_2-x_3)^2+(y_2-y_3)^2\right]^{3/2}} & \text{if } \sqrt{(x_2 - x_3)^2 + (y_2 - y_3)^2} > r_c. \end{cases} \quad (4.23)$$

$$\frac{\partial U_{13}}{\partial x_2} = 0 \quad (4.24)$$

$$\frac{\partial \mathcal{L}}{\partial y_2} = -\frac{\partial U_{13}}{\partial y_2} - \frac{\partial U_{23}}{\partial y_2} - \frac{Z_1 Z_2 e^2 (y_1 - y_2)}{\left[(x_1 - x_2)^2 + (y_1 - y_2)^2\right]^{3/2}}$$

$$\frac{(v_1/a_1) e^{\sqrt{(x_1-x_2)^2+(y_1-y_2)^2}-r_1)/a_1}}{\left[1 + e^{\sqrt{(x_1-x_2)^2+(y_1-y_2)^2}-r_1)/a_1}\right]^2} \frac{(x_1 - x_2)}{\sqrt{(y_1 - y_2)^2 + (y_1 - y_2)^2}}$$

$$- \frac{(v_3/a_3) e^{\sqrt{(x_2-x_3)^2+(y_2-y_3)^2}-r_3)/a_3}}{\left[1 + e^{\sqrt{(x_2-x_3)^2+(y_2-y_3)^2}-r_3)/a_3}\right]^2} \frac{(y_2 - y_3)}{\sqrt{(x_2 - x_3)^2 + (y_2 - y_3)^2}} \quad (4.25)$$

where,

$$\frac{\partial U_{23}}{\partial y_2} = \begin{cases} -\frac{Z_2 Z_3 e^2}{R_c^3}(y_2 - y_3) & \text{if } \sqrt{(x_2 - x_3)^2 + (y_2 - y_3)^2} \leq r_c, \\ -\frac{Z_2 Z_3 e^2 (y_2 - y_3)}{\left[(x_2 - x_3)^2 + (y_2 - y_3)^2\right]^{3/2}} & \text{if } \sqrt{(x_2 - x_3)^2 + (y_2 - y_3)^2} > r_c. \end{cases} \tag{4.26}$$

$$\frac{\partial U_{13}}{\partial y_2} = 0 \tag{4.27}$$

$$\frac{\partial \mathcal{L}}{\partial x_3} = -\frac{\partial U_{13}}{\partial x_3} + \frac{(v_2/a_2) e^{\sqrt{(x_1 - x_3)^2 + (y_1 - y_3)^2} - r_2)/a_2}}{\left[1 + e^{\sqrt{(x_1 - x_3)^2 + (y_1 - y_3)^2} - r_2)/a_2}\right]^2} \frac{(x_1 - x_3)}{\sqrt{(x_1 - x_3)^2 + (y_1 - y_3)^2}}$$

$$- \frac{\partial U_{23}}{\partial x_3} + \frac{(v_3/a_3) e^{\sqrt{(x_2 - x_3)^2 + (y_2 - y_3)^2} - r_3)/a_3}}{\left[1 + e^{\sqrt{(x_2 - x_3)^2 + (y_2 - y_3)^2} - r_3)/a_3}\right]^2} \frac{(x_2 - x_3)}{\sqrt{(x_2 - x_3)^2 + (y_2 - y_3)^2}} \tag{4.28}$$

where,

$$\frac{\partial U_{13}}{\partial x_3} = \begin{cases} \frac{Z_1 Z_3 e^2}{r_c^3}(x_1 - x_3) & \text{if } \sqrt{(x_1 - x_3)^2 + (y_1 - y_3)^2} \leq r_c, \\ \frac{Z_1 Z_3 e^2 (x_1 - x_3)}{\left[(x_1 - x_3)^2 + (y_1 - y_3)^2\right]^{3/2}} & \text{if } \sqrt{(x_1 - x_3)^2 + (y_1 - y_3)^2} > r_c. \end{cases} \tag{4.29}$$

$$\frac{\partial U_{23}}{\partial x_3} = \begin{cases} \frac{Z_2 Z_3 e^2}{r_c^3}(x_2 - x_3) & \text{if } \sqrt{(x_2 - x_3)^2 + (y_2 - y_3)^2} \leq r_c, \\ \frac{Z_2 Z_3 e^2 (x_2 - x_3)}{\left[(x_2 - x_3)^2 + (y_2 - y_3)^2\right]^{3/2}} & \text{if } \sqrt{(x_2 - x_3)^2 + (y_2 - y_3)^2} > r_c. \end{cases} \tag{4.30}$$

$$\frac{\partial \mathcal{L}}{\partial y_3} = -\frac{\partial U_{13}}{\partial y_3} + \frac{(v_2/a_2)e^{\sqrt{(x_1-x_3)^2+(y_1-y_3)^2}-r_2)/a_2}}{\left[1+e^{\sqrt{(x_1-x_3)^2+(y_1-y_3)^2}-r_2)/a_2}\right]^2}\frac{(y_1-y_3)}{\sqrt{(x_1-x_3)^2+(y_1-y_3)^2}}$$

$$-\frac{\partial U_{23}}{\partial y_3} + \frac{(v_3/a_3)e^{\sqrt{(x_2-x_3)^2+(y_2-y_3)^2}-r_3)/a_3}}{\left[1+e^{\sqrt{(x_2-x_3)^2+(y_2-y_3)^2}-r_3)/a_3}\right]^2}\frac{(y_2-y_3)}{\sqrt{(x_2-x_3)^2+(y_2-y_3)^2}} \quad (4.31)$$

where,

$$\frac{\partial U_{13}}{\partial y_3} = \begin{cases} \frac{Z_1 Z_3 e^2}{r_c^3}(y_1-y_3) & \text{if } \sqrt{(x_1-x_3)^2+(y_1-y_3)^2} \le r_c, \\ \frac{Z_1 Z_3 e^2 (y_1-y_3)}{\left[(x_1-x_3)^2+(y_1-y_3)^2\right]^{3/2}} & \text{if } \sqrt{(x_1-x_3)^2+(y_1-y_3)^2} > r_c. \end{cases} \quad (4.32)$$

$$\frac{\partial U_{23}}{\partial y_3} = \begin{cases} \frac{Z_2 Z_3 e^2}{r_c^3}(y_2-y_3) & \text{if } \sqrt{(x_2-x_3)^2+(y_2-y_3)^2} \le r_c, \\ \frac{Z_2 Z_3 e^2 (y_2-y_3)}{\left[(x_2-x_3)^2+(y_2-y_3)^2\right]^{3/2}} & \text{if } \sqrt{(x_2-x_3)^2+(y_2-y_3)^2} > r_c. \end{cases} \quad (4.33)$$

4.6 Initial conditions of the system

The system under consideration basically consists of three particles in two dimensions (x and y coordinates). Hence, from the Lagrange's equations of motion, six second order differential equations are obtained. By a change of variable twelve first order differential equations are constructed. These twelve first order differential equations can be solved only if twelve initial conditions are known. These twelve initial conditions are the positions and velocities of the x and y components of the deuteron, α-particle and the target. The position of the target is conveniently chosen to be at the origin, and is initially at rest. The deuteron and the α-particle constituting the ^{6}Li nucleus, is arbitrarily oriented at an angle θ which is measured from their centre of mass to the direction of the y-axis. Therefore, the 12 initial

conditions are,

$$
\begin{aligned}
x_1(0) &= R - r_1 sin(\theta) \\
\dot{x}_1(0) &= V + v_1 cos(\theta) \\
y_1(0) &= b + r_1 cos(\theta) \\
\dot{y}_1(0) &= v_1 sin(\theta) \\
x_2(0) &= R + r_2 sin(\theta) \\
\dot{x}_2(0) &= V - v_2 cos(\theta) \\
y_2(0) &= b - r_2 cos(\theta) \\
\dot{y}_2(0) &= -v_2 sin(\theta) \\
x_3(0) &= 0 \\
\dot{x}_3(0) &= 0 \\
y_3(0) &= 0 \\
\dot{y}_3(0) &= 0
\end{aligned} \tag{4.34}
$$

here, subscripts 1, 2 and 3 denote the deuteron, α-particle and the target, respectively, and, V=$\sqrt{(2E_{lab})/m}$ is the velocity of the projectile. R is the initial distance of the centre of mass of the projectile from the target and b is the impact parameter. v_1, v_2 and r_1, r_2 are the velocities and distances of the deuteron and the α-particle with respect to their centre of mass.

4.7 Model of ^{6}Li

Initially, for obtaining numerical solutions arbitrary values of v_1, v_2 and r_1, r_2 were used. In general, chaotic solutions are obtained from arbitrary values of v_1, v_2 and r_1, r_2. Afterwards the values of v_1, v_2 and r_1, r_2 are changed and we observed the

nature of the solutions. The process was continued until stable solutions (free from chaos) were obtained. After repeated trial and error, we choose the values, $r_1 = 2r_2$ = 1.513 fm , $v_1 = 2v_2 = 0.645 \times 10^7$ m.s^{-1} because we could consistently obtain three distinct types of trajectories. These three types of trajectories are : scattering-like, incomplete fusion and no-capture breakup, and these are discussed in section 4.9. Next an attempt was made to derive the values of v_1, v_2 and r_1, r_2 from some fundamental properties of the ^{6}Li nucleus like spin and breakup threshold energy (binding energy).

It was found that these values can be derived by considering a cluster model of the ^{6}Li nucleus which is based upon semiclassical ideas. The motivation for the model is Bohr's model of the hydrogen atom in which the electron revolves around the proton in classical orbits. It has been known for quite some time that ^{6}Li exists as a cluster of a deuteron and an α-particle, and fully quantum mechanical treatment is available in the literature [27]. However, we need a model which is consistent with the idea of classical trajectories. The nucleus ^{6}Li is considered to be composed of a deuteron and an alpha-particle, rotating in circular orbits about their centre of mass with a fixed distance of separation (see fig. 4.2). The positions and velocities of the deuteron and the α-particle are determined from consideration of the total energy and the angular momentum of the system. Hence, two postulates are proposed for the ^{6}Li cluster model : (a) The total energy of the deuteron and the α-particle system is equal to the breakup threshold energy (binding energy) of the ^{6}Li nucleus, and (b) The total angular momentum of rotation of the deuteron and the α-particle about an axis through its centre of mass is equal to $\sqrt{I(I+1)}\hbar$, where I is the spin quantum number of the ^{6}Li nucleus. The calculations are as follows : The deuteron and the α-particle cluster (^{6}Li projectile) are rotating with angular velocity ω about their common centre of mass. Since, the mass of the α-particle is twice the mass of the deuteron, hence, $r_1 = 2r_2$, and $v_1 = 2v_2$. Here, v_1, v_2 and r_1, r_2 are the velocities and distances of the deuteron and the α-particle with respect to their centre of mass.

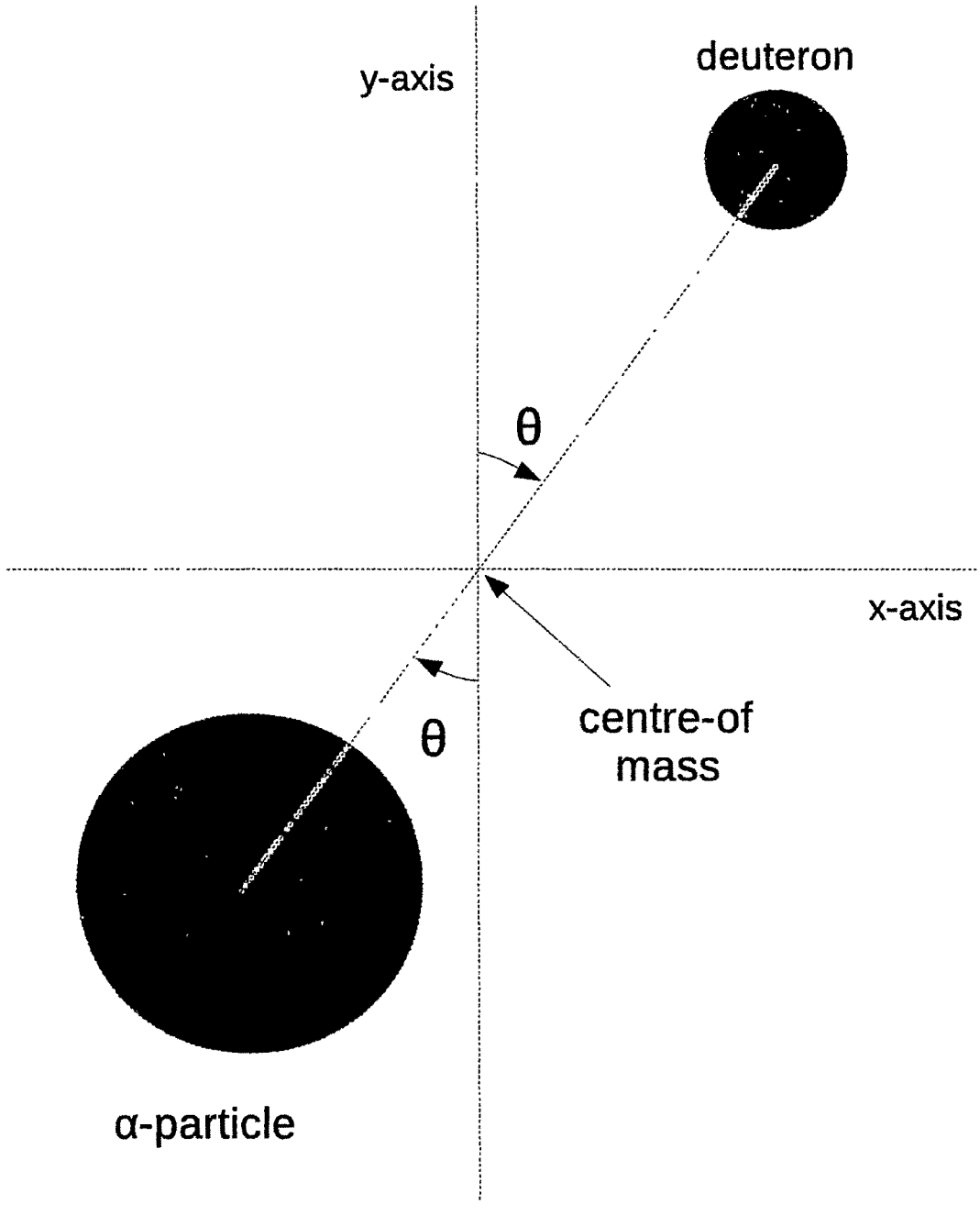

Figure 4.2: Model of ^{6}Li proposed for obtaining boundary conditions

The total energy is given by the sum of the kinetic and potential energies of the two particles,

$$E = \frac{1}{2}m_1v_1^2 + \frac{1}{2}m_2v_2^2 + \frac{Z_1Z_2e^2}{r} - \frac{V_0}{1+e^{(r-r_0)/a}} \tag{4.35}$$

The centrifugal force needed for rotation is provided by the resultant of the Coulomb and nuclear forces,

$$\frac{m_1v_1^2}{r_1} = \frac{\frac{V_0}{a}e^{(r-r_0)/a}}{[1+e^{(r-r_0)/a}]^2} - \frac{Z_1Z_2e^2}{r^2}$$

$$\frac{1}{2}m_1v_1^2 = \frac{\frac{V_0}{2a}r_1e^{(r-r_0)/a}}{[1+e^{(r-r_0)/a}]^2} - \frac{Z_1Z_2e^2r_1}{2r^2} \tag{4.36}$$

Similarly, for the other particle,

$$\frac{1}{2}m_2v_2^2 = \frac{\frac{V_0}{2a}r_2e^{(r-r_0)/a}}{[1+e^{(r-r_0)/a}]^2} - \frac{Z_1Z_2e^2r_2}{2r^2} \tag{4.37}$$

After substituting (4.36) and (4.37) in (4.35), we obtain an expression for the total energy. Here, r=r_1+r_2 is the total distance between the deuteron and the α-particle.

$$E = \frac{\frac{V_0}{2a}re^{(r-r_0)/a}}{[1+e^{(r-r_0)/a}]^2} - \frac{V_0}{1+e^{(r-r_0)/a}} + \frac{Z_1Z_2e^2}{2r} \tag{4.38}$$

Taking, E = 1.48 MeV, the breakup threshold energy of ^{6}Li ($\rightarrow$ ^{2}H+^{4}He), and numerically solving the above equation for the Woods-Saxon parameters (V_0, r_0, a)= (75.5 MeV, 1.85 fm, 0.71 fm) ([28]), we obtain r= 2.27 fm. Using the conditions, r_1= $2r_2$ and r=r_1+r_2, we obtain, r_1= $2r_2$ = 1.513 fm.

To determine the angular velocity of rotation, we use the second postulate which states that the total angular momentum of rotation of the two body system is equal to $\sqrt{2}\hbar$, which is the spin of the ^{6}Li nucleus. Hence,

$$I_1\omega + I_2\omega = \sqrt{2}\hbar \tag{4.39}$$

here, ω is the angular velocity of rotation. I_1 and I_2 are the moments of inertia of

the deuteron and the α-particle, respectively, and are given by,

$$I_1 = \frac{3}{5} m_1 R_1^2 + m_1 r_1^2 \tag{4.40}$$

$$I_2 = \frac{3}{5} m_2 R_2^2 + m_2 r_2^2 \tag{4.41}$$

In the above expression we have assumed the deuteron and the α-particle to be spheres of radii R_1 and R_2, respectively. Determining radius from the approximate relation, R $=1.33A^{1/3}$ fm, we get $\omega = 0.427\times10^{22}$ rad.s^{-1}, and hence, $v_1 = r_1\omega = 0.645\times10^{7}$ m.s^{-1}, and $v_2 = r_2\omega = 0.323\times10^{7}$ m.s^{-1}.

4.8 Numerical solutions

For obtaining numerical solutions, we convert the six second order differential equations (Eqs. 4.10, 4.11, 4.12, 4.13, 4.14, 4.15) into twelve first order differential equations through a change of variable. The twelve first order differential equations are easily solved by applying Euler's method. The actual solution is obtained through the FORTRAN programming language. The twelve first order differential equations are,

$$\dot{x_1} = w_1 \quad ; \quad m_1\dot{w_1} = \frac{\partial \mathcal{L}}{\partial x_1} \tag{4.42}$$

$$\dot{y_1} = z_1 \quad ; \quad m_1\dot{z_1} = \frac{\partial \mathcal{L}}{\partial y_1} \tag{4.43}$$

$$\dot{x_2} = w_2 \quad ; \quad m_2\dot{w_2} = \frac{\partial \mathcal{L}}{\partial x_2} \tag{4.44}$$

$$\dot{y_2} = z_2 \quad ; \quad m_2\dot{z_2} = \frac{\partial \mathcal{L}}{\partial y_2} \tag{4.45}$$

$$\dot{x_3} = w_3 \quad ; \quad m_3\dot{w_3} = \frac{\partial \mathcal{L}}{\partial x_3} \tag{4.46}$$

$$\dot{y_3} = z_3 \quad ; \quad m_3\dot{z_3} = \frac{\partial \mathcal{L}}{\partial y_3} \tag{4.47}$$

The Euler's method is used to solve each of the above first order differential

equations. For a first order differential equation of the form,

$$\dot{y} = f(t) \tag{4.48}$$

Euler's solution is given as,

$$y_{n+1} = y_n + h * f(t) \tag{4.49}$$

where, 'n' is the iteration step and 'h' is an infinitesimal increment of the variable 't'. In our problem, the variable 't' can be identified with the time variable. Applying, Euler's solution to each of the above differential equations,

$$x_{1(n+1)} = x_{1(n)} + h * w_1 \quad ; \quad w_{1(n+1)} = w_{1(n)} + \frac{h}{m_1}\frac{\partial \mathcal{L}}{\partial x_1} \tag{4.50}$$

$$y_{1(n+1)} = y_{1(n)} + h * z_1 \quad ; \quad z_{1(n+1)} = z_{1(n)} + \frac{h}{m_1}\frac{\partial \mathcal{L}}{\partial y_1} \tag{4.51}$$

$$x_{2(n+1)} = x_{2(n)} + h * w_2 \quad ; \quad w_{2(n+1)} = w_{2(n)} + \frac{h}{m_2}\frac{\partial \mathcal{L}}{\partial x_2} \tag{4.52}$$

$$y_{2(n+1)} = y_{2(n)} + h * z_2 \quad ; \quad z_{2(n+1)} = z_{2(n)} + \frac{h}{m_2}\frac{\partial \mathcal{L}}{\partial y_2} \tag{4.53}$$

$$x_{3(n+1)} = x_{3(n)} + h * w_3 \quad ; \quad w_{3(n+1)} = w_{3(n)} + \frac{h}{m_3}\frac{\partial \mathcal{L}}{\partial x_3} \tag{4.54}$$

$$y_{3(n+1)} = y_{3(n)} + h * z_3 \quad ; \quad z_{3(n+1)} = z_{3(n)} + \frac{h}{m_3}\frac{\partial \mathcal{L}}{\partial y_3} \tag{4.55}$$

For obtaining the solutions, the values of the variables (initial conditions) have to be provided at the first step. The above numerical recipe automatically calculates the values of the variables in the second step. Taking these values as input, the new values of the variables are obtained in the third step. The process is continued and ideally we could obtain solutions for any desired number of steps. However, in reality the number of steps that can be carried out is limited by the memory and the processing speed of the computer. Hence, the initial distance between target and projectile is chosen in such a way that the projectile travels a sufficient distance

after interaction with the target so that the nature of the trajectory (scattering-like, incomplete fusion and no capture breakup) can be determined. The calculations are done through the FORTRAN programming language which can easily handle iterative calculations under a DO loop [Ref. Appendix A].

4.9 Nature of solutions and trajectories

Some of the typical trajectories obtained from the numerical solutions are shown in Fig. 4.3. Fig. 4.3(a) shows a scattering-like event, Fig. 4.3(b) shows incomplete fusion in which the deuteron is captured by the target, whereas Fig. 4.3(c) shows no-capture breakup in which none of the breakup fragments are captured by the target. All these trajectories have one feature in common and that is the projectile (or its fragments) are carrying away the angular momentum. In complete fusion event the projectile fuses with the target to form the compound nucleus, and the total angular momentum is manifested as the spin of the compound nucleus. Our model is incapable of handling complete fusion events. This is because the target is considered to be a point particle, and hence it cannot possess internal excitation energy and angular momentum. However, we can argue that every no-breakup event (including scattering-like events) below the cutoff impact parameter (to be discusssed in the section 4.11) has to be interpreted as a complete fusion event. This is because we had employed the sharp cutoff model for fusion, which assumes that complete and incomplete fusion event takes place within a cut-off impact parameter. Our model is effective for studying the breakup of the projectile. Hence, in the next chapter we employ the model to study fusion suppression which we explain as taking place due to the breakup of the projectile.

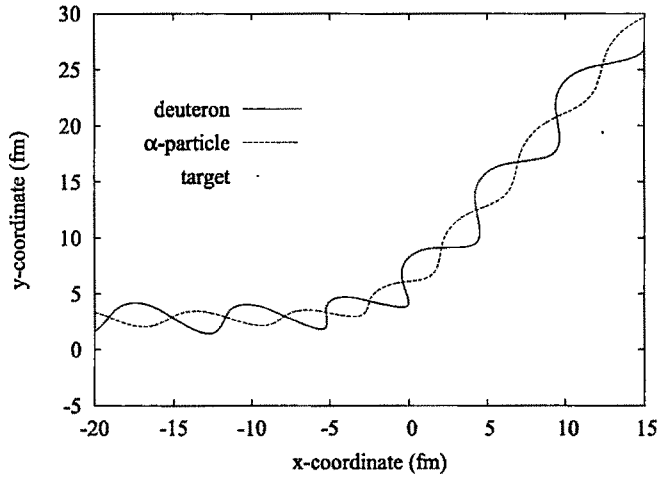

(a) Scattering-like

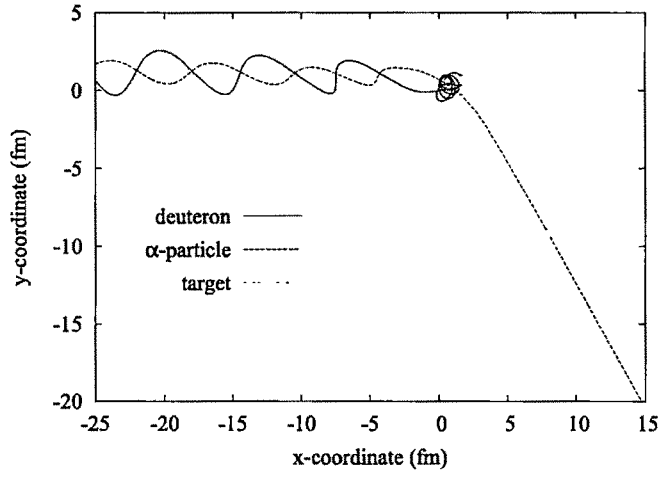

(b) Incomplete fusion

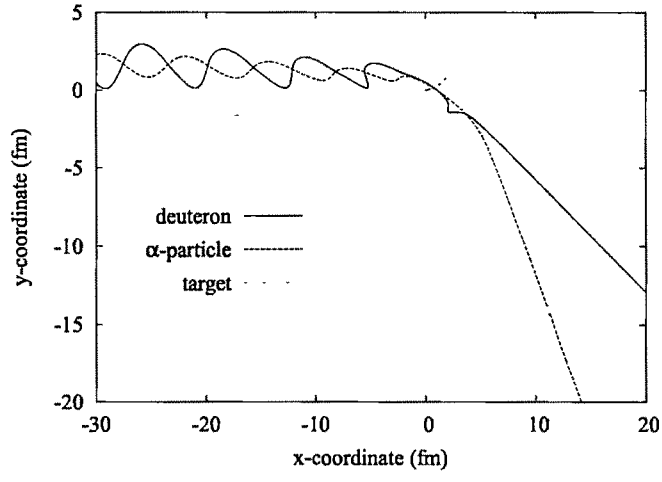

(c) No-capture breakup

Figure 4.3: Typical trajectories of the projectile fragments obtained from numerical solutions.

4.10 Classification of breakup and no breakup trajectories

In this chapter we shall provide an explanation of fusion suppression for the reactions $^6Li+^{144}Sm$, $^6Li+^{152}Sm$ and $^6Li+^{209}Bi$. As explained earlier fusion suppression takes place due to the breakup of a projectile. Hence, explanation of fusion suppression essentially rests upon the concept of breakup (or no-breakup) for a particular trajectory. Hence, some facts and arguments are presented in order to establish the point that breakup of the projectile takes place. In technical terms, breakup would mean that the distance of separation between the deuteron and the α-particle increases with time. In quantum mechanical language, the position of a particle can be calculated from their wave function and the associated probability distribution. However, in our model the positions are determined by the classical Newtonian equations, and breakup would mean that the distance of separation between the positions of the deuteron and the α-particle increases with time. A total of about 18000 trajectories were studied. We found that in more than 99 percent of the cases, the distance of separation between the deuteron and the α-particle were concentrated in two regions ; one between $0 - 2.27$ fm and the other between $80 - 100$ fm. The former region represents the no-breakup case, whereas the latter region represents the breakup case. The second region tended to increase when the iteration (time variable) was increased. This clearly indicates that breakup of the projectile has taken place. The determination of the number of breakup and no-breakup trajectories is done through a Fortran programme. Here, 2.27 fm is the distance that we had obtained between the deuteron and the α-particle in our simplified cluster model of ^{6}Li nucleus (see section 4.7). In less than 1 percent of the cases, the solutions turned chaotic, and these were ignored in the calculations. This is probably due to the fact that the differential equations picked up the right initial conditions (during random Monte Carlo simulation) for the solutions to turn chaotic.

In our programme breakup trajectory is identifed by setting the condition that the distance of separation between the deuteron and the α-particle is greater than 2.27 fm when they are far away from the target after interaction. It may be mentioned that out of the three types of trajectories obtained by us, incomplete fusion and no-capture breakup fall under the category of breakup, whereas scattering-like fall under the category of no-breakup. The Fortran code for determination of breakup and nobreakup trajectories is given in Appendix A.

4.11 Determination of cutoff impact parameter for fusion

For an explanation of fusion suppression factor we need to have an idea of the relative number of projectiles undergoing breakup. For this, the cutoff impact parameter for fusion must be determined. The cutoff impact parameter for fusion can be determined from the cutoff angular momentum for fusion. The cutoff angular momentum for fusion is determined through a comparison of the fusion cross section of the single barrier penetration model (SBPM) and the fusion cross section predicted by the computer code CCFULL [17].

According to SBPM, fusion between two nuclei takes place due to quantum mechanical tunnelling over the fusion barrier. Since, many partial waves are involved, the total fusion cross section is given by the sum of the partial fusion cross sections [29],

$$\sigma = \frac{\pi}{k^2}\sum_{\ell=0}^{\infty}(2\ell+1)T_\ell P_\ell \tag{4.56}$$

where, T_ℓ is the transmission coefficient for the ℓ^{th} partial wave, P_ℓ is the probability for fusion once the barrier is crossed and $k^2{=}2\mu E_{cm}/\hbar^2$. Using WKB approximation and treating the Coulomb barrier as inverted parabolas, Hill and Wheeler [30] arrived

at a simple expression for the transmission coefficients,

$$T_\ell(E_{cm}) = \frac{1}{1 + exp\left(\frac{2\pi}{\hbar\omega_\ell}(E_\ell - E_{cm})\right)} \tag{4.57}$$

where, E_ℓ is the fusion barrier for the ℓ^{th} partial wave, and $\hbar\omega_l$ is the curvature of the parabolic barrier. We assume a sharp cutoff model for P_ℓ, which is based on the idea that fusion is more probable for head-on collisions rather than peripheral collisions [31]. Hence,

$$P_\ell = \begin{cases} 1 & \text{if} \quad \ell \leq L_c \\ 0 & \text{if} \quad \ell > L_c \end{cases} \tag{4.58}$$

where, L_c is the cutoff angular momentum quantum number. Hence, the sum in Eq. (4.56) can be replaced by an integral having L_c as its upper limit. Finally, we obtain σ_{fus} as a function of L_c [31],

$$\sigma_{fus} = \frac{R_b^2\hbar\omega_0}{2E_{cm}} ln\left[\frac{1 + e^{-y_0}}{1 + e^{-z}}\right] \tag{4.59}$$

where,

$$z = y_0 + \frac{\pi\hbar L_c(L_c + 1)}{\omega_0 R_b^2 \mu} \tag{4.60}$$

and,

$$y_0 = \frac{2\pi(E_0 - E_{cm})}{\hbar\omega_0} \tag{4.61}$$

If the Coulomb barrier parameters $\hbar\omega_0$, E_0 and R_b are known, then Eq. (4.59) can be solved to find L_c for every pair of σ_{fus} and E_{cm}. σ_{fus} is taken from the output of the computer code CCFULL. Once L_c is known, the cutoff impact parameter (b_c) can be determined from the relation [32],

$$b_c = \frac{L_c\hbar}{\sqrt{2mE_{lab}}} \tag{4.62}$$

which is derived from the condition that the angular momentum of the projectile is

L_c times $\hbar$. The position of the projectile (needed for locating the impact parameter) is given by the centre of mass of the deuteron α-particle cluster of the ^{6}Li nucleus.

4.12 Methodology for finding fusion suppression

Our methodology in explaining fusion suppression is essentially to find the fraction of projectiles undergoing breakup at each impact parameter (perpendicular distance between the velocity vector of the projectile and target). We define this quantity as the breakup fraction which is the ratio of the number of trajectories undergoing breakup and the total number of trajectories [6],

$$\text{Breakup Fraction } (B_i) = \frac{\text{number of breakup trajectories}}{\text{total number of trajectories}} \tag{4.63}$$

where, subscript i denotes the impact parameter at which B_i is evaluated.

The breakup fraction is a well defined quantity for each impact parameter and needs to be evaluated precisely in view of the problem we have. Initially, we kept a fixed distance of separation between the target and the projectile, and varied angle θ for all possible angles between 0^0 and 360^0. The breakup fraction evaluated in this mannner was very low, and we found that it couldn't explain the fusion suppression factor. There was an additional problem as the precise value of the breakup fraction at each impact parameter tend to vary with the distance of separation between the target and projectile. After some trial and error we found that the breakup fraction tends to have a maximum value for θ=0^0. Hence, for a particular impact parameter the breakup fraction is determined by taking θ=0^0, and randomly varying the distance of separation between the target and the projectile. The random variation of the distance between the target and projectile is done in order to eliminate the effects of the dependence of the breakup fraction on the distance between the target and the projectile. As the projectile is composed of a deuteron and an α-particle, hence the position of the projectile is calculated from the centre of mass of the

deuteron and the α-particle.

After evaluation of the breakup fractions, fusion suppresion is explained through introduction of a simple formula [6]. According to it, the fusion suppression factor is given by the average of the breakup fractions (B_i) evaluated at different impact parameters with weightage given by the fusion probability (P_i). The range of impact parameters starts from zero (i.e., a head-on collision) and is increased in steps of 0.2 fm until the cutoff impact parameter (b_c) is reached. Therefore,

$$\text{Fusion Suppression} = \frac{\sum_i B_i P_i}{\sum_i P_i} \tag{4.64}$$

For a sharp cutoff model,

$$P_i = \begin{cases} 1 & \text{if} \quad i \leq b_c \\ 0 & \text{if} \quad i > b_c \end{cases} \tag{4.65}$$

4.13 Results and Discussion

The formalism described above is now applied for finding the fusion suppression for the three reactions : ^{6}Li+^{209}Bi, ^{6}Li+^{152}Sm and ^{6}Li+^{144}Sm. In order to obtain numerical solutions, Woods-Saxon parameters (v, r, a) of the nuclear potentials have to be provided. The following parameters are used : $V_{d-\alpha}$ = (75.5 MeV, 1.85 fm, 0.71 fm), $V_{d-^{209}\text{Bi}}$ = (91.0 MeV, 1.16 fm, 0.83 fm), $V_{\alpha-^{209}\text{Bi}}$ = (60.0 MeV, 1.392 fm, 0.656 fm) [21, 28], $V_{d-^{152}\text{Sm}}$ = (91.82 MeV, 1.013 fm, 0.938 fm), $V_{\alpha-^{152}\text{Sm}}$ = (60.5 MeV, 1.107 fm, 0.607 fm) [8, 33, 34], $V_{d-^{144}\text{Sm}}$ = (99.72 MeV, 1.15 fm, 0.85 fm) and $V_{\alpha-^{144}\text{Sm}}$ = (185.0 MeV, 1.40 fm, 0.52 fm) [35]. For calculating the breakup fraction, a sample of 50 trajectories are chosen for each impact parameter. As explained above, the random sampling of the trajectories is done in which the initial distance between the target and projectile is randomly varied between two limits.

Table 4.1: Breakup fraction versus impact parameter at different energies for ^{6}Li+^{209}Bi.

Impact Parameter (fm)	Breakup fraction for ^{6}Li+^{209}Bi at E_{lab}					
	34 MeV	36 MeV	38 MeV	40 MeV	44 MeV	48 MeV
0.0	0.06	0.22	0.26	0.24	0.30	0.36
0.2	0.12	0.24	0.34	0.26	0.46	0.24
0.4	0.20	0.14	0.40	0.48	0.40	0.46
0.6	0.32	0.12	0.36	0.46	0.50	0.52
0.8	0.32	0.40	0.46	0.44	0.44	0.58
1.0	0.30	0.38	0.66	0.52	0.58	0.50
1.2	0.28	0.36	0.50	0.44	0.64	0.54
1.4	0.32	0.54	0.64	0.44	0.64	0.74
1.6	0.32	0.64	0.54	0.66	0.54	0.68
1.8	0.54	0.48	0.62	0.54	0.66	0.64
2.0	0.50	0.58	0.50	0.60	0.52	0.54
2.2	0.60	0.66	0.66	0.58	0.58	0.48
2.4	0.42	0.50	0.62	0.66	0.64	0.64
2.6	0.34	0.30	0.48	0.56	0.56	0.52
2.8	0.52	0.38	0.52	0.46	0.42	0.52
3.0	0.28	0.46	0.36	0.54	0.28	0.50
3.2	0.22	0.18	0.32	0.28	0.34	0.36
3.4	0.16	0.26	0.24	0.30	0.42	0.36
3.6	0.22	0.20	0.24	0.14	0.26	0.20
3.8	0.14	0.16	0.18	0.2	0.18	0.36
4.0	0.04	0.08	0.16	0.14	0.20	0.26
4.2	0.06	0.06	0.20	0.08	0.06	0.12
4.4	0.10	0.0	0.12	0.08	0.10	0.08
4.6	0.02	0.0	0.0	0.10	0.06	0.06
4.8	0.0	0.0	0.0	0.06	0.08	0.0
5.0	0.0	0.0	0.0	0.0	0.04	0.0
5.2	0.0	0.0	0.0	0.0	0.02	0.0
5.4	0.0	0.0	0.0	0.0	0.0	0.0

Table 4.2: Breakup fraction versus impact parameter at different energies for ^{6}Li+^{152}Sm.

Impact Parameter (fm)	Breakup fraction for ^{6}Li+^{152}Sm at E_{lab}					
	28 MeV	30 MeV	32 MeV	34 MeV	36 MeV	40 MeV
0.0	0.02	0.08	0.24	0.14	0.48	0.24
0.2	0.12	0.12	0.18	0.34	0.30	0.48
0.4	0.16	0.20	0.22	0.24	0.36	0.44
0.6	0.24	0.12	0.16	0.22	0.30	0.32
0.8	0.16	0.12	0.22	0.32	0.38	0.38
1.0	0.20	0.24	0.26	0.14	0.46	0.50
1.2	0.32	0.24	0.30	0.30	0.54	0.58
1.4	0.28	0.40	0.54	0.54	0.38	0.66
1.6	0.38	0.36	0.40	0.62	0.52	0.66
1.8	0.26	0.26	0.36	0.52	0.60	0.60
2.0	0.42	0.38	0.44	0.46	0.58	0.64
2.2	0.26	0.40	0.48	0.48	0.58	0.60
2.4	0.30	0.48	0.54	0.54	0.48	0.46
2.6	0.28	0.40	0.50	0.64	0.58	0.56
2.8	0.38	0.36	0.36	0.24	0.58	0.68
3.0	0.28	0.28	0.36	0.38	0.34	0.44
3.2	0.36	0.28	0.22	0.32	0.28	0.34
3.4	0.26	0.24	0.18	0.16	0.24	0.20
3.6	0.26	0.24	0.12	0.18	0.26	0.22
3.8	0.10	0.26	0.10	0.06	0.18	0.32
4.0	0.16	0.24	0.12	0.06	0.14	0.12
4.2	0.14	0.20	0.20	0.06	0.10	0.12
4.4	0.14	0.08	0.08	0.12	0.12	0.12
4.6	0.10	0.12	0.0	0.10	0.16	0.10
4.8	0.04	0.04	0.0	0.00	0.06	0.08
5.0	0.0	0.04	0.0	0.00	0.0	0.04
5.2	0.0	0.0	0.0	0.0	0.00	0.0

Table 4.3: Breakup fraction versus impact parameter at different energies for ^{6}Li+^{144}Sm.

Impact Parameter (fm)	Breakup fraction for ^{6}Li+^{144}Sm at E_{lab}					
	30 MeV	32 MeV	34 MeV	36 MeV	38 MeV	40 MeV
0.0	0.36	0.44	0.60	0.48	0.52	0.50
0.2	0.58	0.56	0.60	0.66	0.62	0.52
0.4	0.74	0.70	0.60	0.66	0.52	0.64
0.6	0.82	0.74	0.78	0.74	0.76	0.58
0.8	0.86	0.58	0.72	0.80	0.76	0.62
1.0	0.74	0.88	0.76	0.80	0.76	0.68
1.2	0.64	0.76	0.88	0.78	0.74	0.78
1.4	0.64	0.58	0.88	0.74	0.70	0.72
1.6	0.38	0.52	0.68	0.72	0.74	0.72
1.8	0.30	0.44	0.40	0.72	0.76	0.76
2.0	0.18	0.34	0.32	0.42	0.66	0.72
2.2	0.20	0.24	0.24	0.52	0.54	0.60
2.4	0.04	0.20	0.22	0.28	0.38	0.38
2.6	0.00	0.04	0.14	0.24	0.22	0.24
2.8	0.00	0.00	0.02	0.06	0.06	0.16
3.0	0.00	0.00	0.00	0.00	0.08	0.06
3.2	0.00	0.00	0.00	0.00	0.00	0.00

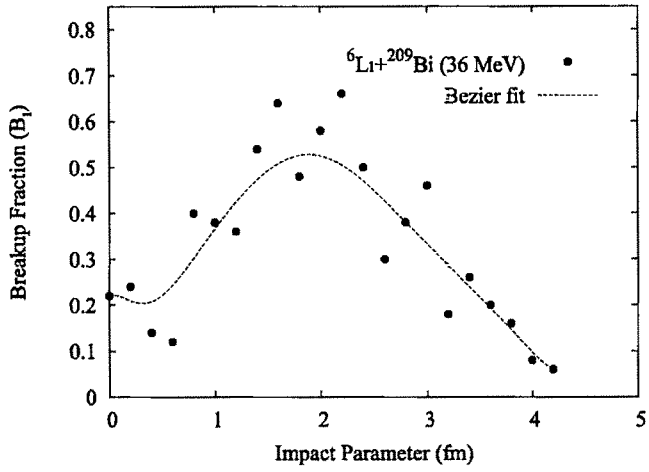

(a) ^{6}Li+^{209}Bi

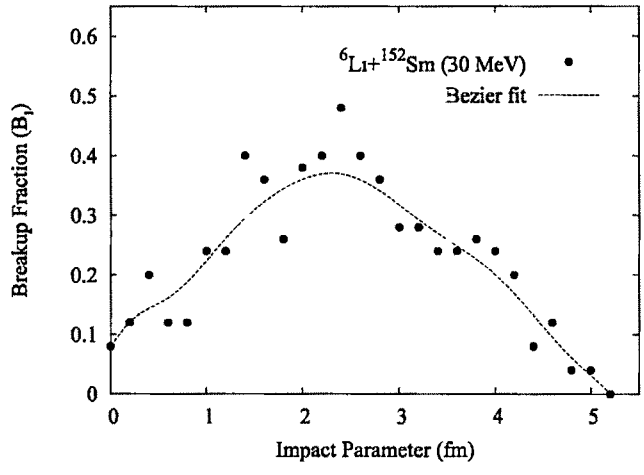

(b) ^{6}Li+^{152}Sm

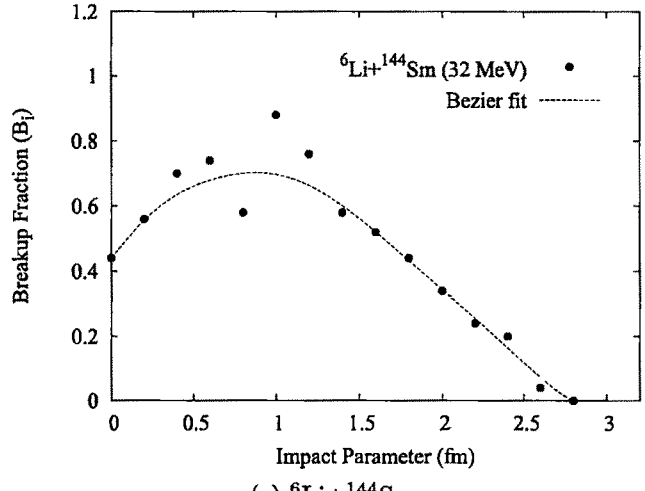

(c) ^{6}Li+^{144}Sm

Figure 4.4: Breakup fraction vs impact parameter at given energies. The Bezier curve is also drawn.

Since, only a sample of 50 trajectories are chosen, the results may be biased if the trajectories don't possess a high degree of randomness. Inbuilt random number generators in Linux Ubuntu produce the same random numbers in every cycle. In order to overcome this problem, we generate successive random numbers by taking the output of the random number generator after it had completed k cycles under a DO loop. The number k is a randomly chosen five digit number. Each time a random number is desired, it is ensured that the value k is different from the previous entries. This method gave us very good random numbers. The lower limit of the distance is taken to be 20 fm, and the upper limit of the distance is actually limited by the computational facilities available to us. A maximum initial distance of 55 fm between target and projectile could only be considered so that sufficient memory is available in the hardware for studying the trajectory of the projectile after interaction with the target. Using the Fortran code given in appendix A, we could determine the distance between the deuteron and the α-particle after interaction with the target. Using the condition of a breakup trajectory (section 4.10), we could identify whether a particular trajectory is a breakup or a no-breakup trajectory. Finding the number of breakup trajectories out of the 50 trajectories, the breakup fraction is calculated. The breakup fraction calculated at different impact parameters is shown in Table 4.1 for ^{6}Li+^{209}Bi, in Table 4.2 for ^{6}Li+^{152}Sm and in Table 4.3 for ^{6}Li+^{144}Sm, respectively [6]. The breakup fraction is calculated at 6 different energies which are $\approx$ 1.1 to 1.5 times the barrier energy, as because in this energy range fusion cross section is suppressed by $\approx$ 36 %, 28 % and 32 %, respectively, for the three reactions [7, 8, 9]. Fig. 4.4 (a),(b) and (c) shows graphical plot of breakup fraction for the three reactions at selected energies [6]. One distinct feature of the breakup fraction, which is also confirmed by the Bezier fit, is that the breakup fraction slowly increases and reaches a maximum, and finally falls to zero for higher impact parameters. For the reaction ^{6}Li+^{144}Sm, the breakup fraction falls off to zero at 2.8 fm which is much lower than the respective values

Table 4.4: Parameters of input file of CCFULL code for $^{6}Li+^{152}Sm$

Line 1	6., 3., 152., 62.
Line 2	1.05, 1, 1.06, 1
Line 3	0.122, 0.26, 0.05, 2
Line 4	1.66, 0.13, 2, 0
Line 5	2.186, 0.87, 0, 1
Line 6	0, 0., 0.3
Line 7	131.0, 1.01, 0.64
Line 8	18., 40., 1
Line 9	30, 0.05

for the other two reactions. This fact is compensated by the comparatively larger values of the breakup fraction.

For determination of the empirical value of fusion suppression (f_{exp}), we first determine the theoretical value of fusion cross section (σ_{theo}), which is expected in the absence of breakup. For the reactions ^{6}Li+^{209}Bi and ^{6}Li+^{144}Sm, σ_{theo} is obtained by running the code CCFULL [17]. For the above reactions, the above barrier fusion cross section (σ_{theo}), with and without coupling, are practically identical [7]. As such the parameters of the input file for lines 2, 6 and 9 of CCFULL code are exactly similar as mentioned in section 3.6. In line 7, the parameters of the Woods–Saxon potential are put. For ^{6}Li+^{209}Bi, the parameters of the Woods-Saxon potential are (V_0, r_0, a)=(107 MeV, 1.12 fm, 0.63 fm) [7], and for ^{6}Li+^{144}Sm the parameters are (V_0, r_0, a)=(47.0 MeV, 1.10 fm, 0.63 fm) [9]. As ^{152}Sm is a highly deformed nucleus, hence for the reaction ^{6}Li+^{152}Sm, σ_{theo} is obtained by running the CCFULL code by considering both target and projectile rotational excited states [8]. The parameters of the input file are shown in Table 4.4. The target (^{152}Sm) is a deformed nucleus in its ground state. Hence, in line 3 we have included both quadrupole (2^+, 0.122 MeV) and hexadecapole (4^+) rotational states with deformation parameters, β_2=0.26, and β_4=0.05. The unbound first excited state (3^+, 2.186 MeV) of the projectile (^{6}Li) with deformation parameter, β_2=0.87 [7], is included in the fifth line. Woods–Saxon parameters [8] of the nuclear potential are put in line 7.

Knowing the experimental value of fusion cross section (σ_{exp}) [7, 8, 9], the em-

pirical fusion suppression factor is determined from the relation,

$$f_{exp} = 1 - \frac{\sigma_{exp}}{\sigma_{theo}} \tag{4.66}$$

and the results are shown in Tables 4.5, 4.6 and 4.7, respectively [6]. Using the value of σ_{theo} and using Eqs. (4.59), (4.60) and (4.61), the cutoff angular momentum (L_c) is determined for the reactions ^{6}Li+^{209}Bi and ^{6}Li+^{144}Sm. The values of the barrier parameters ($\hbar\omega_0$, E_0 and R_b) needed in the above calculations are known from the output of the CCFULL code. The justification for this comes from the fact that the energy region of consideration falls in region I (energy immediately above the barrier) [31, 29], where fusion and total reaction cross sections practically coincide. For the reaction ^{6}Li+^{152}Sm, L_c is determined as above, but this time, σ_{theo} is given by the results of the single barrier penetration model (SBPM) because Eq. (4.59) is derived on the assumption that σ_{theo} is approximated by the results of the SBPM. The SBPM cross section for ^{6}Li+^{152}Sm can be obtained by running the CCFULL code with Woods-Saxon parameters of the nuclear potential given in Ref. [8]. The Woods-Saxon parameters are (V_0, r_0, a)=(131.0 MeV, 1.01 fm, 0.64 fm). Then from Eq. (4.62), the cutoff impact parameter (b_c) is determined for the three reactions. Using the cutoff impact parameter (b_c), the calculated value of fusion suppression (f_{cal}) is evaluated using eqs. (4.63) and (4.64), and the results are shown in Tables 4.5, 4.6 and 4.7 [6].

Table 4.5: Table showing calculations for the calculated fusion cross section (σ_{cal}) at various energies for the reaction ^{6}Li+^{209}Bi. The σ_{exp} values are from Ref. [7]. Units are MeV for E, millibarn for σ, and fm for b_c.

E_{lab}	E_{cm}	σ_{exp}	σ_{theo}	f_{exp}	L_c	b_c	$\sum_i B_i P_i$	$\sum_i P_i$	f_{cal}	σ_{cal}
34	32.96	225.8±4.5	343.2	0.342	13.30	4.25	6.30	22.25	0.283	246.0
36	34.92	344.7±4.5	537.0	0.358	14.49	4.50	7.34	23.50	0.312	369.3
38	36.86	451.0±8	709.0	0.364	16.11	4.87	9.38	25.35	0.370	446.7
40	38.81	558±18	862.8	0.353	17.69	5.21	9.26	27.05	0.342	567.7
44	42.70	703±58	1122.3	0.373	20.62	5.79	9.92	29.95	0.331	750.8
48	46.58	896±18	1331.6	0.327	23.24	6.25	10.26	32.25	0.318	908.2

Table 4.6: Table showing calculations for the calculated fusion cross section (σ_{cal}) at various energies for the reaction ^{6}Li+^{152}Sm. The σ_{exp} values are from Ref. [8]. Units are MeV for E, millibarn for σ, and fm for b_c. σ_{theo} values in the fourth column are obtained by consideration of target and projectile rotational excited states. SBPM values of σ_{theo}, needed for calculating L_c, are obtained from CCFULL code with Woods-Saxon parameters (131 MeV, 1.01 fm, 0.64 fm) [8], and are slightly less than the values in the fourth column.

E_{lab}	E_{cm}	σ_{exp}	σ_{theo}	f_{exp}	L_c	b_c	$\sum_i B_i P_i$	$\sum_i P_i$	f_{cal}	σ_{cal}
28.0	26.94	198±9	273.7	0.277	11.32	3.99	5.19	20.95	0.248	205.8
30.0	28.86	304±10	439.0	0.308	11.98	4.08	5.79	21.40	0.270	320.5
32.0	30.78	418±12	596.7	0.299	13.32	4.39	6.58	22.95	0.287	425.6
34.0	32.71	563±15	737.6	0.237	14.72	4.70	7.18	24.50	0.293	521.4
36.0	34.63	637±16	860.5	0.260	16.05	4.99	9.00	25.95	0.346	562.8
40.0	38.48	797±20	1064.1	0.251	18.54	5.46	9.90	28.30	0.350	691.9

Table 4.7: Table showing calculations for the calculated fusion cross section (σ_{cal}) at various energies for the reaction ^{6}Li+^{144}Sm. The σ_{exp} values are from Ref. [9]. Units are MeV for E, millibarn for σ and, fm for b_c.

E_{lab}	E_{cm}	σ_{exp}	σ_{theo}	f_{exp}	L_c	b_c	$\sum_i B_i P_i$	$\sum_i P_i$	f_{cal}	σ_{cal}
30.0	28.80	236±15	338.7	0.303	12.44	4.23	6.48	22.15	0.293	239.5
32.0	30.72	335±18	496.8	0.326	12.97	4.27	7.02	22.35	0.314	340.8
34.0	32.64	417±27	634.6	0.343	14.16	4.52	7.84	23.60	0.332	423.2
36.0	34.56	502±30	754.5	0.335	15.39	4.78	8.62	24.90	0.346	493.4
38.0	36.48	607±31	858.4	0.293	16.58	5.01	8.82	26.00	0.338	568.3
40.0	38.40	674±33	948.8	0.290	17.71	5.22	8.68	27.10	0.320	645.2

For calculating f_{cal}, we take the ratio between the values of $\sum_i P_i$ (in column 9) and $\sum_i B_i P_i$ (in column 8) of the respective Tables. It is to be noted that the breakup fraction values (B_i) and the corresponding values of $\sum_i P_i$ and $\sum_i P_i B_i$ are determined in steps of 0.2 fm. However, P_i and $P_i B_i$ have to be summed up precisely upto the cut off impact parameter (b_c). In some of the cases, the cut off impact parameter lies at a value where the breakup fraction becomes zero. In the rest of the cases (34 MeV for ^6Li+^{209}Bi, and 28, 30, 32, 34 MeV for ^6Li+^{152}Sm) the cutoff impact parameter lies at a value where the breakup fraction is not zero. In all these cases the cutoff impact parameter value lies between successive multiples of 0.2 fm. For these cases, we used linear extrapolation for determining the precise values of P_i and $P_i B_i$ at the position of the cutoff impact parameter (b_i),

$$P_i = \left(\frac{b_i - k_j}{k_{j+1} - k_j}\right) \tag{4.67}$$

$$B_i P_i = \left(\frac{B_{j+1} - B_j}{k_{j+1} - k_j}\right)(b_i - k_j) + B_j \tag{4.68}$$

Here, k_j and k_{j+1} are the successive impact parameters between which the cutoff impact parameter (b_i) is located, and B_j and B_{j+1} are the respective values of the breakup fraction. From the f_{cal} values, we determine the calculated fusion cross section from the relation,

$$\sigma_{cal} = \sigma_{theo}(1 - f_{cal}). \tag{4.69}$$

A comparison of the experimental and calculated fusion cross sections is shown in Fig. 4.5 (a), (b) and (c) for the three reactions, where uncertainties in the experimental fusion cross section are shown by the error bars [6]. It can be concluded that there is very good agreement between the values of σ_{exp} and σ_{cal}.

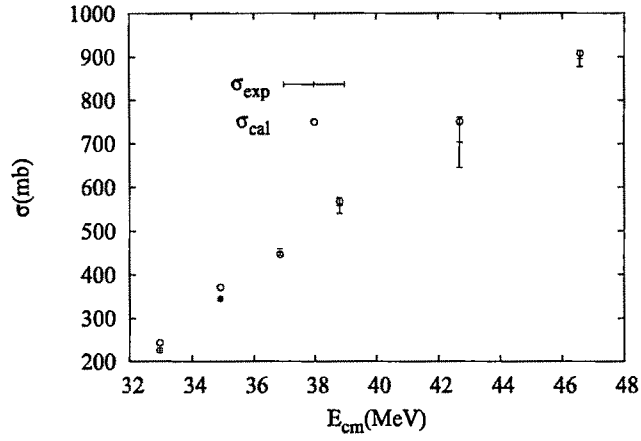

(a) ^{6}Li+^{209}Bi

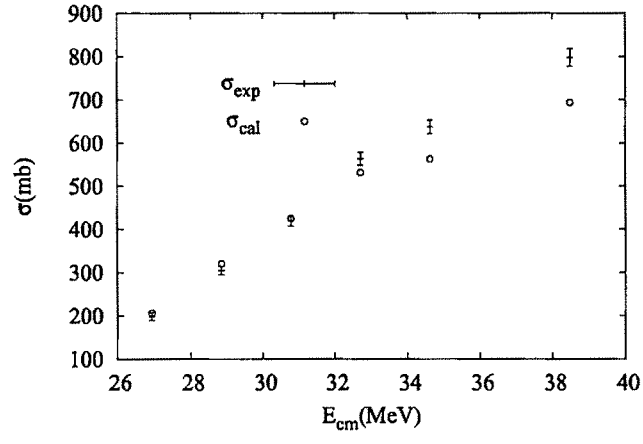

(b) ^{6}Li+^{152}Sm

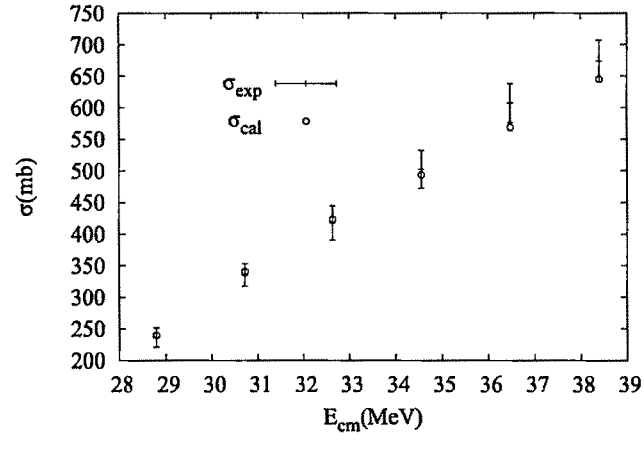

(c) ^{6}Li+^{144}Sm

Figure 4.5: Calculated (σ_{cal}) and experimental fusion cross sections (σ_{exp}) vs E_{cm} (MeV) for the 3 reactions. The experimental fusion cross sections are taken from Refs. [7, 8, 9].

In the cases discussed above (where breakup fraction is not zero at cutoff impact parameter), the breakup of the projectile extends beyond the cutoff impact parameter for fusion. This has been the case in the low energy region for the reactions $^6Li+^{209}Bi$ and $^6Li+^{152}Sm$. This is indeed expected because at lower energies the projectile spends more time in the vicinity of the target nucleus which would lead to its breakup. Inspite of the fact that breakup of the projectile is extending beyond the cutoff impact parameter, we are getting approximately constant values of fusion suppression for all energies considered, and this is in agreement with the experimental values. For ^{6}Li+^{152}Sm, σ_{cal} is slightly lower than σ_{exp} for higher energies. This is because of the fact that the cutoff angular momentum (L_c), as calculated from Eq. (4.59), is slightly lowered from the true value as SBPM values of σ_{fus} are used in the calculations. The agreement is excellent for the reaction ^{6}Li+^{144}Sm, followed by ^{6}Li+^{209}Bi and ^{6}Li+^{152}Sm. In fact, for the system ^{6}Li+^{144}Sm, if the small experimental uncertainty is ignored, σ_{cal} values follow the exact trend of the σ_{exp} (Table 4.7) values evaluated at different energies. The reason is that ^{144}Sm is least deformed, ^{209}Bi is intermediate and ^{152}Sm is most deformed.

4.14 Relationship between E_{cm} and L_c

The energy (E_{cm}) dependence of cutoff L_c has also been studied. The values of L_c have been calculated using both the values of fusion cross section, viz., σ_{theo} and σ_{exp}, and the results are shown in Fig. 4.6 [6]. As expected, a perfect linear relationship between L_c(calculated from σ_{theo}) and E_{cm} is observed. We also observe a very good linear relationship between L_c(calculated from σ_{exp}) and E_{cm}. For comparison, the best fit line using least square method is also drawn. Equations of the best-fit line are,

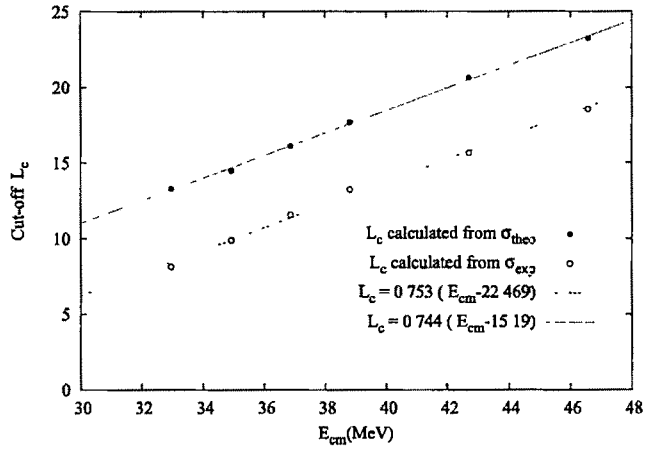

(a) ^{6}Li+^{209}Bi

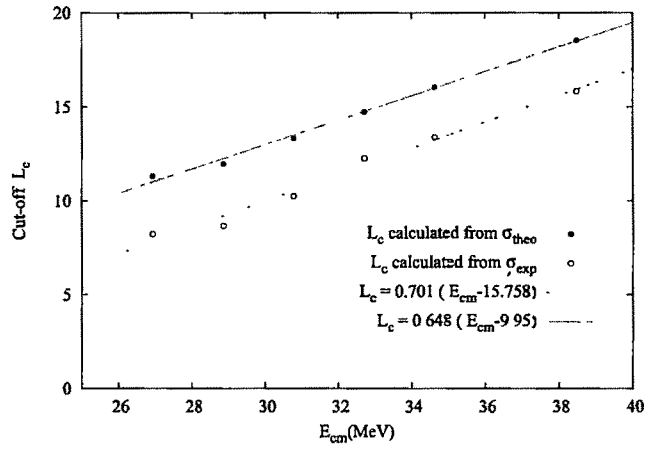

(b) ^{6}Li+^{152}Sm

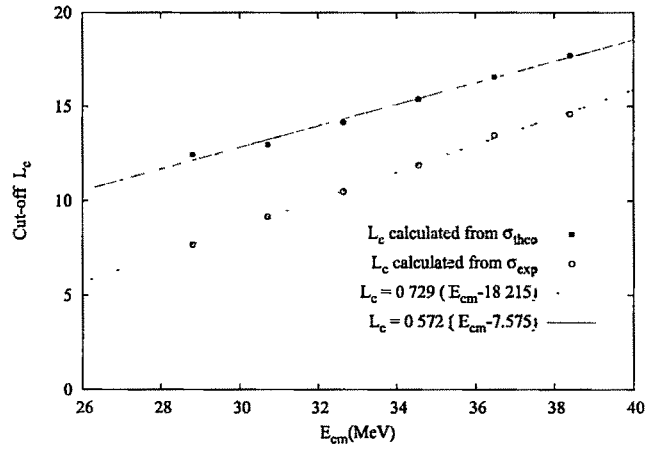

(c) ^{6}Li+^{144}Sm

Figure 4.6: Cutoff angular momentum (L_c) vs. E_{cm} (MeV), where L_c is calculated using σ_{theo} as well as σ_{exp}. The straight line is the linear fit using least square method.

For ^{6}Li+^{209}Bi, with L_c calculated from σ_{theo},

$$L_c = 0.753(E_{cm} - 22.469) \tag{4.70}$$

For ^{6}Li+^{209}Bi, with L_c calculated from σ_{exp},

$$L_c = 0.744(E_{cm} - 15.19) \tag{4.71}$$

For ^{6}Li+^{152}Sm, with L_c calculated from σ_{theo},

$$L_c = 0.701(E_{cm} - 15.758) \tag{4.72}$$

For ^{6}Li+^{152}Sm, with L_c calculated from σ_{exp},

$$L_c = 0.648(E_{cm} - 9.95) \tag{4.73}$$

For ^{6}Li+^{144}Sm, with L_c calculated from σ_{theo},

$$L_c = 0.729(E_{cm} - 18.215) \tag{4.74}$$

For ^{6}Li+^{144}Sm, with L_c calculated from σ_{exp},

$$L_c = 0.572(E_{cm} - 7.575) \tag{4.75}$$

The conclusion made in Ref. [31] that for loosely bound systems the energy (E_{cm}) dependence of L_c is on the verge of transition of a linear dependence and a dependence on $L_c(L_c+1)$ doesn't seem to hold, at least for these three systems. One reason may be that the systems studied in Ref. [31] are low-medium targets, whereas the targets of the present system are relatively heavier. A qualitative understanding of the linear relationship between L_c and E_{cm} is given below. The angular momentum

carried by the projectile can be approximately calculated by equating the energy of the projectile with total potential energy, V(r), between the projectile and target. V(r) is given by,

$$V = V_C(r) + V_N(r) + \frac{\hbar^2 l(l+1)}{2\mu r^2} \tag{4.76}$$

The cut-off angular momentum for fusion, L_c, is given by the value of the angular momentum ℓ in the above equation at the position of the fusion barrier (r=R_B). Calculations done with the proximity potential (Prox 88 of chapter 2) reproduced the linear relationship between L_c (calculated from σ_{theo}) and E_{cm}. The results are shown in Table 4.8.

Table 4.8: Cut-off angular momentum for fusion, L_c, and E_{cm} calculated from proximity potential.

$^6Li+^{209}Bi$		$^6Li+^{152}Sm$		$^6Li+^{144}Sm$	
L_c	E_{lab} (MeV)	L_c	E_{lab} (MeV)	L_c	E_{lab} (MeV)
13.3	36.93	11.32	29.50	12.44	30.96
14.49	38.05	11.98	30.09	12.97	31.50
16.11	39.72	13.32	31.42	14.16	32.80
17.69	41.54	14.72	32.97	15.39	34.29
20.62	45.43	16.05	34.60	16.58	35.85
23.24	49.48	18.54	38.08	17.71	37.46

Comparison with the values of L_c and E_{lab} of Tables 4.5, 4.6 and 4.7 shows a qualitatively good agreement. The fact that the linear relationship is nicely explained is due to the existence of the fusion barrier (or the potential pocket) for the highest energies of the above three reactions. This may not be the case for even higher energies because in that case the potential pocket may disappear, and L_c would be given by the angular momentum, ℓ, for which the potential pocket exists in Eq. 4.76.

4.15 Summary and Outlook

In this chapter, we explain the fusion suppression of three reactions induced by ^{6}Li projectile, namely, ^{6}Li+^{209}Bi, ^{6}Li+^{152}Sm and ^{6}Li+^{144}Sm. Some other authors (eg. Diaz Torrez) have also succeeded in explaining fusion suppression through the introduction of a breakup probability function whose parameters are determined from sub-barrier fusion cross section data. However, we have attempted to explain fusion suppression purely from first principles without the need for introducing any adhoc inputs. Considering the projectile to be a cluster of a deuteron and an α-particle, we construct the classical equations of motion for the system of projectile and target in two-dimensions. As the system has six degrees of freedom, hence we obtain six-second order differential equations. Numerical solutions for the above equations can be obtained only if twelve initial conditions are known. These initial conditions are the positions and velocities of the x and y components of the three particles. Using stable (not chaotic) solutions as an indicator, we obtain the initial conditions for the deuteron and the α-particle which constitute the ^{6}Li nucleus. We propose a semi-classical model of the ^{6}Li nucleus from which the initial conditions of the deuteron and the α-particle are derived. The model utilizes the binding energy (breakup threshold energy) and the spin of the ^{6}Li nucleus for deriving these initial conditions. After studying the numerical solutions, we could identify three distinct kinds of trajectories : scattering-like, incomplete fusion and no capture breakup. Next, we define the breakup condition for a trajectory. If distance between deuteron and α-particle after interaction with the target is greater than 2.27 fm, then its a breakup trajectory, otherwise it is not. Then the breakup fraction at different impact parameters (in steps of 0.2 fm) is obtained. Next we determine the cutoff impact parameter for fusion by using rigourous quantum mechanical concepts. Then we introduce a formula for explaining fusion suppression, according to which fusion suppression is given by the average of breakup fractions evaluated at impact parameters ranging from a head on collision upto the cutoff impact parameter for

fusion. On application of the above formula, we find that there is very good agreement between the calculated (σ_{cal}) and the experimental (σ_{exp}) fusion cross sections for all the three systems. For the system ^{6}Li+^{152}Sm, σ_{cal} falls below σ_{exp} at higher energies because of deformed nature of the target. The relationship between cutoff angular momentum (L_c) and the energy (E_{cm}) is also studied, and we found that there is an excellent linear relationship between the two. By using the proximity potential, an understanding of the linear behaviour is provided.

In future, the fusion suppression of other ^{6}Li induced reactions may be studied provided Woods-Saxon parameters of the nuclear potential are obtained through optical model analysis of elastic scattering data. Some of the reactions for which precise fusion suppression factors are available are ^{6}Li+^{208}Pb [36], ^{6}Li+^{159}Tb [37] and ^{6}Li+^{90}Zr [38], and fusion suppression analysis could be carried out for these reactions. Reactions induced by ^{9}Be (^{7}Li) are a bit complicated as they involve a neutron transfer (proton pickup) to (from) target to form the nucleus ^{8}Be [24, 26]. However, fusion suppression factor of the same order as ^{6}Li induced reactions have been observed for reactions induced by ^{9}Be and ^{7}Li. Modelling the breakup of ^{9}Be induced reactions has been done by Diaz Torrez through the introduction of an empirically obtained breakup probability function [24]. Similar analysis could also be tried for ^{7}Li induced reactions [39], although the number of experiments is quite limited. Modelling the breakup of ^{7}Li and ^{9}Be induced reactions, without the introduction of an empirically obtained breakup probability function may also be attempted. However, this may require some serious theoretical effort. A complete quantum mechanical model of fusion suppression could be attempted in future. Much progress has to be done in computational techniques (both in theory and in practice) before succeeding in such an attempt.

Bibliography

[1] K. Siwek-Wilczynska and J. Wilczynski, *Phys. Rev. C*, **69**, 024611, (2004)

[2] N.G. Nicolis, *Eur. Phy. J. A*, **21**, 265, (2004)

[3] M. Dasgupta, D. J. Hinde, N. Rowley and A. M. Stefanini, *Annu. Rev. Nucl. Part. Sci.*, **48**, 401, (1998)

[4] C. K. Phookan and K. Kalita, *Nucl. Phys. A*, **899**, 29, (2013)

[5] I. Dutt and R. K. Puri, *Phys. Rev. C*, **81**, 064609, (2010).

[6] C. K. Phookan and K. Kalita, *Journal of Physics G : Nuclear and Particle Physics*, **40**, 125107, (2013)

[7] M. Dasgupta, P. R. S. Gomes, D. J. Hinde, S. B. Moraes, R. M. Anjos, A. C. Berriman, R. D. Butt, N. Carlin, J. Lubian, C. R. Morton, J. O. Newton, and A. Szanto de Toledo, *Phys. Rev. C*, **70**, 024606, (2004)

[8] P. K. Rath, S. Santra, N. L. Singh, K. Mahata, R. Palit, B. K. Nayak, K. Ramachandran, V. V. Parkar, R. Tripathi, S. K. Pandit, S. Appanababu, N. N. Deshmukh, R. K. Choudhury, and S. Kailas, *Nucl. Phys. A*, **874**, 14, (2012)

[9] P.K. Rath, S. Santra, N. L. Singh, R. Tripathi, V. V. Parkar, B. K. Nayak, K. Mahata, R. Palit, Suresh Kumar, S. Mukherjee, S. Appannababu, and R. K. Choudhury, *Phys. Rev. C*, **79**, 051601, (2009)

[10] P.R.S.Gomes, I. Padron, E. Crema, O. A. Capurro, J. O. Fernandez Niello, A. Arazi, G. V. Mart, J. Lubian, M. Trotta, A. J. Pacheco, J. E. Testoni, M. D. Rodrguez, M. E. Ortega, L. C. Chamon, R. M. Anjos, R. Veiga, M. Dasgupta, D. J. Hinde, and K. Hagino, *Phys. Rev. C*, **73**, 064606, (2006)

[11] M. Zadro, P.Figuera, A. Di Pietro, F. Amorini, M. Fisichella, O. Goryunov, M. Lattuada, C. Maiolino, A. Musumarra, V. Ostashko, M. Papa, M. G. Pellegriti, F. Rizzo, D. Santonocito, V. Scuderi, and D. Torresi, *Phys. Rev. C*, **80**, 064610, (2009)

[12] M.K. Pradhan, A. Mukherjee, P.Basu, A. Goswami, R. Kshetri, Subinit Roy, P. Roy Chowdhury, and M. Saha Sarkar, *Phys. Rev. C*, **83**, 064606, (2011)

[13] Y. W. Wu, Z. H. Liu, C. J. Lin, H. Q. Zhang, M. Ruan, F. Yang, and Z. C. Li, *Phys. Rev. C*, **68**, 044605, (2003)

[14] C.S. Palshetkar, S. Santra, A. Chatterjee, K. Ramachandran, Shital Thakur, S. K. Pandit, K. Mahata, A. Shrivastava, V. V. Parkar, and V. Nanal, *Phys. Rev. C*, **82**, 044608, (2010)

[15] V.V. Parkar, R. Palit, S.K. Sharma, B. S. Naidu, S. Santra, P. K. Joshi, P. K. Rath, K. Mahata, K. Ramachandran, T. Trivedi, and A. Raghav, *Phys. Rev. C*, **82**, 054601, (2010)

[16] Z.H. Liu, C. Signorini, M. Mazzocco, M. Ruan, H.Q. Zhang, T. Glodariu, Y.W. Wu, F. Soramel,C.J. Lin, and F. Yang, *European Phys. J. A*, **26**, 73, (2005)

[17] K. Hagino, N. Rowley and A.T. Kruppa, *Comp. Phys. Comm.*, **123**, 143, (1999)

[18] C. Beck, N. Keeley and A. Diaz-Torres, *Phys. Rev. C*, **75**, 054605, (2007) and references therein.

[19] N. J. Upadhyay, A. Deltuva and F. M. Nunes, *Phys. Rev. C*, **85**, 054621, (2012)

[20] A. Deltuva, A. M. Moro, E. Cravo, F. M. Nunes, and A. C. Fonseca, *Phys. Rev. C*, **76**, 064602, (2007)

[21] K. Hagino, M. Dasgupta and D. J. Hinde, *Nucl. Phys. A*, **738**, 475, (2004)

[22] A. Diaz-Torres, *Comp. Phys. Comm.*, **182**, 1100, (2011)

[23] A. Diaz-Torres, D. J. Hinde, J. A. Tostevin, M. Dasgupta, and L. R. Gasques, *Phys. Rev. Lett.*, **98**, 152701, (2007)

[24] R. Rafiei, R. du Rietz, D. H. Luong, D. J. Hinde, M. Dasgupta, M. Evers, and A. Diaz-Torres, *Phys. Rev. C*, **81**, 024601, (2010)

[25] James Cohen, *Phys. Rev. A*, **64**, 043412, (2001)

[26] M. Dasgupta, L.R. Gasquez, D.H. Luong, R. du Rietz, R. Rafei, D. J. Hinde, C.J. Lin, M. Evers, A. Diaz-Torres, *Nucl. Phys. A*, **834**, 147c, (2010)

[27] T. Matsumoto, D. Ichinkhorloo, Y. Hirabayashi, K. Kat and S. Chiba, *Phys. Rev. C*, **83**, 064611, (2011) and references therein.

[28] I. J. Thompson and M. A. Nagarjan, *Phys. Lett.*, **106B**, 163, (1981)

[29] C. A. Bertulani and P. Danielewicz, *Introduction to Nuclear Reactions, IOP Publishing*, page 218, (2004)

[30] D. L. Hill and J. A. Wheeler, *Phys. Rev.*, **89**, 1102, (1953)

[31] E. F. Aguilera and J. J. Kolata, *Phys. Rev. C*, **85**, 014603, (2012)

[32] K. S. Krane, *Introductory Nuclear Physics, Wiley India Pvt. Ltd.*, page 409, (2011)

[33] P. Christensen, A. Berinde, I. Neamu, N. Scintei, *Nucl. Phys. A*, **129**, 337, (1969)

[34] E. Obiajunwa, L. H. Rosier, J. V. de Wiele, *Nucl. Phys. A*, **500**, 341, (1989)

[35] C. M. Perey aand F. G. Perey, *Atomic Data and Nuclear data Tables*, **17**, 1, (1976)

[36] Y. W. Wu, Z. H. Liu, C. J. Lin, H. Q. Zhang, M. Ruan, F. Yang, and Z. C. Li, *Phys. Rev. C*, **68**, 044605, (2003)

[37] M.K. Pradhan, A. Mukherjee, P.Basu, A. Goswami, R. Kshetri, Subinit Roy, P. Roy Chowdhury, and M. Saha Sarkar, *Phys. Rev. C*, **83**, 064606, (2011)

[38] H. Kumawat, V. Jha, V. V. Parkar, B. J. Roy, S. K. Pandit, R. Palit, P. K. Rath, C. S. Palshetkar, Sushil K. Sharma, Shital Thakur, A. K. Mohanty, A. Chatterjee, and S. Kailas, *Phys. Rev. C*, **86**, 024607, (2012)

[39] A. Shrivastava, A. Navin, N. Keeley, K. Mahata, K. Ramachandran, V. Nanal, V.V. Parkar, A. Chatterjee, S. Kailas, *Phys. Lett. B*, **633**, 463, (2006)

Chapter 5

Reduced reaction cross section induced by radioactive projectiles

5.1 Introduction

The last two decades has seen a sudden rise in the study of reaction cross section [1, 2, 3, 4] between a variety of target and projectile. This has been possible due to tremendous improvement in experimental facilities over the years. The availability of intense beams of loosely bound nuclei [5], and the radioactive ion beam has added impetus to this exciting field of study. As a result a huge database of reaction cross section data for a range of target and projectile has become available. For purposes of comparison, various reduction procedures have been proposed which are aimed at eliminating trivial geometrical effects of size and charge. Also, using these reduction procedures it is possible to say whether there is an enhancement or reduction of fusion cross section with respect to some benchmark cross section. Of late, Gomes's reduction procedure [6] has been widely followed in which the dependence of the reaction cross section on the barrier radius (R_B) is eliminated, and the energy is scaled with respect to the barrier height (V_B).

For purposes of comparing reaction cross section data using a variety of target

and projectile, various authors have compared the reduced reaction cross section (σ_{red}) against the reduced energy (E_{red}). Recently, it was noted that the trajectory of the reduced cross section for tightly bound, normal loosely bound and radioactive halo projectiles are clearly separated [7, 8, 9]. Both, neutron halo and proton halo nuclei are considered in case of radioactive halo nuclei. It was also noted that the reason for the separation of the trajectories is that the Coulomb barrier is slightly lowered, and the barrier radius is marginally increased for radioactive halo systems in comparison with normal loosely bound systems [9]. In the first part of our work, a satisfactory explanation of the above fact is provided by using some common global nuclear potentials. The potentials chosen are the latest version of the Bass potential, the Christensen and Winther potential, the Broglia and Winther potential, Aage Winther potential, the Proximity potential and the Denisov potential. Straight forward application of the nuclear potentials can explain the shift in the barrier parameters for the case of reactions induced by the neutron halo nucleus ^6He. However, for the reaction induced by the proton halo nucleus (^8B), the shift of the barrier parameters in the right direction can only be explained if we take into consideration the increase in radius of ^8B with respect to its normal counterpart (^{10}B). Hence, first we shall be explaining the shift in the barrier parameters of radioactive halo systems with respect to normal loosely bound systems and compare them with the shift obtained from experimental reduced reaction cross section data. In the next part of the study, we obtain a theoretical fit for the reaction cross section of reactions induced by radioactive projectiles. The explanation is done on the basis of the modified Wong's formula [10]. In section 5.2, we provide the necessary formalism and in the next section (5.3) we review the procedure for the determination of the fusion barrier. In section 5.4 we discuss the nuclear potentials used, and in the next section (5.5) we discuss the nature (or shape) of the potentials. In Section 5.6, we present the results (including discussion), and in the last section (5.7) we provide a summary of our results.

5.2 Formalism

The total reaction cross-section is given by the sum of the fusion and quasi-elastic cross sections. Quasi-elastic reaction cross section includes the sum of the elastic, inelastic and the transfer cross sections,

$$\sigma_R = \sigma_{fus} + \overbrace{\sigma_{el} + \sigma_{inel} + \sigma_{trans}}^{\sigma_{quasi}}$$

However, in some of the systems, σ_{quasi} is quite insignificant, and we have, $\sigma_R \approx \sigma_{fus}$. This is quite true for low intensity (10^{4-5} pps) radioactive ion beams. For the study of reaction cross section, Wong's formula [11, 12] provides a convenient expression in terms of three parameters characterizing the barrier,

$$\sigma_R = \frac{R_b^2 \hbar\omega_0}{2E_{cm}} ln\Big\{1 + exp\Big[\frac{2\pi(E_{cm} - E_0)}{\hbar\omega_0}\Big]\Big\} \tag{5.1}$$

where, $\hbar\omega_0$ is the curvature of the Coulomb barrier (ℓ=0). E_0 and R_b are the height and position of the Coulomb barrier, respectively. In a naive picture, the position and height of the Coulomb barrier is given by [9],

$$R_b = k_b(A_P^{1/3} + A_T^{1/3}) \text{ fm} \tag{5.2}$$

$$E_0 = \frac{Z_P Z_T e^2}{k_r(A_P^{1/3} + A_T^{1/3})} \text{ MeV} \tag{5.3}$$

In order to reduce the complexity of reaction cross data among various combinations of target and projectile, the concept of reduced reaction cross section has emerged. Gomes devised a reduction procedure in order to eliminate the dependence of the reaction cross section on the atomic and mass number of the target and projectile. Hence, in Gomes' reduction procedure, the cross section is divided by the square of $(A_P^{1/3} + A_T^{1/3})$, and the energy is divided by $Z_P Z_T/(A_P^{1/3} + A_T^{1/3})$. Applying the above

reduction, Wong's formula reduces to,

$$\sigma_{red} = \frac{k_b^2 \epsilon_0}{2E_{red}} ln\Big\{1 + exp\Big[\frac{2\pi(E_{red} - V_{red})}{\epsilon_0}\Big]\Big\} \tag{5.4}$$

where,

$$\sigma_{red} = \frac{\sigma}{A_P^{1/3} + A_T^{1/3}} \tag{5.5}$$

$$E_{red} = E_{cm} \frac{A_P^{1/3} + A_T^{1/3}}{Z_P Z_T e^2} \tag{5.6}$$

$$V_{red} = E_0 \frac{A_P^{1/3} + A_T^{1/3}}{Z_P Z_T e^2} = \frac{1}{k_r} \tag{5.7}$$

$$\epsilon_0 = \hbar\omega_0 \frac{A_P^{1/3} + A_T^{1/3}}{Z_P Z_T e^2} \tag{5.8}$$

The values of the constants k_b and k_r can be obtained from the best fit of the reduced experimental reaction cross-section at various energies. In this manner the reduced reaction cross section for a variety of systems have been obtained. According to the study conducted in Ref. [7, 9], the following facts are reported. For tightly bound projectiles, the best fitting can be done with $k_b = 1.56$, $k_r = 1.65$ and ϵ_0=0.14. For normal loosely bound projectiles (^6Li, ^7Li and ^9Be), the Wong's model fit can be done with $k_b = 1.64$, $k_r = 1.76$ and ϵ_0=0.34. For radioactive halo projectiles (^6He and ^8B), the fitting can be done with $k_b = 1.79$, $k_r = 1.83$ and ϵ_0=0.49. The above fact can be interpreted by saying that in moving from normal to radioactive halo systems, the barrier is lowered by 4% and its position is increased by about 9% [9]. Hence, the trajectories for the three types of systems (tightly bound, loosely bound and radioactive halo) are clearly separated in the reduced reaction cross section analysis (σ_{red} vs E_{red}). This is diagrammatically shown in Fig 5.1. In the above study, different sets of reactions were considered for normal weakly bound systems as well as for radioactive halo systems. For radioactive halo systems, the following four reactions were considered : ^6He+^{27}Al, ^6He+^{64}Zn, ^5He+^{209}Bi and ^8B+^{58}Ni. The corresponding reactions induced by normal nuclei are : ^4He+^{27}Al, ^4He+^{64}Zn,

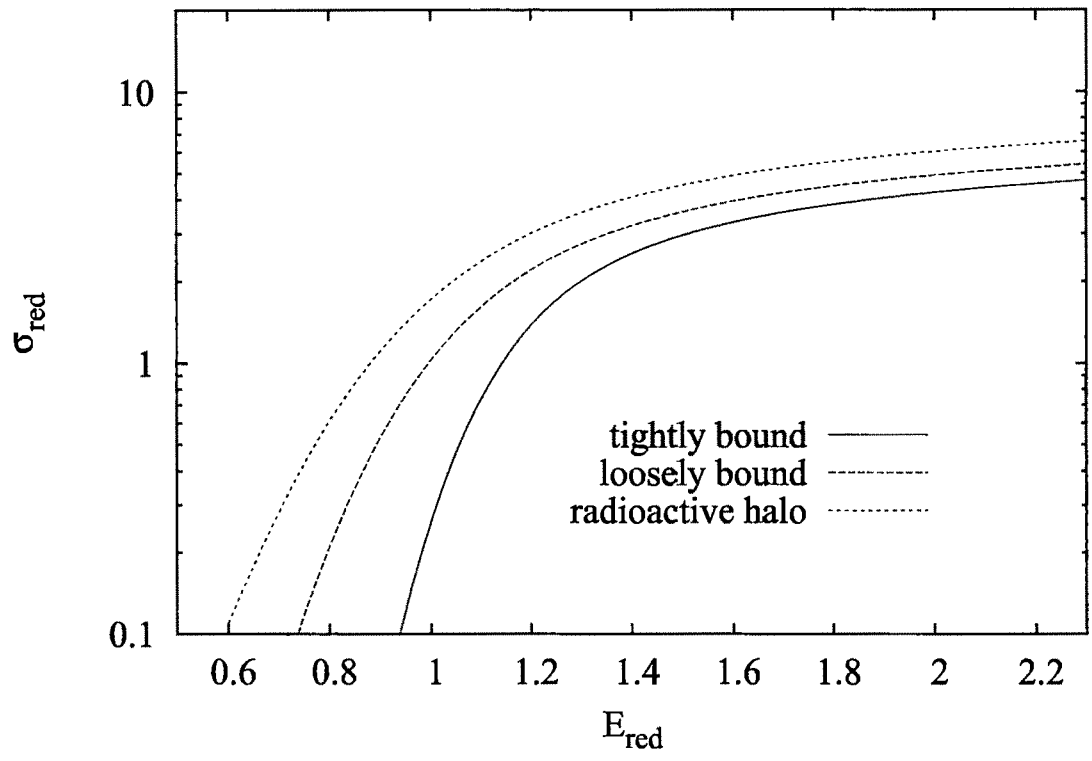

Figure 5.1: Diagram showing σ_{red} vs E_{red} for various systems. The trajectories for tightly bound, loosely bound and radioactive halo systems are clearly separated.

^4He+^{209}Bi and ^{10}B+^{58}Ni. Here, ^4He is the normal counterpart of the neutron halo nucleus ^6He, and ^{10}B is the normal counterpart of the proton halo nucleus ^8B. We shall be showing that in moving from normal to radioactive halo systems, the barrier parameters (V_B, R_B) are shifted as mentioned above. The shift in the barrier parameters is determined by taking an average of the shifts for the above reactions, as well as the average of the shifts for the different nuclear potentials.

5.3 Determination of the barrier parameters

The interaction potential between the target nucleus and the projectile can be written as the sum of nuclear, Coulomb and centrifugal potentials. Hence,

$$V = V_C(r) + V_N(r) + \frac{\hbar^2 l(l+1)}{2\mu r^2} \tag{5.9}$$

where, r is the distance between the centres of the target and projectile, ℓ is the angular momentum quantum number, and μ is the reduced mass of the system. The maximum value of the above potential for ℓ=0 is called the height of the fusion (or Coulomb) barrier (V_B), and the corresponding value of r is called the position of the barrier (R_B). As a few of the target nuclei are deformed, hence for accurate determination of the Coulomb barrier (V_B,R_B), we use Wong's prescription [11] for the Coulomb potential between two deformed nuclei,

$$V_C(r,\theta) = \frac{Z_1 Z_2 e^2}{r} + \sqrt{\frac{9}{20\pi}}\frac{Z_1 Z_2 e^2}{r^3}\sum_{i=1}^{2} R_i^2 \beta_{2i} P_2(cos\theta_i) + \left(\frac{3}{7\pi}\right)\frac{Z_1 Z_2 e^2}{r^3}\sum_{i=1}^{2} R_i^2 [\beta_{2i} P_2(cos\theta_i)]^2 \quad (5.10)$$

here, R_1, R_2 and β_{21}, β_{22} are the charge radii and the deformation parameters of the two nuclei, respectively. θ_i is the angle between the collision axis and the symmetry axis of the i^{th} nucleus, and is averaged with respect to angles from 0 to $\pi/2$ (see Fig. 2.5).

5.4 Nuclear potentials

We shall be using six different versions of the nuclear potential for the determination of the barrier parameters. These are the Bass potential (Bass 80), Christensen and Winther potential (CW 76), Broglia and Winther potential (BW 91), Aage Winther potential (AW 95), proximity potential (Prox 88) and the Denisov potential (Denv 02). We had used the above potentials as the barrier parameters could be easily and accurately determined with the minimum number of parameters. Apart from the Denisov potential, all the other potentials are discussed in section 2.5. A brief description of the Denisov potential is given below :

5.4.1 Denisov potential (Denv 02)

Denisov [13] calculated the semi-microscopic potential for various colliding nuclei in the framework of extended Thomas-Fermi approximation where the proton and neutron densities of each ion are obtained in the Hartree-Fock-Bogoliubov approximation with SkM parameter set of the Skyrme force [14]. By evaluating 7140 ion-ion potentials at 15 distances around the touching point, Denisov gave the following analytical expression for the nuclear potential,

$$V_N(r) = -1.989843\frac{R_1R_2}{R_1+R_2}\Phi(r-R_1-R_2-2.65)\Big[1+0.003525139\Big(\frac{A_1}{A_2}+\frac{A_2}{A_1}\Big)^{3/2} - 0.4113263(I_1+I_2)\Big] \quad (5.11)$$

with,

$$I_i = \frac{N_i - Z_i}{A_i} \qquad (i=1,2) \quad (5.12)$$

where, N ,Z and A are the number of neutrons, protons and mass number of the nuclei, respectively. R_i is the effective nuclear radius and is given as,

$$R_i = R_{ip}\Big(1-\frac{3.413817}{R_{ip}^2}\Big) + 1.284589\Big(I_i - \frac{0.4A_i}{A_i+200}\Big) \qquad (i=1,2) \quad (5.13)$$

where, the proton radius (R_{ip}) is given by [15],

$$R_{ip} = 1.24A_i^{1/3}\Big[1+\frac{1.646}{A_i} - 0.191\Big(\frac{A_i-2Z_i}{A_i}\Big)\Big] \quad (5.14)$$

.The function Φ is given by Eq. (5.15) for, -5.65 $\leq$ s $\leq$ 0, and by Eq. (5.16) for s $\geq$ 0.

$$\Phi(s) = 1 - \frac{s}{0.7881663} + 1.229218s^2 - 0.2234277s^3 - 0.1038769s^4$$
$$- \frac{R_1 R_2}{R_1 + R_2}(0.1844935s^2 + 0.07570101s^3) + (I_1 + I_2)(0.04470645s^2 + 0.03346870s^3) \quad (5.15)$$

$$\Phi(s) = \Big[1 - s^2[0.05410106\frac{R_1 R_2}{R_1 + R_2} exp(-s/1.760580)$$
$$- 0.5395420(I_1 + I_2)exp(-s/2.424408)]\Big] \times exp(-s/0.7881663) \quad (5.16)$$

5.5 Nature of the potentials

In this section we show the shape or nature of the potentials for the reactions ^4He+^{209}Bi, ^6He+^{209}Bi, ^4He+^{64}Zn and ^6He+^{64}Zn. For plotting the potential curves from Eq. 5.9, we use the simplified expression for the Coulomb potential between projectile and target which assumes that the projectile is a point charge in comparison to the target.

$$V_C = \begin{cases} \frac{Z_1 Z_2 e^2}{2r_c}\left(3 - \frac{r^2}{r_c^2}\right) & \text{if } r \leq r_c, \\ \frac{Z_1 Z_2 e^2}{r} & \text{if } r > r_c, \end{cases} \quad (5.17)$$

where, r_c is the radius of the target nucleus. Using the six different versions of the nuclear potentials (section 5.4), we plot the potentials for the above mentioned reactions in Figs. 5.2 and 5.3, respectively. We see that the maximum value of the potentials is quite distinct for all the six different types of potentials used. This peak value of the potential (for ℓ=0) is the Coulomb barrier (V_B) and the corresponding value of r is the position of the Coulomb barrier (R_B). Also, among the reactions induced by the normal projectile and the corresponding halo projectile, we observe

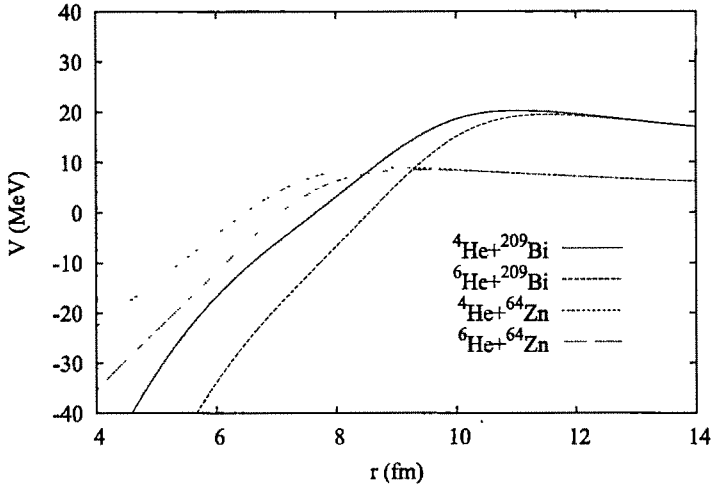

(a) Bass 80

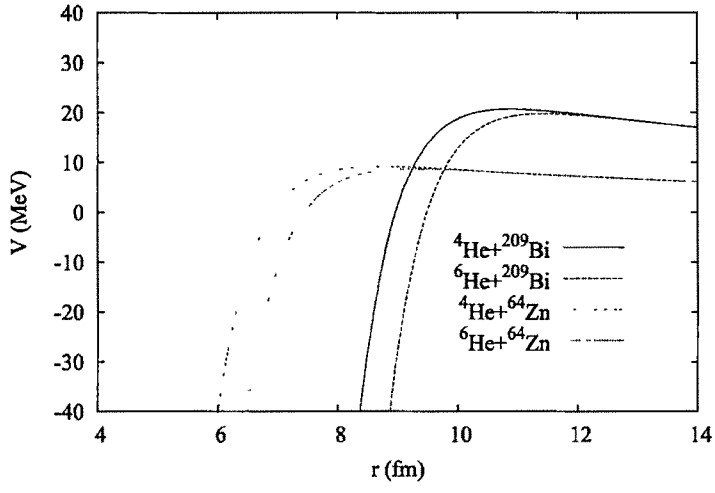

(b) CW 76

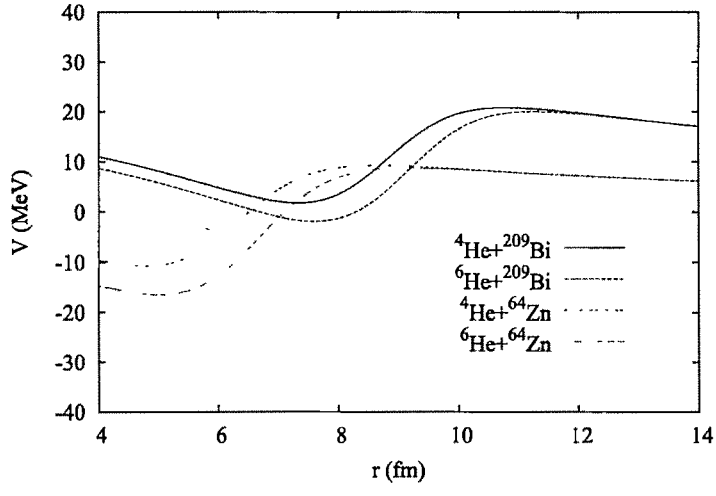

(c) BW 91

Figure 5.2: Total potential (MeV) vs distance (fm) for the reactions ^4He+^{209}Bi, ^6He+^{209}Bi, ^4He+^{64}Zn and ^6He+^{64}Zn using the nuclear potentials Bass 80, CW 76 and BW 91.

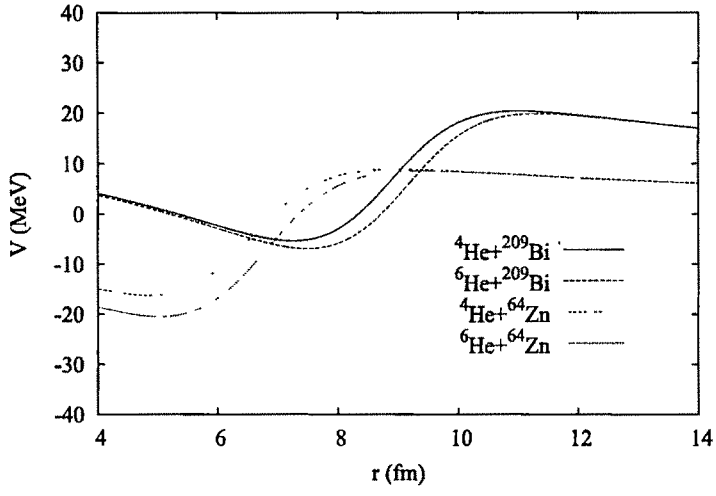

(a) AW 95

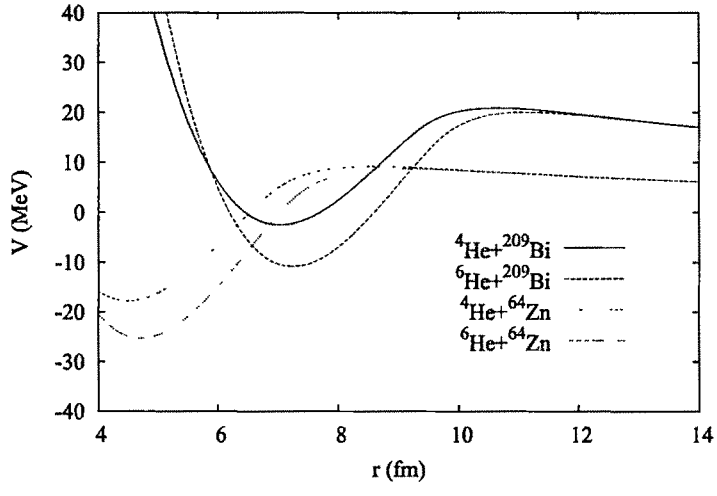

(b) Prox 88

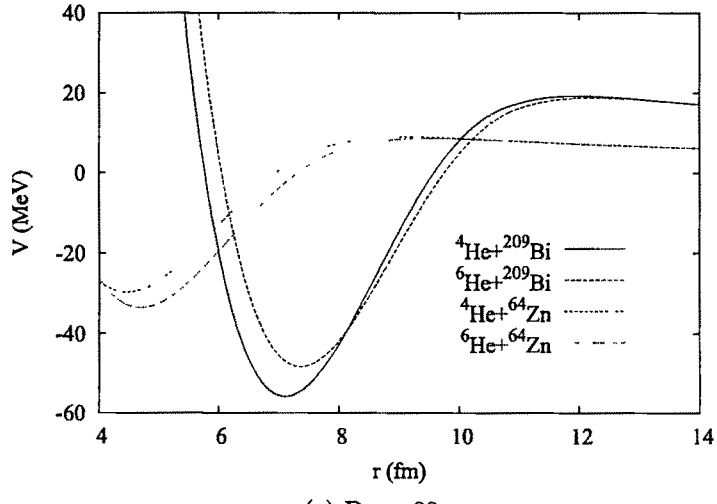

(c) Denv 02

Figure 5.3: Total potential (MeV) vs distance (fm) for the reactions ^4He+^{209}Bi, ^6He+^{209}Bi, ^4He+^{64}Zn and ^6He+^{64}Zn using the nuclear potentials AW 95, Prox 88 and Denv 02.

that noticeable differences of the total potential begin to show only for distances less than R_B. Also for r < R_B, the potential is more steeper for the halo projectile case than the normal projectile case which suggests that the magnitude of the force is greater for the halo projectile case than in comparison to the normal projectile case. Also, we notice that in moving from normal to radioactive halo projectiles, V_B is lowered and R_B is increased by small amount.

5.6 Results and Discussion

Using the different nuclear potentials we have found the height and position of the Coulomb barrier for the three reactions induced by the neutron halo nucleus ^6He, namely, ^6He+^{27}Al, ^6He+^{64}Zn and ^6He+^{209}Bi. Also the corresponding values induced by the normal nucleus (^4He) for the three reactions, namely, ^4He+^{27}Al, ^4He+^{64}Zn and ^4He+^{209}Bi are also determined. The static deformation parameters used for the target nuclei are as follows : 0.31 (^{27}Al) [16], 0.242 (^{64}Zn) and 0.1828 (^{58}Ni) [17]. The results are shown in Table 5.1. As can be seen, the height of the barrier (V_B) is slightly reduced and the position (R_B) is marginally raised for reactions induced by the halo nuclei in comparison to the normal nuclei. However, for the reaction ^8B+^{58}Ni (induced by the proton halo nuclei ^8B) straight application of the potentials give erroneous results as the barrier parameters are shifted in the opposite direction. This is because the rms matter radius of ^8B is larger than its normal counterpart ^{10}B even though there are lesser number of nucleons. The excess proton tend to form a halo outside the core which increases its matter radius [18]. This increase in the radius of proton halo nucleus is not accounted in the calculation of matter radii for the above potentials (Eqs. 2.10, 2.16, 2.19, 2.22, 2.27, 2.31 and 5.13). However, the increase of the radius of neutron halo nuclei is automatically accounted as the radius formulae for the different potentials show a direct dependence with the nucleon number. Taking experimental results into

Table 5.1: Coulomb barrier heights (in MeV) and positions (in fm) for the reactions $^{4,6}He+^{27}Al$, $^{4,6}He+^{64}Zn$, $^{4,6}He+^{209}Bi$ and $^{10,8}B+^{58}Ni$ using the potentials Bass 80, CW 76, BW 91, AW 95, Prox 88 and Denv 02.

Potential	Bass 80		CW 76		BW 91		AW 95		Prox 88		Denv 02	
	V_B	R_B	V_B	R_B	V_B	R_B	V_B	R_B	V_B	R_B	V_B	R_B
$^{4}He+^{209}Bi$	20.30	11.01	20.69	10.88	20.81	10.79	20.41	11.02	20.89	10.64	19.23	11.97
$^{6}He+^{209}Bi$	19.51	11.51	19.76	11.43	20.01	11.25	19.88	11.34	20.03	11.13	18.78	12.20
$^{4}He+^{64}Zn$	9.01	8.91	9.25	8.72	9.31	8.64	8.96	9.00	9.24	8.58	9.01	9.18
$^{6}He+^{64}Zn$	8.58	9.38	8.74	9.27	8.81	9.18	8.62	9.40	8.78	9.07	8.67	9.52
$^{4}He+^{27}Al$	4.31	7.98	4.47	7.73	4.50	7.66	4.26	8.14	4.42	7.68	4.51	7.93
$^{6}He+^{27}Al$	4.09	8.46	4.20	8.28	4.23	8.21	4.08	8.54	4.18	8.18	4.29	8.30
$^{10}B+^{58}Ni$	19.00	9.89	19.84	9.55	19.89	9.48	20.59	9.16	19.41	9.61	18.99	10.18
$^{8}B+^{58}Ni$	18.20	10.37	18.98	10.01	18.99	9.96	19.65	9.63	18.54	10.10	18.29	10.66

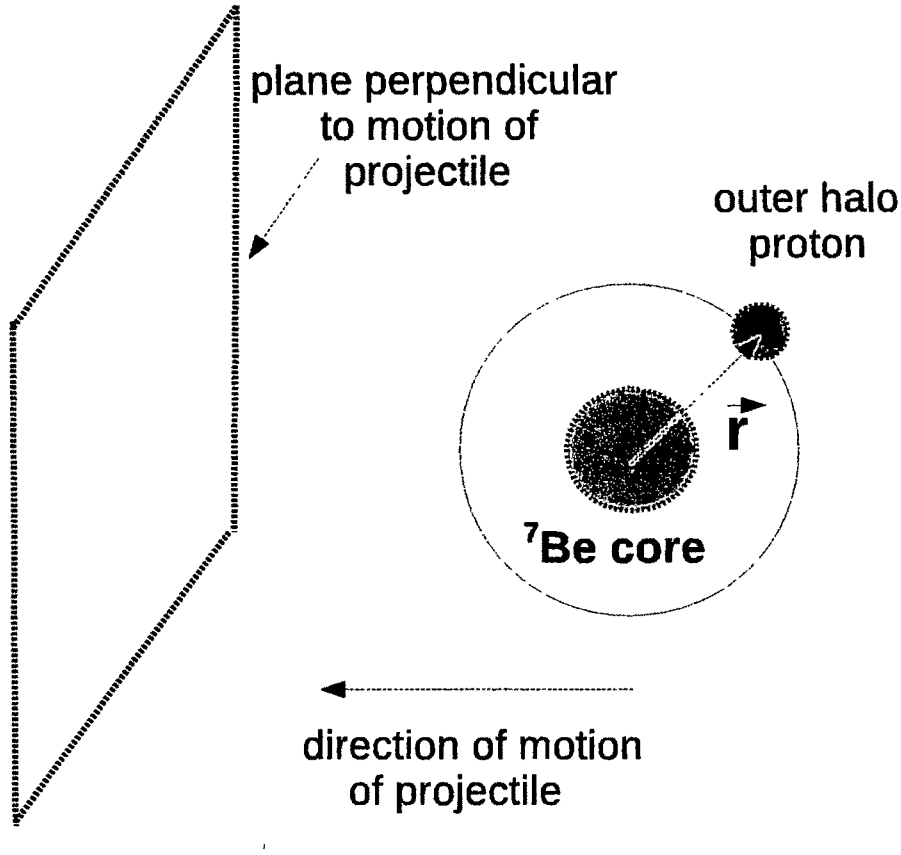

Figure 5.4: Diagram showing determination of effective radius of ^{8}B projectile.

consideration, we calculate effective radii for ^8B and ^{10}B, and then evaluate V_B and R_B for the reactions ^8B+^{58}Ni and ^{10}B+^{58}Ni. For ^{10}B, the radius is taken as 2.49 fm which is the average of experimentally reported values of 2.42 [19] and 2.56 fm [20].

Since, ^8B has a small one proton separation energy (S_p = 137 keV), hence it has exceptional proton halo character. Also, it has been shown that standard treatments like point Coulomb multipole expansion doesn't apply in case of ^8B nucleus [21]. The outer proton resides at a halo radius of r_h=4.2 fm, which is much larger than the experimental matter radius (2.33 fm) of its core (^7Be) (see Fig. 5.4). Straight forward calculation (Eq. 15 of Ref. [18]) yields r.m.s. matter radius of 2.60 fm for ^8B. However, instead of using the r.m.s. matter radius, we calculate an effective radius of ^8B nucleus by the following method. For an ^8B projectile incident on a target

nucleus, the effective radius would be the projection of $\vec{r}$ on a plane perpendicular to the direction of motion of the projectile, where $\vec{r}$ is the vector from the centre of the ^8B nucleus to the outer halo proton (see Fig. 5.4). The length of $\vec{r}$ is taken as 5.01 fm which is the sum of the halo radius (r_h) and the proton radius ($r_p = 0.81$ fm) [18]. For random orientations of ^8B projectile, we calculate the average of the projections with the condition that if the projection is less than 2.33 fm (radius of ^7Be core), then consider the projection as 2.33 fm. Straight forward Monte Carlo simulation yields the value 2.84 fm, which we consider as the effective radius of the ^8B projectile. With these new values of radii, we find the barrier parameters for $^{10,8}B$+^{58}Ni, and these are shown in Table 5.1. The percentage change in the barrier parameters can be determined by,

$$\Delta V_B(\%) = \frac{V_B^N - V_B^H}{V_B^N} \times 100 \quad ; \quad \Delta R_B(\%) = \frac{R_B^N - R_B^H}{R_B^N} \times 100 \tag{5.18}$$

where, V_B^N, R_B^N and V_B^H, R_B^H stand for the barrier parameters of reactions induced by normal nuclei (^4He, ^{10}B) and halo nuclei (^6He, ^8B), respectively.

Using the barrier parameters from Table 5.1, $\Delta V_B(\%)$ and $\Delta R_B(\%)$ are calculated and these values are shown in Fig. 5.5(a) and 5.5(b), respectively. The highest shift in the barrier parameters is observed for $^{4,6}He$+^{27}Al, followed by $^{4,6}He$+^{64}Zn, $^{10,8}B$+^{58}Ni and $^{4,6}He$+^{209}Bi. Among the potentials the highest shift in the barrier parameters is observed for CW 76, which is marginally ahead of BW 91. They are followed by Prox 88, Bass 80, Denv 02 and AW 95. For the reactions $^{4,6}He$+^{27}Al, $^{4,6}He$+^{64}Zn, $^{10,8}B$+^{58}Ni and $^{4,6}He$+^{209}Bi, the average values of $\Delta V_B(\%)$ for the six potentials turn out to be 5.63, 4.99, 4.50 and 3.68, respectively. The corresponding values for $\Delta R_B(\%)$ are -6.06, -5.29, -4.95 and -3.88, respectively. This gives an overall average of 4.70 for $\Delta V_B(\%)$ and -5.05 for $\Delta R_B(\%)$. For comparison the values reported in Ref. [9] are $\approx$ 4% and -9%, respectively. Therefore, a qualitative

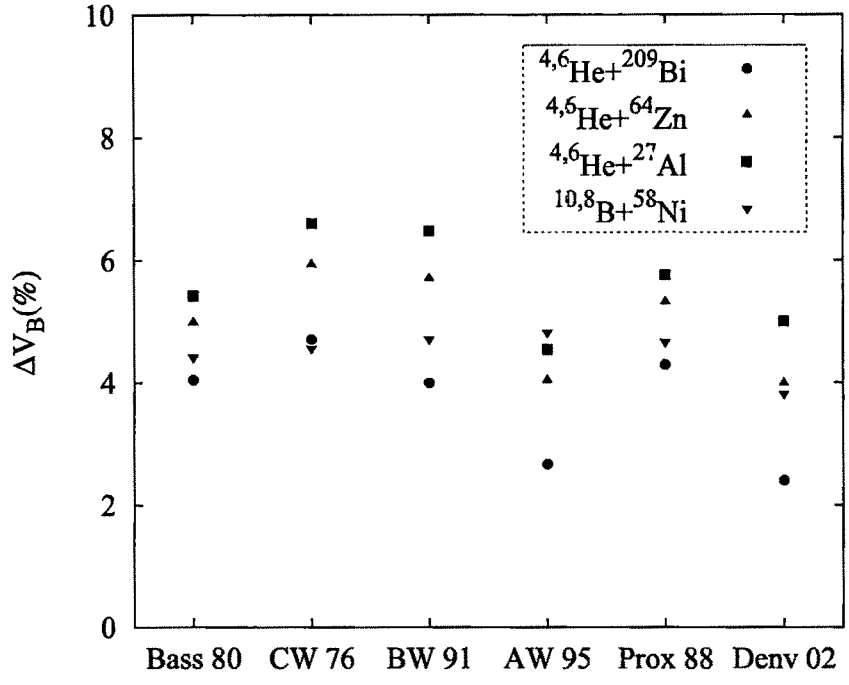

(a) ΔV_B

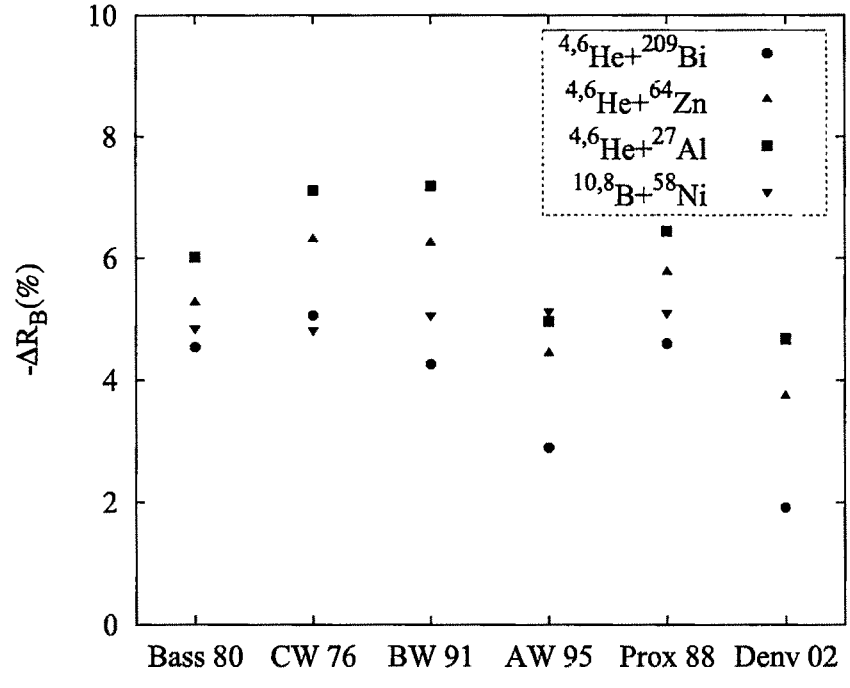

(b) ΔR_B

Figure 5.5: Percentage change in the barrier parameters of radioactive halo systems with respect to normal loosely bound systems for the six different nuclear potentials. The radioactive halo systems are ^6He+^{27}Al, ^6He+^{64}Zn, ^6He+^{209}Bi and ^8B+^{58}Ni. The normal loosely bound systems are ^4He+^{27}Al, ^4He+^{64}Zn, ^4He+^{209}Bi and ^{10}B+^{58}Ni. Fig. (a) shows percentage changes in V_B, and Fig. (b) shows percentage changes in R_B.

explanation for the shift in the barrier parameters in moving from normal to radioactive halo systems is contained within the global parametrization of nuclear potentials. As explained earlier, this shift in the barrier parameters ultimately explains the separation of the trajectories of normal loosely bound systems and radioactive halo systems in the reduced experimental reaction cross section analysis.

It would be interesting to observe the shift in the barrier parameters for Berellium (Be) projectile induced systems. Be has many isotopes out of which ^{7}Be and ^{9}Be are loosely bound, whereas the isotope ^{11}Be has proven neutron halo properties. Using the six nuclear potentials, we did similar calculations as above to determine the barrier parameters for reactions induced by the above projectiles on the targets ^{27}Al, ^{64}Zn and ^{209}Bi. The results are shown in Table 5.2. As expected we notice that the barrier height (V_B) is reduced, whereas the barrier position (R_B) is slightly raised as we move from normal loosely bound to radioactive halo systems. Again using Eq. (5.18) we find the shift in the barrier parameters. However, this time we determine two sets for the shift in the barrier parameters, one each for reactions induced by the two loosely bound nuclei (^{7}Be and ^{9}Be) with respect to reactions induced by the halo nucleus (^{11}Be). The average values of $\Delta V_B(\%)$ for the six potentials for the reactions $^{7,11}Be+^{27}Al$, $^{7,11}Be+^{64}Zn$ and $^{7,11}Be+^{209}Bi$ are 5.79, 7.04 and 4.72 respectively. The corresponding values of $\Delta R_B(\%)$ are -6.31, -7.66 and -4.84, respectively. Similarly, for the reactions $^{9,11}Be+^{27}Al$, $^{9,11}Be+^{64}Zn$ and $^{9,11}Be+^{209}Bi$ the average values of $\Delta V_B(\%)$ are 4.12, 3.05 and 1.57, respectively. The corresponding values of $\Delta R_B(\%)$ are -2.98, -3.32 and -2.22, respectively. This gives an overall average of 4.38 and -4.56 for $\Delta V_B(\%)$ and $\Delta R_B(\%)$, respectively, which is a qualitatively good agreement with the values of $\approx$ 4% and -9% [9]. The above results suggest that the reduced reaction cross section for reactions induced by the neutron halo projectile ^{11}Be is very likely to fall on the same trajectory as that of radioactive halo projectiles [9]. Also, the reduced reaction cross section for reactions induced by the loosely bound projectiles (^{7}Be, ^{9}Be) will certainly lie on

Table 5.2: Coulomb barrier heights (in MeV) and positions (in fm) for the reactions $^{7,9,11}Be+^{27}Al$, $^{7,9,11}Be+^{64}Zn$ and $^{7,9,11}Be+^{209}Bi$ using the potentials Bass 80, CW 76, BW 91, AW 95, Prox 88 and Denv 02.

Potential	Bass 80		CW 76		BW 91		AW 95		Prox 88		Denv 02	
	V_B	R_B	V_B	R_B	V_B	R_B	V_B	R_B	V_B	R_B	V_B	R_B
$^{7}Be+^{209}Bi$	40.25	11.08	40.46	11.15	40.59	11.07	40.46	11.11	41.41	10.73	39.31	11.35
$^{9}Be+^{209}Bi$	39.16	11.43	39.31	11.50	39.64	11.35	39.73	11.33	40.26	11.07	38.32	11.87
$^{11}Be+^{209}Bi$	38.29	11.72	38.41	11.78	38.86	11.60	39.10	11.53	39.35	11.35	37.54	12.13
$^{7}Be+^{64}Zn$	17.83	8.97	18.01	8.97	18.11	8.89	17.78	9.07	18.32	8.67	18.28	8.94
$^{9}Be+^{64}Zn$	17.24	9.31	17.37	9.33	17.49	9.23	17.31	9.34	17.69	9.01	17.61	9.30
$^{11}Be+^{64}Zn$	16.78	9.60	16.88	9.61	17.02	9.51	16.91	9.58	17.20	9.28	17.11	9.59
$^{7}Be+^{27}Al$	8.53	8.06	8.69	7.97	8.74	7.91	8.46	8.20	8.76	7.75	9.11	7.77
$^{9}Be+^{27}Al$	8.23	8.39	8.35	8.33	8.40	8.25	8.20	8.48	8.43	8.09	8.72	8.12
$^{11}Be+^{27}Al$	7.99	8.67	8.09	8.61	8.15	8.54	8.00	8.72	8.19	8.36	8.43	8.41

the same trajectory as that of the normal loosely bound projectiles [9]. This would ensure that the above calculated shift (which matches the experimental shift from reduced reaction cross section analysis) in the barrier parameters is obtained as we move from normal to radioactive halo systems.

Out of the reactions considered above, we have obtained a Wong's model fit for the total reaction cross section for the reactions $^{6}He + {}^{27}Al$ and $^{7}Be+{}^{27}Al$. We use the barrier parameters obtained from the Bass 80 and the AW 95 potentials for use in the Wong's formula, as our earlier work [4] had shown that these two potentials are best in reproducing the barrier parameters. The results are shown in Figs. 5.6 and 5.7, where the fusion cross section (σ_{reac}) predicted by the unmodified Wong's formula (UWF) (with barrier parameters calculated from Bass 80 and AW 95 potentials) is compared with experimental data. There is not much difference in the predictions of UWF-Bass 80 and UWF-AW 95 for the two reactions. However, for the reaction $^{7}Be+{}^{27}Al$, the prediction is below the experimental data. This is due to a proton transfer of ^{7}Be to the target which tends to increase the experimental reaction cross section. The unmodified Wong's formula assumes the projectile and target to be inert and no breakup and transfer (of nucleons) is allowed.

As suggested in [10], the total reaction cross section for all types of systems (tightly bound, loosely bound and halo) can be described by the modified Wong's formula (MWF).

$$\sigma = \frac{IMR_b^2\hbar\omega_0}{2E_{cm}} ln\Big\{1 + exp\Big[\frac{2\pi(E_{cm} - E_0)}{\hbar\omega_0} + P\Big]\Big\} \tag{5.19}$$

where, I, M and P are three dimensionless parameters whose values are derived by fitting the data. Here, the parameter I accounts for the Coulomb barrier dependency of the cross section, M indicates increase of the cross section for loosely bound and halo systems, and P makes an adjustment of the Coulomb barrier with respect to the collision energy in case the cross section starts to increase sharply. The parameters

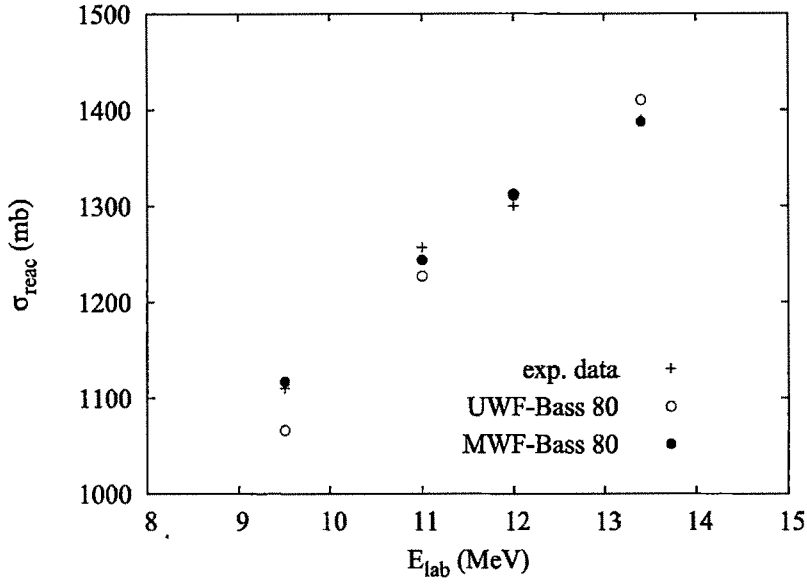

(a) $^{6}He+^{27}Al$ (Bass 80)

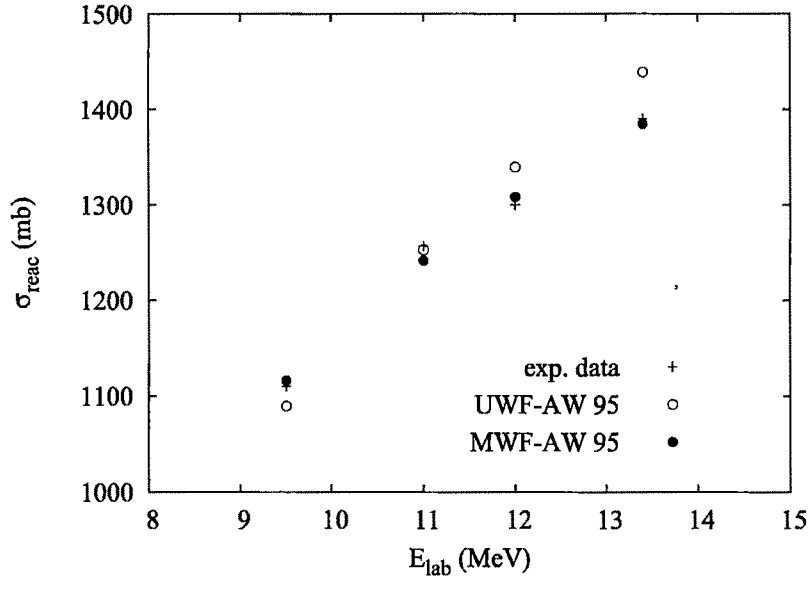

(b) $^{6}He+^{27}Al$ (AW 95)

Figure 5.6: Fitting of reaction cross section (σ_{reac}) using the unmodified Wong's formula (UWF) and the modified Wong's formula (MWF) for the reaction $^{6}He+^{27}Al$. The barrier parameters are taken from Bass 80 and AW 95 potentials. Expt. data is taken from [22]

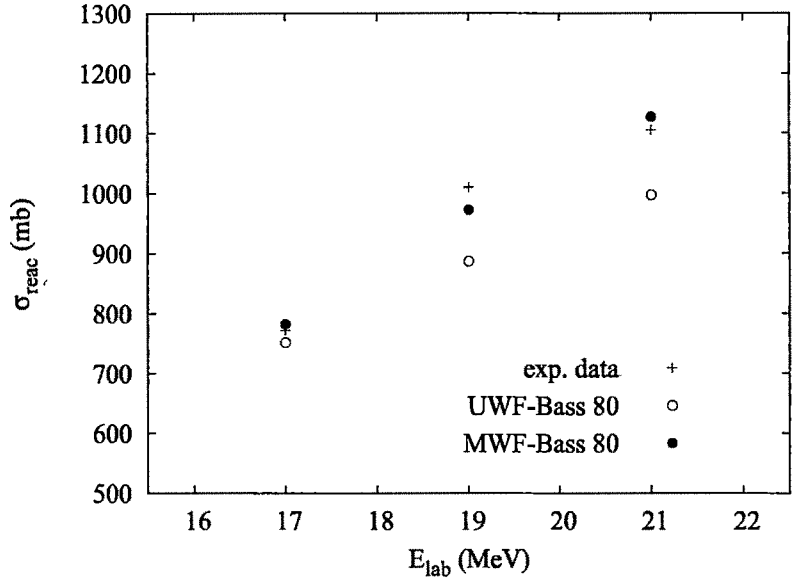

(a) $^{7}Be+^{27}Al$ (Bass 80)

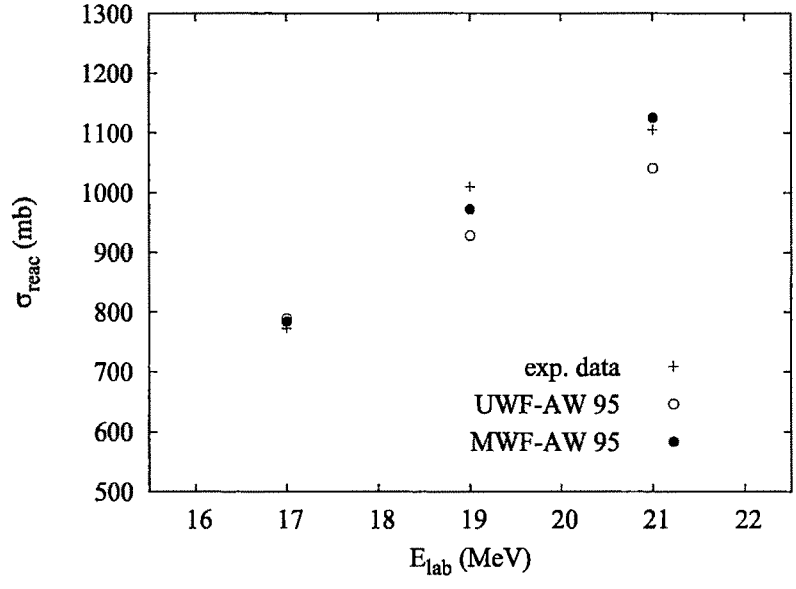

(b) $^{7}Be+^{27}Al$ (AW 95)

Figure 5.7: Fitting of reaction cross section (σ_{reac}) using the unmodified Wong's formula (UWF) and the modified Wong's formula (MWF) for the reaction $^{7}Be+^{27}Al$. The barrier parameters are taken from Bass 80 and AW 95 potentials. Expt. data is taken from [16].

Table 5.3: Values of the parameters I, M, P and the minimized χ^2-values obtained by fitting the experimental reaction cross-section data with the modified Wong's formula (MWF) for the reactions $^6He + ^{27}Al$ and $^7Be + ^{27}Al$. The barrier parameters are derived from the Bass 80 and AW 95 potentials.

Parameter	$^7Be+^{27}Al$		$^6He+^{27}Al$	
	Bass 80	AW 95	Bass 80	AW 95
I	0.8	0.8	0.6	0.6
M	1.59	1.53	1.52	1.48
P	-0.23	-0.24	0.17	0.17
χ^2	1.95	1.95	0.28	0.29

are derived in way such that the deviation of the calculated and the experimentally measured cross section is minimum. Initially, we make a choice of the parameter I taking into account its direct dependence with the barrier height [10]. The χ^2 minimization technique of the best fit distribution is utilized to derive the other two parameters (M and P). The χ^2 value for a particular fitting of observed or experimental (O) value and the expected or theoretical value (E) is given by,

$$\chi^2 = \sum_{i=1}^{n} \frac{(O_i - E_i)^2}{E_i} \tag{5.20}$$

Initially the expected values (E) are determined from the modified Wong's formula with arbitrary values of the parameters (I, M and P). Then using Fortran programming χ^2 values are minimized by simultaneous change of the variables x (=IM) and P. Then, the total reaction cross section is obtained for the three reactions by using the modified Wong's formula (MWF) and the results are shown in Figs. 5.6 and 5.7. We see that the fitting is quite good and there is vast improvement over the predictions of the unmodified Wong's formula (UWF). This is because the modified Wong's formula (MWF) is a phenomenological formula with additional parameters (I, M and P) to explain the increase in the reaction cross-section induced by halo and radioactive projectiles. The values of the parameters and the minimized χ^2 values are given in Table 5.3. We note that the value of M is in good agreement with

the values given in [10]. For the reaction $^{6}He + ^{27}Al$, the value of the parameter P is more or less in agreement with the values in [10]. However, for the reaction $^{7}Be + ^{27}Al$, parameter P is not in agreement with the value reported in [10] which is probably due to the fact that there is a substantial transfer cross section.

5.7 Summary and Outlook

Reduced reaction cross section analysis of a variety of reactions has revealed that the trajectories for reduced reaction cross section for reactions initiated by normal loosely bound projectiles, and radioactive halo projectiles are clearly separated when plotted against their reduced energy. Also, it has been pointed out that the reason for the separation of the trajectories is that the barrier parameters (V_B, R_B) are slightly shifted. This result can be explained within the global parametrization of nuclear potentials if the correct radius of nucleus is taken into consideration. Direct application of the potentials Bass 80, CW 76, BW 91, AW 95, Prox 88 and Denv 02 can explain the shift of the barrier parameters of reactions induced by the neutron halo nucleus (^{6}He). For the proton halo system ($^{8}B + ^{58}Ni$), the shift cannot be explained by straight application of the potentials. The potentials predict a decrease in radius of proton halo nucleus (^{8}B) with respect to the normal counterpart (^{10}B), but experimentally an increase in matter radius is observed. Taking experimental data into consideration, the average matter radius for ^{10}B is determined. Since, ^{8}B has exceptional proton halo character, we determine an effective radius for ^{8}B. The experimental shift in the barrier parameters for the proton halo system can be satisfactorily explained by taking into consideration the radii for ^{10}B and ^{8}B. Similar analysis is carried out for reactions induced by Be projectile. We found that the calculated shift of the barrier parameters for radioactive halo system (induced by ^{11}Be) with respect to normal loosely bound systems (induced by ^{7}Be and ^{9}Be) matches the experimentally obtained shift of the barrier parameters obtained from reduced cross

section analysis of reactions induced by ^{6}He and ^{8}B projectiles. For the reactions $^{6}He + {}^{27}Al$ and $^{7}Be{+}^{27}Al$ (induced by radioactive projectiles), we have obtained a best fit for the total reaction cross section using the modified Wong's formula (MWF). This phenomenological formula contains three dimensionless parameters whose values are chosen by the χ^2 minimization technique. The total reaction cross section is reproduced quite satisfactorily for the two reactions.

We note that only one proton halo system has been taken into consideration for study of the reduced reaction cross section. Hence, more experimental data regarding proton halo systems is needed in order to make a universal conclusion regarding its reduced reaction cross section. More study (experimental and theoretical) is needed for accurate determination of r.m.s. matter and charge radii of proton halo nuclei. This would help us in better treatment of the nuclear potentials of proton halo nuclei.

Bibliography

[1] K. Siwek-Wilczynska and J. Wilczynski, *Phys. Rev. C*, **69** (2004) 024611.

[2] N.G. Nicolis, *Eur. Phy. J. A*, **21** (2004) 265.

[3] M. Dasgupta, D. J. Hinde, N. Rowley and A. M. Stefanini, *Annu. Rev. Nucl. Part. Sci.*, **48** (1998) 401.

[4] C. K. Phookan and K. Kalita, *Nucl. Phys. A*, **899** (2013) 29.

[5] C. K. Phookan and K. Kalita, *Journal of Physics G : Nucl. and Part. Physics*, **40** (2013) 125107.

[6] P. R. S. Gomes, J. Lubian, I. Padron, and R. M. Anjos, *Phys. Rev. C*, **71** (2005) 017601.

[7] E. F. Aguilera, *Journal of Physics : Conference Series* , **387** (2012) 012001.

[8] E. F. Aguilera, E. Martinez-Quiroz, D. Lizcano, A. Gmez-Camacho, J. J. Kolata, L. O. Lamm, V. Guimares, R. Lichtenthler, O. Camargo, F. D. Becchetti, H. Jiang, P. A. DeYoung, P. J. Mears, and T. L. Belyaeva, *Phys. Rev. C*, **79** (2009) 021601.

[9] J. J. Kolata and E. F. Aguilera, *Phys. Rev. C*, **79** (2009) 027603.

[10] Jin Lei, J. S. Wang, S. Mukherjee, Q Wang and R. Wada, *Phys. Rev. C* , **86** (2012) 057603.

[11] C. Y. Wong, *Phys. Rev. Lett.*, **31** (1973) 766.

[12] C. Y. Wong, *Phys. Lett. B*, **42** (1972) 186.

[13] V. Yu. Denisov, *Phys. Lett. B*, **526** (2002) 315.

[14] M. Brack,C. Guet, H. B. Hakanson, *Phys. Rep.*, **123** (1985) 275; M. Brack and R. K. Bhaduri, *Semi-Classical Physics*, Addison-Wesley, Reading, MA, (1997) ; J. Bartel, Ph. Quentin, M. Brack, C. Guet, H. B. Hakanson,*Nucl. Phys. A*, **386** (1982) 79.

[15] B. Nerlo-Pomorska, K. Pomorski, *Z. Phys. A*, **348** (1994) 169.

[16] K. Kalita, S. Verma, R. Singh, J. J. Das, A. Jhingan, N. Madhavan, S. Nath, T. Varughese, P. Sugathan, V. V. Parkar, K. Mahata, K. Ramachandran, A. Shrivastava, A. Chatterjee, S. Kailas, S. Barua, P. Basu, H. Majumdar, M. Sinha, R. Bhattacharya, and A. K. Sinha, *Phys. Rev. C*, **73** (2006) 024609.

[17] S. Raman, C. W. Nestor and P. Tikkanen, *Atomic Data and Nuclear Data Tables*, **78** (2001) 1.

[18] F. Carstoiu, L. Trache, C. A. Gagliardi, R. E. Tribble and A. M. Mukhamedzhanov, *Phys. Rev. C*, **63** (2001) 054310.

[19] M. Lassaut and R. J. Lombart, *Z. Phys. A*, **341** (1992) 125.

[20] E. Liatard, J. F. Bruandet, F. Glasser, S. Kox, Tsan Ung Chan, G. J. Costa, C. Heitz, Y. El Masri, F. Hanappe, R. Bimbot, D. Guillemaud-Mueller and A. C. Mueller *Europhys. Lett.*, **13** (1990) 401.

[21] H. Esbensen and G. F. Bertsch, *Phys. Rev. C*, **59** (2002)3240.

[22] E.A. Benjamim, A. Lpine-Szily, D.R. Mendes Junior, R. Lichtenthler, V. Guimares, P.R.S. Gomes, L.C. Chamon, M.S. Hussein, A.M. Moro, A. Arazi, I. Padron, J. Alcantara Nuez, M. Assuno, A. Barioni, O. Camargo Jr., R.Z. Denke, P.N. de Faria, K.C.C. Pires, *Phys. Lett. B*, **647** (2007) 30.

Chapter 6

Conclusion

In the present thesis we have carried out a theoretical investigation on the properties of reactions induced by loosely bound projectiles. To some extent, our work is motivated by the huge amount of experimental data that has become available in the last decade and a half. The properties studied by us are the fusion barrier, fusion cross section, fusion suppression and also the reduced reaction cross section analysis of radioactive systems. In chapter 2, the fusion barrier parameters (V_B, R_B) of thirteen reactions induced by the loosely bound projectiles, ^{6}Li, ^{7}Li and ^{9}Be are studied. For evaluation of the fusion barriers, eight different versions of the proximity potential are employed. The potentials Bass 80 and BW 91 are found to be most effective in reproducing the values of V_B and R_B, respectively. The parametrized formula $\left(V_B = 1.44 Z_1 Z_2 (R_B - 0.75)/R_B^2\right)$ connecting V_B and R_B has also been tested for the above reactions, and the formula is found to be extremely effective. For the reaction ^{6}Li+^{152}Sm, the deviation of the barrier parameters from the experimental values are quite large. On applying the correction to the Coulomb potential for the deformed target (^{152}Sm), the new values of the barrier parameters are found to be much closer to the empirical values.

In the third chapter we studied the fusion cross section for the reactions ^6Li+^{209}Bi, ^9Be+^{208}Pb, ^7Li+^{209}Bi and ^6Li+^{152}Sm. Wong's formula is used for determination

of the fusion cross section, and the barrier parameters needed for use in the Wong's formula are taken from chapter 2. For all the reactions, the fusion cross section is in agreement with the results of the single barrier penetration model (SBPM). We also note that the experimental results are much below the theoretical expectations. This is because of the fact that fusion suppression is dominant in these reactions which takes place due to breakup of the projectile. For the reaction $^{6}Li+^{152}Sm$ we also observe that the fusion cross section for the deformed target case is in much better agreement with the theoretical predictions than in case of spherical target. This proves that target deformation has a great role to play in the study of fusion cross section.

In the fourth chapter we present a semiclassical model for the explanation of fusion suppression. The problem is essentially separated into two parts. In the first part the cutoff impact parameter for fusion is determined, and in the second part we find the fraction of projectiles undergoing breakup within this cutoff impact parameter. The cutoff impact parameter for fusion is obtained through rigorous quantum mechanical concepts as fusion is a quantum mechanical barrier transmission problem having no classical analogue. We applied the classical trajectory method in order to determine the fraction of projectiles undergoing breakup within the cutoff impact parameter for fusion. Studying the numerical solutions, a breakup condition for a trajectory is defined. Then for each impact parameter, the breakup fraction is determined by taking a sample of 50 trajectories. Then, a simple formula for explanation of fusion suppression is proposed, according to which fusion suppression is given by the average of the breakup fractions evaluated at impact parameters ranging from head-on collision up to the cutoff impact parameter. On application of the above formula, we find that there is very good agreement between σ_{cal} and σ_{exp} for the three systems ^{6}Li+^{209}Bi, ^{6}Li+^{152}Sm and ^{6}Li+^{144}Sm. The agreement of our results with experimental data also suggests that the above barrier breakup of ^{6}Li nucleus in the field of a heavy target nucleus can be fruitfully studied by applying classi-

cal Newtonian laws. This is especially important in view of the fact that quantum mechanical methods (like CDCC), employed for studying breakup, can work only under approximations which may not lead to accurate results under all conditions. Another contribution in this chapter is the development of a semiclassical model of the ^{6}Li nucleus. The model is essential for obtaining the initial conditions for solving the classical equations of motion.

In the fifth chapter, we present an analysis of reaction cross section induced by radioactive projectiles (^{6}He, ^{8}B and ^{7}Be). It is now well known that the reduced reaction cross section (vs reduced energy) shows separate trajectories for tightly bound, loosely bound and radioactive halo systems. Also it has been pointed out that this existence of well-defined paths is due to the separation of the barrier parameters for the three types of systems. In this work we sought an explanation for the shift in the barrier parameters of radioactive halo systems with respect to normal loosely bound systems by using six different nuclear potentials. The calculated shift of the barrier parameters closely matches the experimental shift of the barrier parameters obtained from reduced reaction cross section analysis. This result proves that the separation of the trajectories of the reduced reaction cross section of different systems is contained within the global parametrization of nuclear potentials. For the proton halo system, the shift can only be explained if new values of the radii (for ^{10}B and ^{8}B) are taken into consideration which is because of the fact that the radius of the halo nucleus (^{8}B) is greater than the normal nucleus (^{10}B). For the reactions $^{6}He + {}^{27}Al$ and $^{7}Be{+}^{27}Al$, fitting of the total reaction cross section is done using the modified Wong's formula (MWF) (PRC, 86, 057603). From the quality of the fit, it can be concluded that for halo and loosely bound systems, the modified Wongs' formula (MWF) gives a better reproduction of the experimental reaction cross section than the unmodified Wongs' formula (UWF).

In our opinion, the work presented here has a lot of scope for future research. Many other potentials, like, single-folding, double-folding and Skyrme energy den-

sity, could be used for the evaluation of the barrier parameters (V_B, R_B) of loosely bound systems. It would be interesting to see how they compare with the predictions of the proximity potentials that has been reported here. For the system ^{6}Li+^{152}Sm, correction of the nuclear potential for the deformed target can also be tried, especially for the potentials Prox 88 and BW 91. For the determination of the fusion cross section above the barrier, improved versions of Wong's formula (Balantekin's correction) can be used for accurate determination of the fusion cross section.

Fusion suppression factor for other ^{6}Li based reactions can also be studied. Instead of using Wood's–Saxon potential, other nuclear potentials can also be used in the classical equations of motion. It would be interesting to observe which other nuclear potentials (apart from Wood's-Saxon) can predict an accurate picture of breakup of the projectile. The model of fusion suppression developed here is a two-dimensional classical trajectory model. The obvious generalization would be a three–dimensional model. It would be interesting to see whether the formula for fusion suppression proposed here for the two–dimensional model (Eq. 4.64) would still be applicable for the three–dimensional model. In the three–dimensional model, the orientation of the projectile is not necessarily confined to a single plane which is the case for the two–dimensional model. Finally, a fully quantum mechanical model of fusion suppression could be attempted in future even though it may be a highly challenging task. For this it would be necessary to develop a fully quantum mechanical version of the model of ^{6}Li nucleus that has been proposed here.

Appendix A

Fortran code for determining breakup and nobreakup trajectories

```
program breakup
implicit none
real::fun1,fun2,r1,a1,r2,a2,r3,a3,k0,k1,k2,k3,k4,k5,r,w1,z1,w2,z2,w3,z3,n1,n2,n3,h,t,x
real::c1,c2,c3,c4,c5,c6,c7,c8,c9,c10,c11,c12,c13,c14,c15,c16,c17,c18,c19,c20,c21,c22,c23,c24
real::r0,e,b,v3,v,v1,v2,rd1,ra,d
real::x1,x2,y1,y2,x3,y3
integer::i,n,m,i1
open(unit=1,file='data22b1',status='unknown')
open(unit=2,file='deutron2',status='unknown')
open(unit=3,file='alpha-particle2',status='unknown')
open(unit=4,file='target2',status='unknown')
read*,m
r1=1.850
a1=0.710
```

r2=1.160

a2=0.830

r3=1.392

a3=0.656

k0=2.880

k1=106.338

k2=109.630

k3=91.460

k4=119.520

k5=239.040

r=6.970

h=0.01

n=1700

n1=2

n2=4

n3=209

t=0

x3=0

w3=0

y3=0

z3=0

r0=2.27

e=33.0

b=0.8

v3=0.47952/sqrt(r0)

v=sqrt(0.31936*e)

v1=2*v3

v2=v3

```
do i1=1,m
rd1=rand()
enddo
ra=25+rd1*30
x1=-ra-(0.666667)*r0*sin(x)
y1=b+(0.66667)*r0*cos(x)
x2=-ra+(0.33333)*r0*sin(x)
y2=b-(0.33333)*r0*cos(x)
w1=v+v1*cos(x)
z1=v1*sin(x)
w2=v-v2*cos(x)
z2=-v2*sin(x)
do i=1,n
c1=k0*(x1-x2)/(fun1(x1,x2,y1,y2))**3
c2=-k1*fun2(x1,x2,y1,y2,r1,a1)*(x1-x2)/fun1(x1,x2,y1,y2)
c3=-k2*fun2(x1,x3,y1,y3,r2,a2)*(x1-x3)/fun1(x1,x3,y1,y3)
if(fun1(x1,x3,y1,y3).lt.r)then
c4=(k4/r**3)*(x1-x3)
else
c4=k4*(x1-x3)/(fun1(x1,x3,y1,y3))**3
endif
w1=w1+h*0.95808*(c1+c2+c3+c4)/n1
x1=x1+h*w1
c5=k0*(y1-y2)/(fun1(x1,x2,y1,y2))**3
c6=-k1*fun2(x1,x2,y1,y2,r1,a1)*(y1-y2)/fun1(x1,x2,y1,y2)
c7=-k2*fun2(x1,x3,y1,y3,r2,a2)*(y1-y3)/fun1(x1,x3,y1,y3)
if(fun1(x1,x3,y1,y3).lt.r)then
c8=(k4/r**3)*(y1-y3)
```

```
else
c8=k4*(y1-y3)/(fun1(x1,x3,y1,y3))**3
endif
z1=z1+h*0.95808*(c5+c6+c7+c8)/n1
y1=y1+h*z1
c9=-k0*(x1-x2)/(fun1(x1,x2,y1,y2))**3
c10=k1*fun2(x1,x2,y1,y2,r1,a1)*(x1-x2)/fun1(x1,x2,y1,y2)
c11=-k3*fun2(x2,x3,y2,y3,r3,a3)*(x2-x3)/fun1(x2,x3,y2,y3)
if(fun1(x2,x3,y2,y3).lt.r)then
c12=(k4/r**3)*(x2-x3)
else
c12=k4*(x2-x3)/(fun1(x2,x3,y2,y3))**3
endif
w2=w2+h*0.95808*(c9+c10+c11+c12)/n2
x2=x2+h*w2
c13=-k0*(y1-y2)/(fun1(x1,x2,y1,y2))**3
c14=k1*fun2(x1,x2,y1,y2,r1,a1)*(y1-y2)/fun1(x1,x2,y1,y2)
c15=-k3*fun2(x2,x3,y2,y3,r3,a3)*(y2-y3)/fun1(x2,x3,y2,y3)
if(fun1(x2,x3,y2,y3).lt.r)then
c16=(k5/r**3)*(y2-y3)
else
c16=k5*(y2-y3)/(fun1(x2,x3,y2,y3))**3
endif
z2=z2+h*0.95808*(c13+c14+c15+c16)/n2
y2=y2+h*z2
c17=k2*fun2(x1,x3,y1,y3,r2,a2)*(x1-x3)/fun1(x1,x3,y1,y3)
c18=k3*fun2(x2,x3,y2,y3,r3,a3)*(x2-x3)/fun1(x2,x3,y2,y3)
if(fun1(x1,x3,y1,y3).lt.r)then
```

```
c19=-(k4/r**3)*(x1-x3)
else
c19=-k4*(x1-x3)/(fun1(x1,x3,y1,y3))**3
endif
if(fun1(x2,x3,y2,y3).lt.r)then
c20=-(k5/r**3)*(x2-x3)
else
c20=-k5*(x2-x3)/(fun1(x2,x3,y2,y3))**3
endif
w3=w3+h*0.95808*(c17+c18+c19+c20)/n3
x3=x3+h*w3
c21=k2*fun2(x1,x3,y1,y3,r2,a2)*(y1-y3)/fun1(x1,x3,y1,y3)
c22=k3*fun2(x2,x3,y2,y3,r3,a3)*(y2-y3)/fun1(x2,x3,y2,y3)
if(fun1(x1,x3,y1,y3).lt.r)then
c23=-(k4/r**3)*(y1-y3)
else
c23=-k4*(y1-y3)/(fun1(x1,x3,y1,y3))**3
endif
if(fun1(x2,x3,y2,y3).lt.r)then
c24=-(k5/r**3)*(y2-y3)
else
c24=-k5*(y2-y3)/(fun1(x2,x3,y2,y3))**3
endif
z3=z3+h*0.95808*(c21+c22+c23+c24)/n3
y3=y3+h*z3
t=t+h
write(2,*)x1,y1
write(3,*)x2,y2
```

```
write(4,*)x3,y3
enddo
d=sqrt((x1-x2)**2+(y1-y2)**2)
print*,d
stop
end

real function fun1(b1,b2,b3,b4)
implicit none
real::b1,b2,b3,b4
fun1=sqrt((b1-b2)**2+(b3-b4)**2)
end function fun1

real function fun2(b5,b6,b7,b8,b9,b10)
implicit none
real::b5,b6,b7,b8,b9,b10
fun2=exp((sqrt((b5-b6)**2+(b7-b8)**2)-b9)/b10)/(1+exp((sqrt((b5-b6)**2+(b7-b8)**2)-
b9)/b10))**2
end function fun2
```